DOKUZ EYLÜL UNIVERSITY

GRADUATE SCHOOL OF NATURAL AND APPLIED SCIENCES

EFFECT OF GEOMETRICAL PARAMETERS ON HEAT TRANSFER AND PRESSURE DROP CHARACTERISTICS OF PLATE FIN AND TUBE HEAT EXCHANGERS

by

Ali J.ABBAS

September, 2008

İZMİR

EFFECT OF GEOMETRICAL PARAMETERS ON HEAT TRANSFER AND PRESSURE DROP CHARACTERISTICS OF PLATE FIN AND TUBE HEAT EXCHANGERS

A Thesis Submitted to the

Graduate School of Natural and Applied Sciences of

Dokuz Eylül University

In Partial Fulfillment of the Requirements for the Degree of Master of Science

in Mechanical Engineering, Thermodynamics Program

by

Ali J.ABBAS

September, 2008

İZMİR

M.Sc. THESIS EXAMINATION RESULT FORM

We have read the thesis entitled **"EFFECT OF GEOMETRICAL PARAMETERS ON HEAT TRANSFER AND PRESSURE DROP CHARACTERISTICS OF PLATE FIN AND TUBE HEAT EXCHANGERS"** completed by **ALİ J. ABBAS** under supervision of **ASSIST. PROF. Dr. AYTUNÇ EREK** and we certify that in our opinion it is fully adequate, in scope and quality, as a thesis for the degree of Master of Science.

.....

Assist. Prof. Dr. Aytunç EREK

Supervisor

....

(Jury Member) (Jury Member)

Prof. Dr. Cahit HELVACI

Director

Graduate School of Natural and Applied Sciences

ACKNOWLEDMENTS

I would like to thank to my supervisor, Assist. Prof. Dr. Aytunç EREK, for his unlimited support and guidance during the study and his contribution to the achievements of this work is significant.

I would also like to thank to my friend, Assist. Mehmet Akif EZAN, for his help and support. Special thanks to my family and all my friends.

Ali J. ABBAS

EFFECT OF GEOMETRICAL PARAMETERS ON HEAT TRANSFER AND PRESSURE DROP CHARACTERISTICS OF PLATE FIN AND TUBE HEAT EXCHANGERS

ABSTRACT

In this study, the influences of the changes in fin geometry on heat transfer and pressure drop of a plate fin and tube heat exchanger are investigated, numerically. A comparison between experimental results (Herchang Ay, JiinYuh Jang and Jer-Nan Yeh, 2002) and numerical ones for temperature distribution and local convective heat transfer coefficients over a plate-fin surface inside the plate finned and three row tubes heat exchangers are performed. In addition, plate fin and one row tube heat exchanger is analyzed numerically for different geometrical parameters. A computational fluid dynamics (CFD) program called Fluent is used in all analysis. In numerical study for plate fin and one row tube heat exchanger, the effects of the distance between two fins, tube center location, fin height, tube thickness, and tube ellipticity on heat transfer and pressure drop across the heat exchanger are investigated. The distance between fins is found to have a considerable effect on pressure drop. It is observed that placing the fin tube at downstream region affects heat transfer positively. Another important result of the study is that increasing ellipticity of the fin tube increases the heat transfer while it, also, results in an important reduction in pressure drop.

Keywords: Plate fin; Heat exchanger; Numerical modeling; Heat transfer; Pressure drop.

DÜZ KANAT BORU TİPİ ISI DEĞİŞTİRGEÇLERİNİN GEOMETRİK PARAMETRELERİNİN ISI TRANSFERİ VE BASINÇ DÜŞÜMÜ KARAKTERİSTİKLERİNE ETKİSİ

ÖZ

Bu çalışmada, düz kanat-boru tipi ısı değiştiricisinde kanat geometrisi değişimlerinin ısı transferi ve basınç düşümüne etkileri sayısal olarak incelenmiştir. 3 sıralı düz kanat-boru tipi ısı değiştirgeci içindeki sıcaklık dağılımları ve kanat üzerindeki yerel ısı taşınım katsayıları için elde edilen sayısal sonuçlar deneysel sonuçlarla (Herchang Ay, JiinYuh Jang and Jer-Nan Yeh, 2002) karşılaştırılmıştır. Buna ek olarak, düz kanat ve tek sıra borulu ısı değiştirgeci, farklı geometrik parametreler için sayısal olarak analiz edilmiştir. Tüm analizlerde, FLUENT adlı, hesaplamalı akışkanlar dinamiği (HAD) programı kullanılmıştır. Düz kanat ve tek sıra borulu ısı değiştirgeci için sayısal analizlerde, iki kanat arası mesafe, boru merkezin yeri, kanat yüksekliği, boru kalınlığı ve boru eliptikliğinin ısı değiştirgeci boyunca, ısı transferi ve basınç düşümüne etkileri incelenmiştir. Kanatlar arası mesafenin basınç düşümü üzerine önemli bir etkisi olduğu bulunmuştur. Borunun akış boyunca ileride yerleştirilmesinin ısı transferine olumlu etkisi olduğu gözlenmiştir. Bu çalışmanın bir diğer önemli sonucu, boru kesitindeki eliptikliğin artmasıyla ısı transferinin artması, basınç düşümünün ise önemli miktarda azalmadır.

Anahtar Kelimeler: Düz kanat, Isı değiştiricisi, Sayısal modelleme, Isı transferi, Basınç düşümü

CONTENTS

Page

CHAPTER ONE

INTRODUCTION

Plate fin and tube heat exchangers are widely employed in such commercial applications as air conditioning system, heaters and radiation. There are various fin patterns such as plate, louver, convex-louver, and wavy. Among these patterns, plate fin configuration is the most popular fin pattern in heat exchanger applications, owing to its simplicity, rigidity, and economical impact. Typical tube geometries used in heat exchangers are circular and elliptical.

Plate fin and tube heat exchangers have been investigated by many researchers due to their widespread usage. A survey of published heat transfer information related to such heat exchanger devices revealed that the most extensive set of results is concerned with circular tube geometry. For circular tube heat exchangers with plate fins, the results reported by Shepherd (1956), Saboya (1974), Sparraw, (1976) and Rosman et al (1984), constitute the most complete information available in the literature. Several heat exchanger configurations with circular tubes were analyzed.

In Shepherd (1956) a pioneering study of arrangements with one row of circular tubes was reported. Global heat transfer coefficients as a function of the Reynolds number were determined assuming isothermal fins (fin efficiency equal to 1). Saboya (1974) using the naphthalene sublimation technique and the heat and mass transfer analogy, experimentally obtained local and global heat and mass transfer coefficients, for one- and two-row circular tube and plate fin heat exchangers. Saboya and Sparrow (1976) extended the study for three-row heat exchangers. The results show low mass transfer coefficients behind the tubes, as compared with the fin average. Rosman (1984) experimentally determined local and global heat transfer coefficients, using the heat and mass transfer analogy for one – two –row circular tube and plate fin heat exchangers, followed by numerical computations of the fin temperature distribution and fin efficiency, and free steam bulk temperature along the fin. The results show that the two –row configuration is more efficient that

the one –row configuration. Jang et al. (1996) investigated the effects of different geometrical parameters on the average heat transfer coefficient and pressure drop for plate fin and tube heat exchangers, numerically and experimentally. Jang et al. (1998) studied fluid flow and heat transfer characteristics over circular fin and tube heat exchangers with staggered arrangement. Abu Madi et al. (1998) tested 28 heat exchanger samples in an open circuit thermal wind tunnel for different geometries, He examined the effect of geometrical variations of flat and corrugated fins and the results are correlated in terms of Colburn and friction factors.

The elliptic tube geometry has a better aerodynamic shape than the circular one; therefore, it is reasonable to expect a reduction in total drag force and an increase in heat transfer when comparing the former to the latter, both submitted to a cross-flow free stream. According to Webb (1980) the performance advantage of the elliptical tubes results from their lower pressure drop due to the smaller wake region on the fin behind the tube. Brauer (1964) reported experimental results comparing the performance of staggered banks of finned elliptic and circular tubes. The elliptic tubes gave 15% more heat transfer and 18% less pressure drop than the circular tubes. In these experiments, the flow was turbulent with the Reynolds number ranging from 4 x 1000 to 100000.

Later, Schulemberg (1966) analyzed the potential of the application of elliptic tubes in industrial heat exchangers. He concluded that, for a given heat transfer duty, a heat exchanger built from finned elliptical tubes requires less heat transfer surface and consumes less power for driving the fans than an exchanger built from finned circular tubes. Rocha et al. (1997) presented numerical computations of the fin temperature distribution and fin efficiency in one- and two-row elliptic tube and plate fin heat exchangers. In their studies, the fin efficiency results were compared with those of Rosman (1984) for plate fin and circular tube heat exchangers and a relative fin efficiency gain of up to 18% was observed with the elliptical arrangement. Bordalo and Saboya (1995) reported pressure drop measurements comparing the two configurations, with one-, two-, and three-row arrangements. The conclusion of those

studies based on experimental evidence is that the elliptic tube configuration performs better than the circular one.

Recently, Bordalo and Saboya (1999) reported pressure drop measurements comparing elliptic and circular tube and plate fin heat exchanger configurations, with one-, two- and three-row arrangements. Reductions of up to 30% of the loss coefficient (pressure drop coefficient per unit row due only to the presence of the tubes) were observed, in favor of the elliptic configuration. Bordalo and Saboya (1999) shown that elliptical arrangements have the potential for a considerably better overall performance than conventional circular arrangements. Ximenes (1981) reported experimental results for mass transfer coefficients in one- and two-row elliptical tube and plate fin heat exchangers. In the elliptic configuration, it was observed that the mass transfer coefficients drop less dramatically behind the tubes than in the circular configuration.

In most applications, continuous fin sheets pierced by regular arrays of tubes are used. The latter arrangement is not only simple and economic, but also increases overall rigidity of the structure. The augmentation of heat transfer is associated with the increased volume, weight, and cost of the heat exchanger because of the addition of fins. However, tube spacing and fin thickness can be selected optimally so that maximum heat can be transferred for a given fin volume. Zabronsky (1955) determined the temperature distribution and efficiency of square fins around circular tubes in heat exchanger application. However, in his analysis, the adiabatic boundary condition at the fin edge has been satisfied exactly; whereas, the isothermal condition at the fin base has been satisfied only approximately. Shah (1985) described an approximate method, referred to as "Sector Method," for determining the efficiency of plate fins. In this method, the fin is divided into a large number of small sectors. The approximate efficiency of each sector is determined from the efficiency curves already available for annular fins. Finally, the weighted average of the sector efficiencies gives the fin efficiency. Kuan et al. (1984) numerically determined the efficiency of a variety of polygonal fins circumscribing tubes of different regular geometry. They found that for most combined tube and fin geometry; the efficiency

can be calculated analytically, replacing the actual fin by an equivalent annular fin of the same surface area. Romero- Mendez et al. (2000) investigated the effects of fin pitches on a single-row fin and tube heat exchanger. Wang et al. (1996 – 2001) studied the effects of number of tube rows, tube diameter, fin pitch, and fin thickness on heat transfer and pressure drop characteristics for different fin surfaces. Figure 1.1 shows a typical plate fin and tube heat exchanger of a heater used in the analyses.

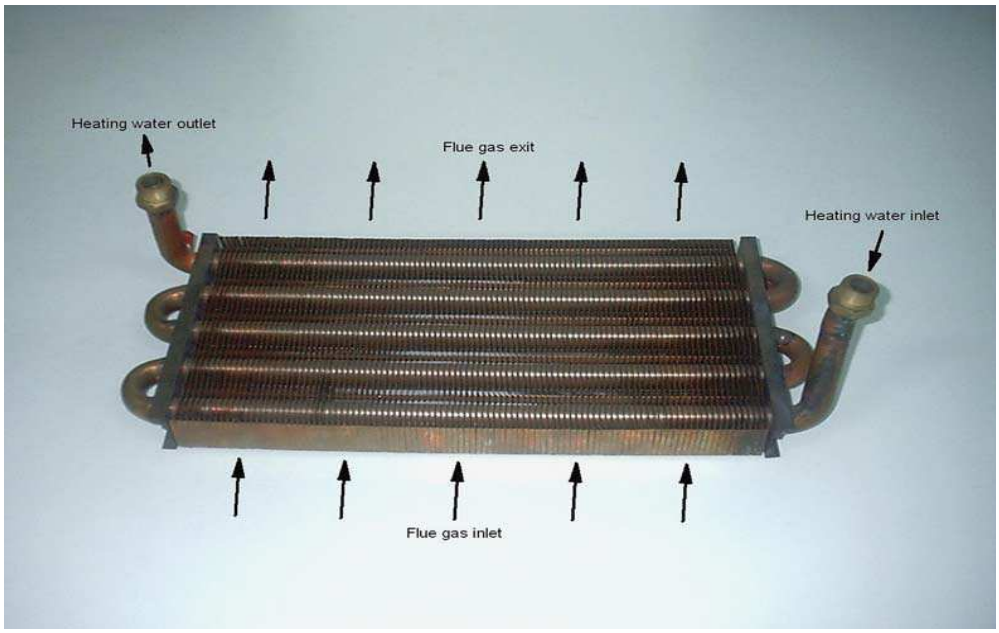

Figure.1.1 View of an analyzed plate fin and tube heat exchanger.

In this study, a comparison between experimental result (Herchang Ay, JiinYuh Jang and Jer-Nan Yeh, 2002) and numerical result of CFD code (FLUENT) programs for temperature distribution and local convective heat transfer coefficients over a plate-fin surface inside the plate finned-tube heat exchangers are performed, In addition, the plate fin and one row tube heat exchanger analyzed for different geometrical parameters, numerically. The effects of tube ellipticity, fin pitch, fin thickness, tube diameter and tube center location on heat transfer and pressure drop of plate fin and tube heat exchangers have been introduced.

CHAPTER TWO

CLASSIFICATION OF HEAT EXCHANGERS

Heat exchangers are devices that provide the flow of thermal energy between two or more fluid at different temperatures. Heat exchangers are used in various applications. In space heating, power production, industrial processes, air-conditioning and refrigeration, heat exchangers are used extensively. In Figure 2.1, a classification of heat exchangers according to 5 main criteria is shown (Kakaç, 1998):

1. Recuperators and regenerators
2. Transfer processes: direct contact and indirect contact
3. Geometry of construction: tubes, plates, and extended surfaces
4. Heat transfer mechanisms
5. Flow arrangements: parallel, counter, and cross flows

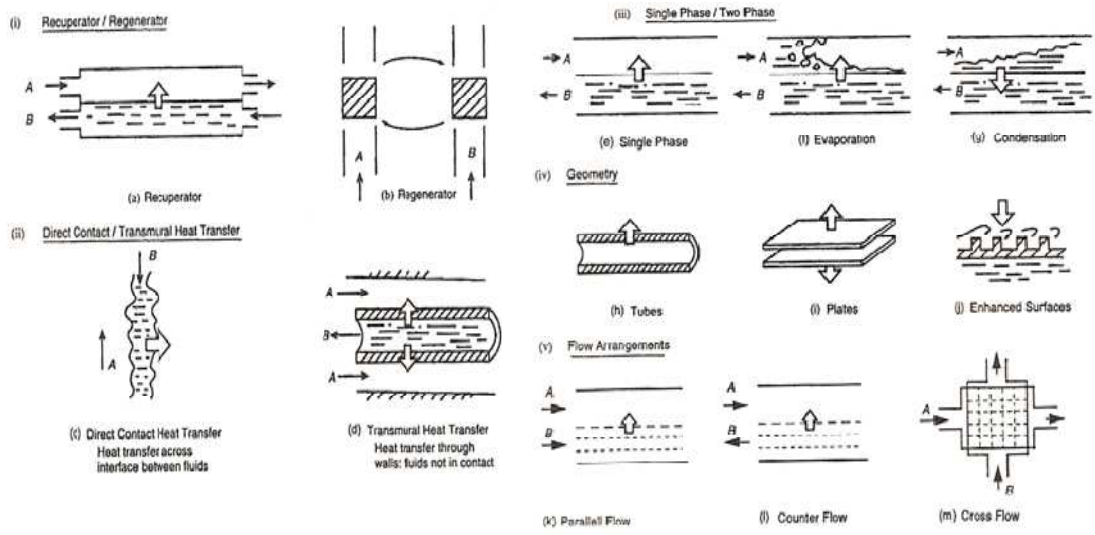

Figure 2.1 Classification of heat exchangers

In this study, the type of heat exchangers is in the category of extended surface heat exchangers according to construction features.

2.1 Recuperation and Regeneration

Recuperators are direct -transfer heat exchangers in which heat transfer occurs between two fluid streams at different temperature levels in a space that is separated by a thin solid wall (a parting sheet or tube wall) .Heat is transferred by convection from the hot (hotter) fluid to the wall surface and by convection from the wall surface To the cold (cooler) fluid. The recuperator is a surface heat exchanger. Some of the recuperative-type exchangers are shown in Figure 2.2.

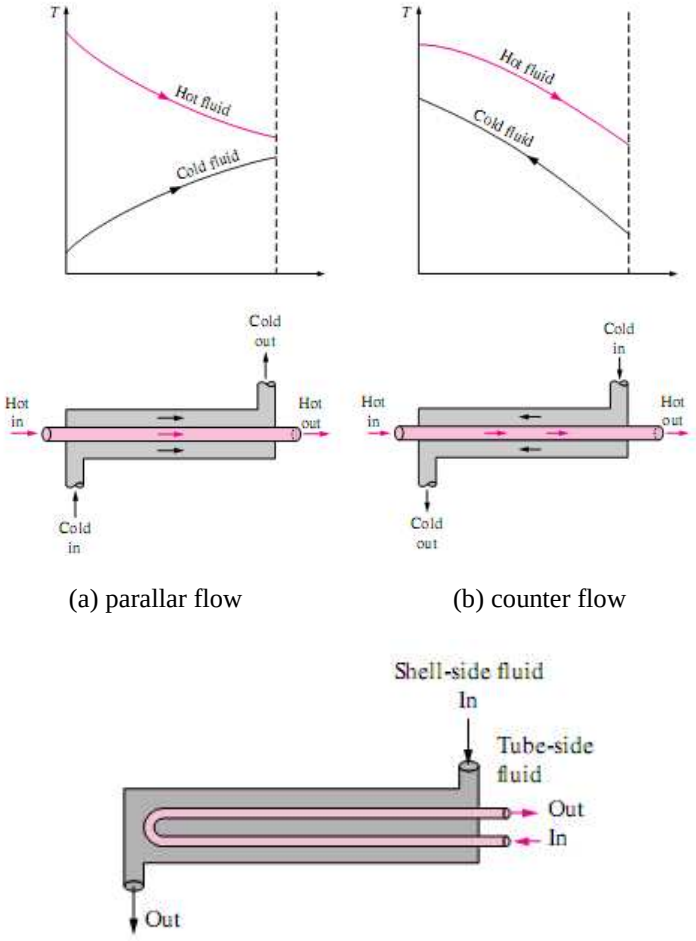

(a) parallar flow (b) counter flow

(c) One-shell pass and two-tube passes

Figure 2.2 Indirect contact types of heat exchangers. (a), (b) Double-pipe type, (c) shell and tube type

In regenerators (storage-type heat exchangers), the same flow passage is alternately occupied by one of the two fluids. The hot fluids stores the thermal energy in the passage during the cold fluid flow through the same passage later,

energy stored will be extracted from the passage. Therefore, thermal energy is not transferred through the wall as in a direct transfer type of heat exchanger. Regenerators can be classified as:

1. Rotary regenerator
   (a) Disk-type
   (b) Drum-type
2. Fixed-matrix regenerator

Rotary regenerators are used in preheating air in large coal-fired steam power plants, gas turbines, and fixed matrix air preheating for blast furnace stoves, steel furnaces, open-hearth steel melting furnaces, and glass furnaces. Rotary regenerators can be classified as:

The disk-type and drum-type regenerators are shown in Figure 2.3, schematically. The heat transfer surface is in a disk form and fluids flow axially in disk-type regenerators. In drum-type regenerators, the matrix is in a hollow drum form and fluids flow radially.

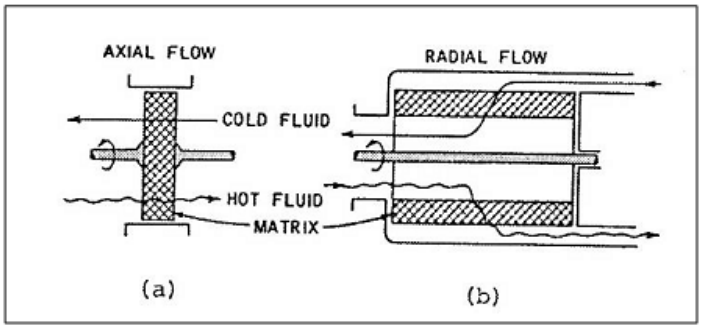

Figure 2.3 Rotary regenerators. (a) Disk type. (b) Drum type

2.2 Transfer Processes

Heat exchangers are classified as direct contact type and indirect contact type (transmural heat transfer) according to transfer processes (Kakaç, 1998).

In direct contact heat exchangers, heat is transferred by partial or complete mixing of the hot and cold fluid streams. As shown in Figure 2.1c, since there is no wall between hot and cold streams. The heat transfer occurs through the interface of two streams. The streams are two immiscible liquids, a gas-liquid pair, or a solid particle-fluid combination in direct contact type heat exchangers. Cooling towers, spray and tray condensers are good examples of such heat exchangers.

In indirect contact type heat exchangers, heat is transferred through a heat transfer surface between the cold and hot fluids, as shown in Figure 2.1d. The fluids are not mixed. This type of heat exchanger examples are shown in Figure 2.2.

Indirect contact and direct contact type heat exchangers are also called recuperators. Tubular (double-pipe, shell and tube), plate, and extended surface heat exchangers; cooling towers; and tray condensers are examples of recuperators.

2.3 Geometry of Construction

Indirect contact type heat exchangers are often described in terms of their construction features. Tubular, plate and extended surface heat exchangers are the major construction types (Kakaç, 1998).

2.3.1 Tubular Heat Exchangers

Circular tubes are used in these heat exchangers. One fluid flows inside the tubes and the other fluid flows outside of the tubes. Tube diameter, number of tubes, tube length, tube pitch, and tube arrangement are the construction parameters; there is a considerable flexibility in tubular heat exchanger design. Tubular heat exchangers can be classified as:

1. Double-pipe
2. Shell and tube
3. Spiral-tube

2.3.1.1 Double-Pipe Heat Exchangers

A typical double-pipe heat exchanger consists of one pipe placed concentrically inside another of larger diameter with appropriate fittings to direct the flow from one section to the next, as shown in Figure 2.4. Double-pipe heat exchangers can be arranged in various series and parallel arrangements to meet pressure drop and mean temperature difference requirements. In sensible heating or cooling of process fluids where the small heat transfer areas (to 50 m^2) are required, double-pipe heat exchangers are used extensively. Double-pipe heat exchangers can be built in modular concept (i.e., in the form of hairpins).

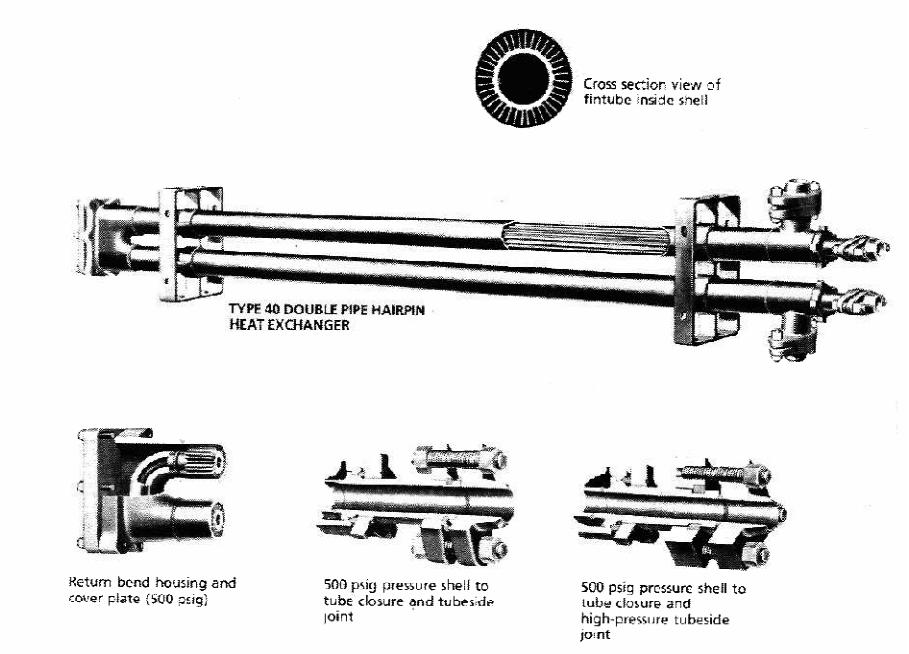

Figure 2.4 Double-pipe hairpin heat exchanger

2.3.1.2 Shell and Tube Heat Exchangers

Shell and tube heat exchangers are built of round tubes mounted in large cylindrical shells with the tube axis parallel to that of the shell. They are used as oil coolers, power condensers, preheaters in power plants, steam generators in nuclear power plants, and in process and chemical industry applications, extensively. A horizontal shell and tube condenser is shown in Figure 2.5. One fluid flows through the tubes while the other flows on the shell side, across or along the tubes. The

baffles are used to promote a better heat transfer coefficient on the shell side and to support the tubes. In a baffled shell and tube heat exchanger, the shell side fluid flows across between pairs or baffles and then flows parallel to the tubes as it flows from one baffle compartment to the next. There are many different shell and tube heat exchangers depending on the application. The most representative tube bundle types are used in shell and tube heat exchangers are shown in Figure 2.6 and 2.7. Since only one tube sheet is used, the U-tube is the least expensive construction. But the tube side cannot be mechanically cleaned because of the sharp U-bend.

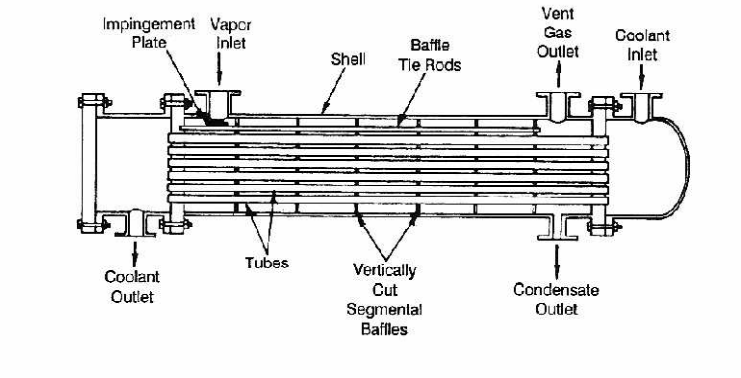

Figure 2.5 Shell and tube heat exchanger as a shell side condenser

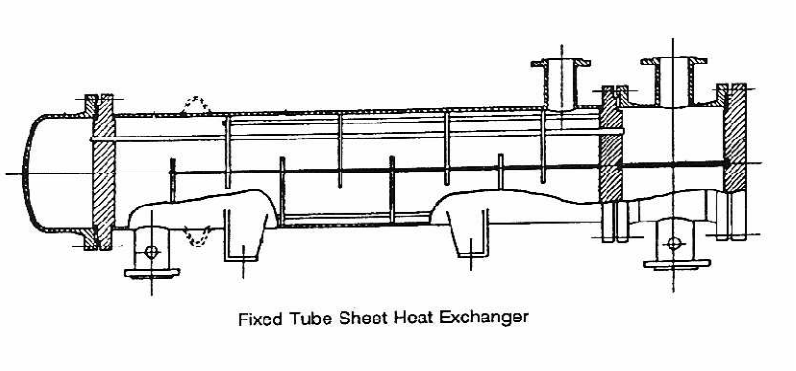

Figure 2.6 Two-pass tube, baffled single-pass shell, shell and tube heat exchanger

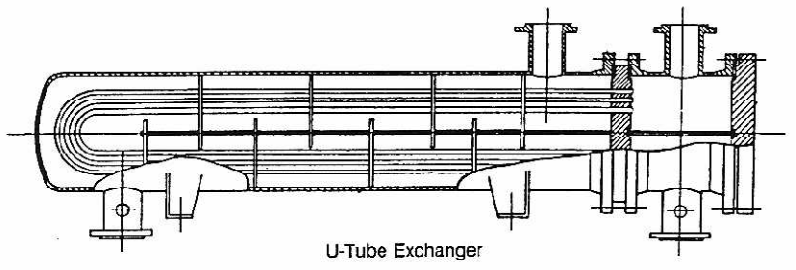

Figure 2.7 U-tube, baffled single-pass shell, shell and tube heat exchanger

2.3.1.3 Spiral-Tube Heat Exchangers

Spiral-tube heat exchangers are spirally wound coils placed in a shell, or coaxial condensers and coaxial evaporators used in refrigeration systems. The heat transfer coefficient is higher than straight tubes. They are suitable for thermal expansion and clean fluids, because it is almost impossible to clean a spiral-tube heat exchanger.

2.3.2 Plate Heat Exchangers

Plate heat exchangers are made of thin plates forming flow channels. The fluid streams are separated by flat plates that are either smooth or between which are sandwiched corrugated fins. They are used for heat transfer between any gas, liquid, and two-phase stream combinations. Plate heat exchangers are classified as:

1. Gasketed-plate
2. Spiral plate
3. Lamella

2.3.2.1 Gasketed-Plate Heat Exchangers

A typical gasketed-plate heat exchanger and the flow paths are shown in Figure 2.8 and 2.9. A gasketed plate consists of a series of corrugated or wavy thin plates that separates the fluids. Gaskets are used to prevent the leakage to the outside and direct the fluids in the plates. The countercurrent flow pattern is generally selected for the fluids. Because of the small flow passages, strong eddying gives high heat transfer coefficients, high-pressure drops, and high local shear that minimizes fouling. Gasketed-plate heat exchangers provide relatively compact and lightweight heat transfer surface. They are typically used for heat exchange between two liquid streams. Because of easy cleaning and sterilization, they are extensively used in the food processing industry.

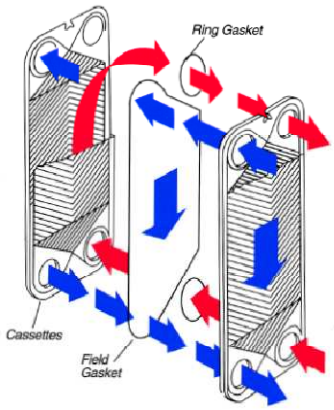

Figure 2.8 Gasketed-plate heat exchanger and flow paths

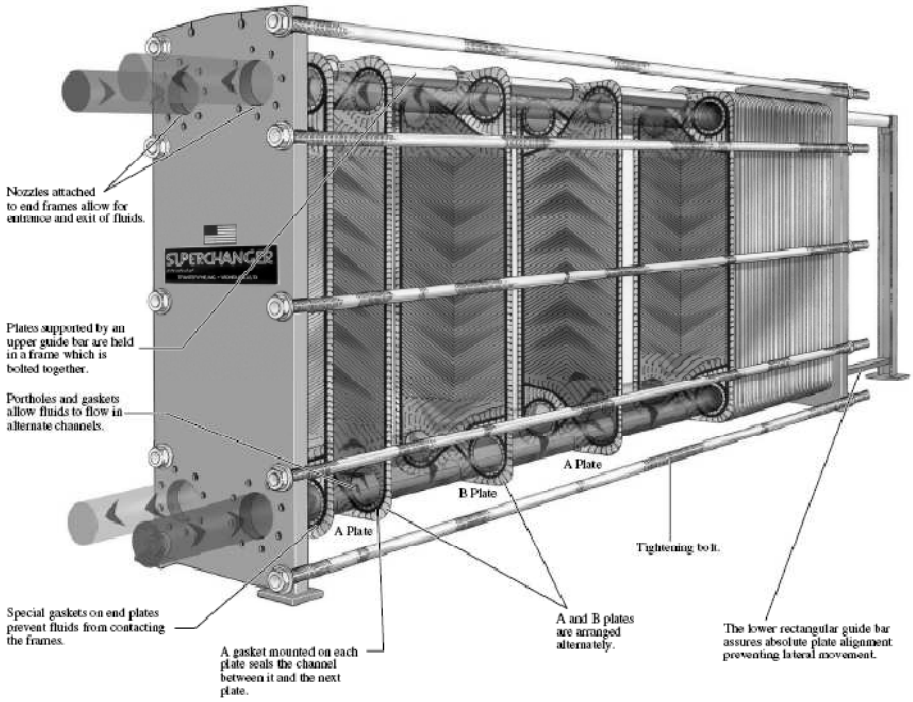

Figure 2.9 Gasketed-plate heat exchanger

2.3.2.2 Spiral Plate Heat Exchangers

As shown in Figure 2.10, spiral heat exchangers are formed by rolling two long, parallel plates into a spiral using a mandrel and welding the edges of adjacent plates to form channels. The distance between the metal surfaces in both spiral channels is

maintained by means of distance pins welded to the metal sheet. The length of the distance pins may vary between 5 and 20 mm. It is possible to choose between different channels spacing according to the flow rate and ideal flow conditions and smallest possible heating surfaces can be obtained.

Two spiral paths introduce a secondary flow, increasing the heat transfer and reducting fouling deposits. These heat exchangers are quite compact, but are relatively expensive due to their specialized fabrication. Sizes range from 0.5 to 500m² heat transfer surface in one single spiral body.

The spiral heat exchanger is particularly effective in handling sludges, viscous liquids, and liquids with solids in suspension including slurries. A cross flow type spiral heat exchanger is shown in Figure 2.11.

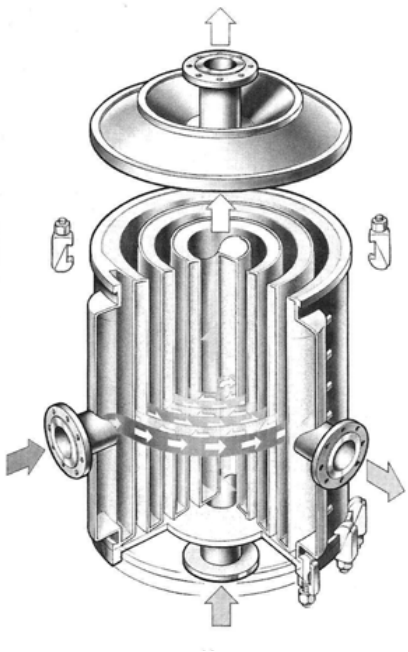

Figure 2.10 Counter-flow spiral heat exchanger

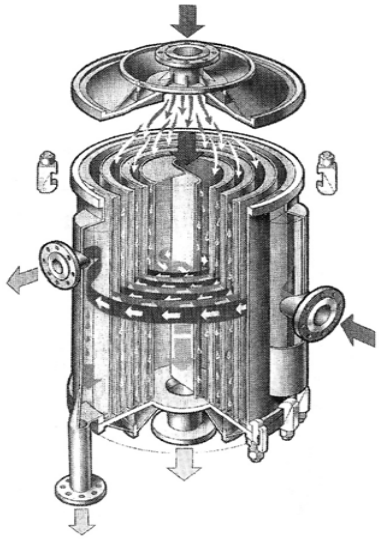

Figure 2.11 Cross-flow spiral heat exchanger

2.3.2.3 Lamella Heat Exchanger

As shown in Figure 2.12, the lamella (Ramen) type heat exchangers consists of a set of parallel, welded, thin plate channels or lamellae (flat tubes or rectangular channels) placed longitudinally in a shell. It is a modification of the floating-head type of shell and tube heat exchanger. These flattened tubes (lamellas) are made up of two strips of plates, profiled and spot or seam welded together in a continuous operation. The lamellas are welded together at both ends by joining the ends with steel bars in between, depending on the space required between lamellas. Both ends of the lamella bundle are joined by peripheral welds to the channel cover, which at the outer ends is welded to the inlet and outlet nozzle. The lamella side is thus completely sealed in by welds. Lamella heat exchangers can be arranged for true countercurrent flow, since there are no shell side baffles. Because of high turbulence, uniform flow distribution, and smooth surfaces, the lamellas do not foul easily. They can be used up to 35 bar, 200°C for Teflon gaskets, and 500°C for asbestos gaskets.

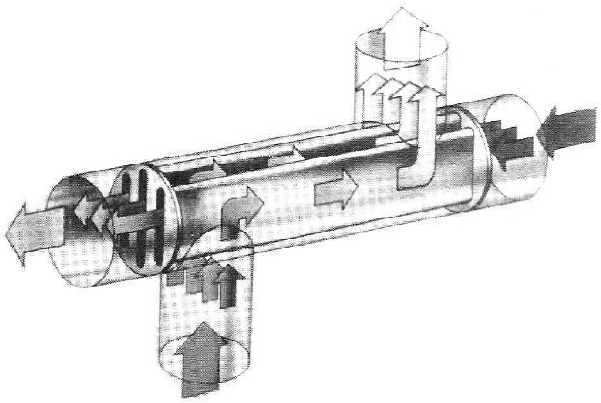

Figure 2.12 Lamella heat exchanger.

2.3.3 Extended Surface Heat Exchangers

Extended surface heat exchangers have fins or appendages on the primary heat transfer surface (tubular or plate) to increase heat transfer area. Since gas side heat transfer coefficient is much lower than liquid side, finned surfaces are used to increase the heat transfer area. Fins are extensively used in gas-to-gas and gas-liquid heat exchangers. The most common types of the extended surface heat exchangers are

1. Plate-fin
2. Tube-fin

2.3.3.1 Plate-Fin Heat Exchangers

Plate-fin type heat exchangers are primarily used in gas-to-gas applications and tube-fin type heat exchangers are used in liquid-air applications. Since mass and volume reduction is important in most of the applications, compact heat exchangers are widely used in air-conditioning, refrigeration and process industries. Basic construction of a plate-fin heat exchanger is shown in Figure 2.13. The fluids are separated by flat plates between which are sandwiched corrugated fins. Figure 2.13 shows the arrangement for parallel flow or counter flow and cross flow between the streams.

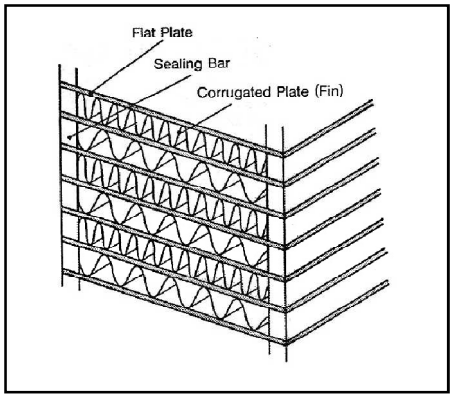

Figure 2.13 Basic construction of a plate-fin heat exchanger

The corrugated sheets that are sandwiched between the plates serve both to give extra heat transfer area and to give structural support to the flat plates. The most common types of corrugated sheets are shown in Figure 2.14.

1. Plain fin
2. Plain-perforated fin
3. Serrated (interrupted, louver) fin
4. Herringbone or wavy fin

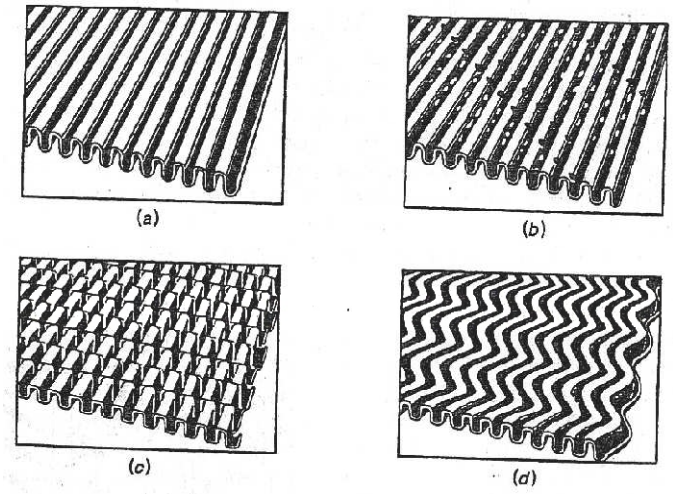

Figure 2.14 Fin types in plate-fin heat exchangers. (a) Plain, (b) perforated, (c) serrated, (d) herringbone

2.3.3.2 Tubular-Fin Heat Exchangers

Tubular-fin heat exchangers are used as gas-to-liquid heat exchangers. Since the gas side heat transfer coefficients are generally much lower than the liquid side, fins are required. As shown in Figures 2.15 and 2.16, a tubular-fin heat exchanger consists of an array of tubes with fins fixed on the outside. The fins may be normal on individual tubes, transverse or helical, or longitudinal (Figure 2.16). Longitudinal fins are commonly used in double-pipe or shell and tube heat exchangers with no baffles. As can be seen from Figure 2.15, continuous plate-fin sheets may be fixed on the array of round, rectangular, or elliptical tubes. Plate fin and tube heat exchangers are commonly used in air-conditioning and refrigerating systems.

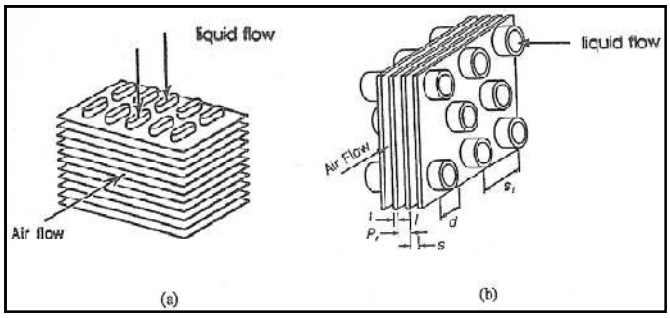

Figure 2.15 Tube-fin heat exchangers (a) Flattened tube-fin, (b) round tube-fin.

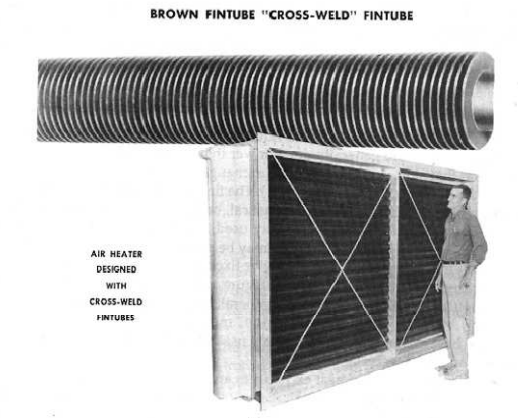

Figure 2.16 Fin-tube air heater

2.4 Flow Arrangement

Heat exchangers may be classified according to the fluid-flow path through the heat exchanger (Kakaç, 1998). Three basic flow arrangements are

1. Parallel flow
2. Counter flow
3. Cross flow

As shown in Figure 2.17a, in parallel flow heat exchangers, the two fluid streams enter together at one end, flow through the same direction, and leave together at the other end. In counter flow heat exchangers, two fluid streams flow in opposite direction (Figure 2.17b). In single-cross flow heat exchangers, one fluid flows through the heat exchanger surface at right angles to the flow path of the other fluid. Cross flow arrangements with both fluids unmixed, and one fluid mixed and the other fluid unmixed are shown in Figures 2.17c and 2.17d, respectively.

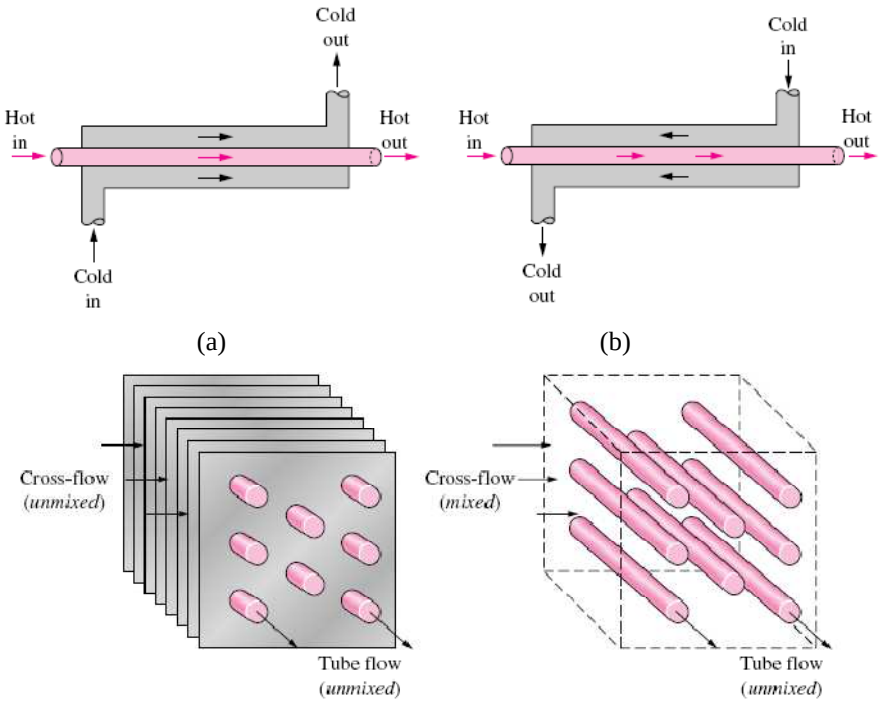

Figure 2.17 Heat exchanger classifications according to flow arrangement. (a) Parallel-flow, (b) counter flow, (c) cross flow-both fluids unmixed, (d) cross flow-fluid 1 mixed, fluid 2 unmixed.

CHAPTER THREE

COMPUTATIONAL FLUID DYNAMICS AND FLUENT PROGRAM

3.1 Computational Fluid Dynamics

Computational fluid dynamics (CFD) is one of the branches of fluid mechanics that uses numerical methods and algorithms to solve and analyze problems that involve fluid flows. Computers are used to perform the millions of calculations required to simulate the interaction of fluids and gases with the complex surfaces used in engineering. In this thesis, computational fluid dynamics code called FLUENT used to solve governing equations.

The ultimate goal of the field of computational fluid dynamics (CFD) is to understand the physical events that occur in the flow of fluids around and within designated objects. Modern engineers apply both experimental and CFD analyses, and two complement each other. Experimental data are often used to validate CFD solutions by matching the computationally and experimentally determined global quantities. CFD is then employed to shorten the design cycle through carefully controlled parametric studies, thereby reducing the required amount of experimental testing.

- **Steps to Solve Flow Problem by CFD**

The basic procedural steps to solve CFD problems are shown below.

1. Define the modeling goals.
2. Create the model geometry and grid.
3. Set up the solver and physical models.
4. Compute and monitor the solution.
5. Examine and save the results.
6. Consider revisions to the numerical or physical model parameters, if necessary.

The Step 2 of the solution process requires a geometry modeler and grid generator. We use GAMBIT for geometry modeling and grid generation. We can also use TGrid to generate volume grids from surface grids imported from GAMBIT.

3.2 GAMBIT and FLUENT Programs

3.2.1 GAMBIT Program

GAMBIT is a software package designed to help analysts and designers build and mesh models for computational fluid dynamics (CFD) and other scientific applications. GAMBIT receives user input by means of its graphical user interface (GUI). The GAMBIT GUI makes the basic steps of building, meshing, and assigning zone types to a model simple and intuitive, yet it is versatile enough to accommodate a wide range of modeling applications. GAMBIT allows constructing and meshing models by means of its graphical user interface (GUI).

- **GUI Components**

The GAMBIT GUI consists of eight components, each of which serves a separate purpose with respect to the creating and meshing of a model. The GUI components are as follows:

1. Graphics window
2. Main menu bar
3. Operation tool pad
4. Form field
5. Global Control tool pad
6. Description window
7. Transcript window
8. Command text box

3.2.2 FLUENT Program

FLUENT is a computational fluid dynamics (CFD) software package to simulate fluid flow problems. FLUENT is a state-of-the-art computer program for modeling fluid flow and heat transfer in complex geometries. FLUENT provides complete mesh flexibility, including the ability to solve your flow problems using unstructured meshes that can be generated about complex geometries with relative ease. It uses the finite-volume method to solve the governing equations for a fluid. It provides the capability to use different physical models such as incompressible or compressible, inviscid or viscous, laminar or turbulent, etc**.** FLUENT allows working in any unit system, including inconsistent units**.** Geometry and grid generation is done using GAMBIT which is the preprocessor bundled with FLUENT. A solution can be obtained by following these seven steps:

1. Create Geometry in GAMBIT
2. Mesh Geometry in GAMBIT
3. Set Boundary Types in GAMBIT
4. Set Up Problem in FLUENT
5. Solve
6. Analyze Results
7. Refine Mesh

Fluent uses a control-volume-based technique to convert a general scalar transport equation to an algebraic equation that can be solved numerically. This control volume technique consists of integrating the transport equation about each control volume, yielding a discrete equation that expresses the conservation law on a control-volume basis.

Discretization of the governing equations can be illustrated most easily by considering the unsteady conservation equation for transport of a scalar quantity ϕ. This is demonstrated by the following equation written in integral form for an arbitrary control volume Δv as follows:

$$\int_{\Delta v} \frac{\partial \rho \phi}{\partial t} dV + \int_{\Delta v} div(\rho \phi \bar{v}).dV = \int_{\Delta v} div(\Gamma_\phi gard\phi).dV + \int_{\Delta v} S_\phi dV \qquad (3.1)$$

Where

ρ : Density

$\vec{v}$: Velocity vector $\left(= u\vec{i} + v\vec{j} \text{ in 2D}\right)$

Γ_ϕ : Diffusion coefficient for ϕ

$grad\phi$: Gradient of $\phi = \left(\frac{\partial \phi}{\partial x}\right)\vec{i} + \left(\frac{\partial \phi}{\partial y}\right)\vec{j}$ in 2D

S_ϕ : Source of ϕ per unit volume

Equation (3.1) is applied to each control volume, or cell, in the computational domain. The two-dimensional, triangular cell shown in Figure (3.1) is an example of such a control volume. Discretization of Equation (3.1) on a given cell yields

$$\frac{\partial \rho \phi}{\partial t} V + \sum_f^{N_{faces}} \rho_f \overrightarrow{v_f} \phi_f . \overrightarrow{A_f} = \sum_f^{N_{faces}} \Gamma_\phi grad\phi_f . \overrightarrow{A_f} + S_\phi V \qquad (3.2)$$

Where

N_{faces} : number of faces enclosing cell

ϕ_f : Value of ϕ convected through face f

$\rho_f \overrightarrow{v_f} . \overrightarrow{A_f}$: Mass flux through the face

$\overrightarrow{A_f}$: Area of face f , $|A| = \left|A_{x\vec{i}} + A_{x\vec{j}}\right|$ in 2D

$\nabla\phi_f$: Gradient of ϕ at face f

V : cell volume

The equations solved by *FLUENT* take the same general form as the one given above and apply readily to multi-dimensional, unstructured meshes composed of arbitrary polyhedra.

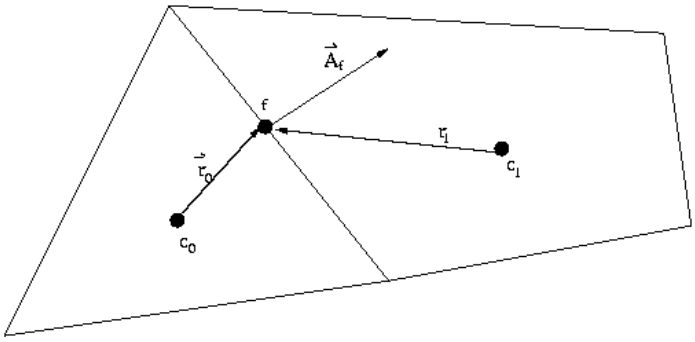

Figure 3.1 Control Volume Used to Illustrate Discretization of a Scalar Transport Equation

Face values ϕ_f are required for the convection terms in Equation (3.2) and must be interpolated from the cell center values. This is accomplished using an upwind scheme.

Upwinding means that the face value ϕ_f is derived from quantities in the cell upstream, or "upwind," relative to the direction of the normal velocity u_n in Equation (3.2). *FLUENT* allows choosing from several upwind schemes: first-order upwind, second-order upwind, power law, and QUICK. In this study using QUICK scheme. The diffusion terms in Equation (3.2) are central-differenced and are always second-order accurate

3.2.2.1 Control-Volume Formulation and Discretization

Discretization equations of a computational domain can be derived from the governing equations in many ways,

- Finite difference,
- Finite element,
- Spectral methods,
- Finite volume (*control volume*) method,

As an outline, the basis of the solver methods perform the following steps (Versteeg and Malalasekera, 1995),

- Approximation of the unknown flow variables by means of simple functions,
- Discretization by substitution of the approximations into the governing flow equations and subsequent mathematical manipulations,
- Solution of the algebraic equations.

A. *Control-Volume Formulation*

The finite volume method is a method for representing and evaluating partial differential equations as algebraic equations. "Finite volume" refers to the small volume surrounding each node point on a mesh. In the finite volume method, volume integrals in a partial differential equation that contain a divergence term are converted to surface integrals, using the divergence theorem. These terms are then evaluated as fluxes at the surfaces of each finite volume.

Finite-volume methods have become popular in CFD as a result, primarily, of two advantages. First, they ensure that the discretization is conservative, i.e., mass, momentum, and energy are conserved in a discrete sense. While this property can usually be obtained using a finite-difference formulation, it is obtained naturally from a finite-volume formulation. Second, finite- volume methods do not require a coordinate transformation in order to be applied on irregular meshes. As a result, they can be applied on unstructured meshes consisting of arbitrary polyhedra in three dimensions or arbitrary polygons in two dimensions. This increased flexibility can be used to great advantage in generating grids about arbitrary geometries.

In this method the calculation domain is divided into a number of non-overlapping control volumes (Figure 3.2) such that there is one control volume surrounding each grid point. The differential equation is integrated over each control volume. Piecewise profiles expressing the variation of ϕ between the grid points are used to evaluate the required integrals. The result is the discretization equation containing the values of ϕ for a group of grid points. The discretization equation obtained in this manner expresses the conservation principle for ϕ for the finite control volume,

just as the differential equation expresses it for an infinitesimal control volume. (Patankar 1980)

$$\begin{bmatrix}\text{Rate of change of}\\ \phi \text{ in the control volume}\\ \text{with respect time}\end{bmatrix} = \begin{bmatrix}\text{Net flux of } \phi \text{ due}\\ \text{to convection into}\\ \text{the control volume}\end{bmatrix} + \begin{bmatrix}\text{Net flux of } \phi \text{ due}\\ \text{to diffusion into}\\ \text{the control volume}\end{bmatrix} + \begin{bmatrix}\text{Net rate of creation of}\\ \phi \text{ inside the control}\\ \text{volume}\end{bmatrix}$$

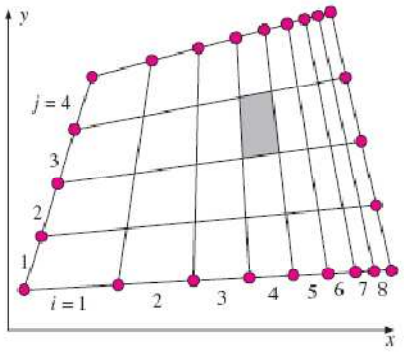

(a)

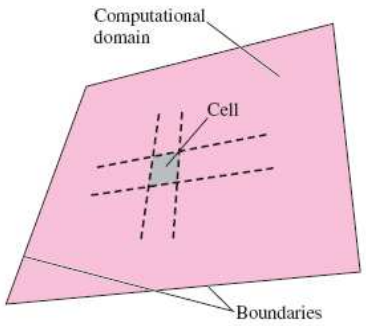

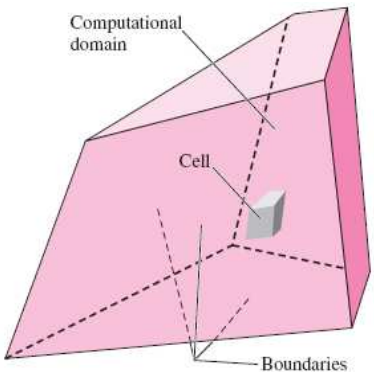

(b) (c)

Figure 3.2 (a) Grid layout for a computation domain (*b*) a two dimensional domain and quadrilateral cell, and (*c*) a three-dimensional domain and hexahedral cell

I. *Discretization for one Dimensional Control Volume*

Control volume approach and discretization of governing equation can be explained via an illustrative example. Because of its simplicity, discretizing a steady and one –dimensional convection and diffusion equation is selected. Governing equation of the problem is, well-known convection and diffusion equation,

$$\frac{\partial}{\partial x}(\rho u\phi)=\frac{\partial}{\partial x}\left(\Gamma\frac{\partial\phi}{\partial x}\right)+\mathrm{S} \qquad (3.3)$$

Where, ϕ is diffusion property, *e.g. temperature,* Γ is the diffusion coefficient, *e.g. thermal conductivity* and S is the source term, *e.g. the rate of heat generation per unit volume.*

The first step in the finite volume method is to divide the domain into discrete control volumes. Discretization equation can be derived for the grid-point cluster, shown in Figure 3.3. Here the central point of the control volume is indicated with P, and the nodes to the west and east, are identified by W and E respectively. The west side face of the control volume is referred to by "w "and the east side control volume face by "e". The distances between the nodes W and P, and between nodes P and E are identified by δx_{WP} and δx_{PE} respectively. Similarly the distances between the nodes w and P, and between nodes P and e are denoted by δx_{wP} and δx_{Pe} respectively (Versteeg and Malalasekera, 1995).

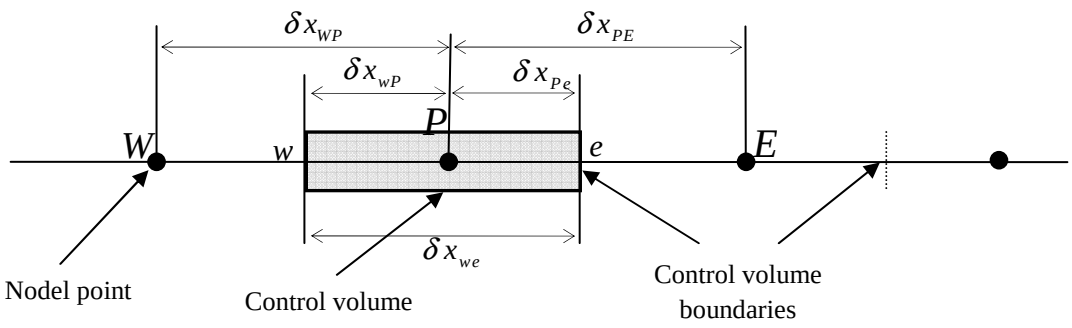

Figure 3.3 Control volume and grid nodes for one-dimensional domain

The key step of the finite volume is the integration of the governing equation (or equations) over a control volume to yield a discretized equation at its nodal point P (Versteeg and Malalasekera, 1995). Integration of the Equation (3.3) over the control volume, as above-mentioned, can be written as follows,

$$\int_{\Delta V} \frac{\partial}{\partial x}(\rho u \phi).dV = \int_{\Delta V} \frac{\partial}{\partial x}\left(\Gamma \frac{\partial \phi}{\partial x}\right).dV + \int_{\Delta V} S.dV \qquad (3.4)$$

Here, linear interpolation functions are used between the grid points, hence, derivatives $d\phi/dx$ can be written from the piecewise-linear profile,

$$(\rho u A \phi)_e - (\rho u A \phi)_w - \left[\left(\Gamma A \frac{\partial \phi}{\partial x}\right)_e - \left(\Gamma A \frac{\partial \phi}{\partial x}\right)_w\right] - \bar{S}\Delta V = 0 \qquad (3.5)$$

In uniform grid linearly interpolated values for Γ_w and Γ_e are given by

$$\Gamma_w = \frac{\Gamma_W + \Gamma_P}{2} \qquad (3.6a)$$

$$\Gamma_e = \frac{\Gamma_P + \Gamma_E}{2} \qquad (3.6b)$$

In Equation (3.5), the diffuse flux terms are evaluated as,

$$\left(\Gamma A \frac{\partial \phi}{\partial x}\right)_e = \Gamma_e A_e \left(\frac{\phi_E - \phi_P}{\delta x_e}\right) \qquad (3.7a)$$

$$\left(\Gamma A \frac{\partial \phi}{\partial x}\right)_w = \Gamma_w A_w \left(\frac{\phi_P - \phi_W}{\delta x_w}\right) \qquad (3.7b)$$

The source term S may be a function of the dependent variable, in such cases, the finite volume method approximates the source term by means of a linear form;

$$\bar{S}\Delta V = S_u + S_P \phi_P \qquad (3.8)$$

Equations (3.7a) to (3.8) can be arranged in Equation (3.5),

$$(\rho uA\phi)_e-(\rho uA\phi)_w-\left[\Gamma_e A_e\left(\frac{\phi_E-\phi_P}{\delta x_e}\right)-\Gamma_w A_w\left(\frac{\phi_P-\phi_W}{\delta x_w}\right)\right]-(S_u+S_P\phi_P)=0 \quad (3.9)$$

here, Γ is used to represent the value of Γ pertaining to the particular control face, e.g. Γ_e refers to interface e If the diffusion coefficient Γ is a function of x, then the value of Γ must be known at the grid points E and P and so on (Erek, 1999).

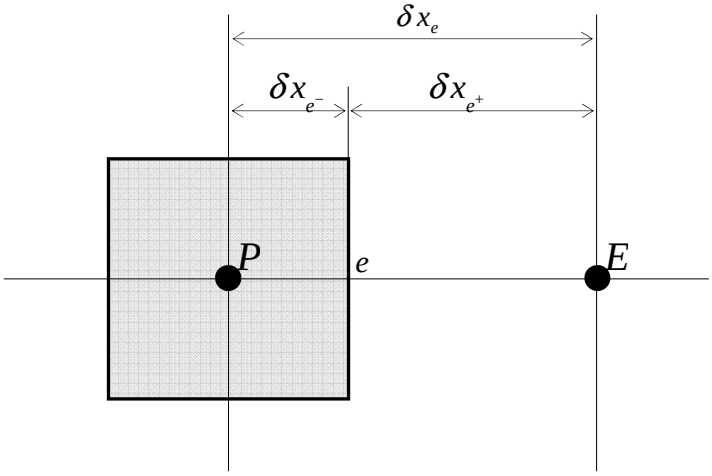

Figure 3.4 Distances for interface e

The interpolation factor f_e is a ratio defined in terms of the distances in Figure 3.4;

$$f_e=\frac{\delta x_{e^+}}{\delta x_e} \quad (3.10)$$

If the interface e is the midway between the grid points, f_e would be 0.5, and Γ_e would be arithmetic mean of Γ_P and Γ_E.Heat flux equations for interface e can be obtained as,

$$q_e=\Gamma_e\frac{T_P-T_E}{\delta x_e} \quad (3.11)$$

and another flux equation can be written, if the control volume that surround the grid point P is filled with a material of uniform diffusion coefficient Γ_P, and the one around E with a material of diffusion coefficient Γ_E, so the steady heat flux for the composite slab between the points P and E leads to,

$$q_e = \frac{T_P - T_E}{\delta x_{e^-}/\Gamma_P + \delta x_{e^+}/\Gamma_E} \qquad (3.12)$$

Equations (3.11) and (3.12) can be arranged to express the desired Γ_e,

$$\Gamma_e = \left(\frac{1-f_e}{\Gamma_P} + \frac{f_e}{\Gamma_E} \right)^{-1} \qquad (3.13)$$

As a particular grid structure, if the interface e is placed midway between P and E, then interpolation factor becomes, $f_e = 0.5$. So the Equation (3.13) can be re-arranged as follows,

$$\Gamma_e^{-1} = 0.5\left(\frac{1}{\Gamma_P} + \frac{1}{\Gamma_E} \right) \quad \text{or} \quad \Gamma_e = \frac{2\Gamma_P\Gamma_E}{\Gamma_P + \Gamma_E} \qquad (3.14)$$

Thus, Γ_e is gained as a harmonic mean of Γ_P and Γ_E, rather than the arithmetic mean, for uniform grid. (Patankar 1980).

To obtain discretised equations for convection-diffusion problem, approximate the terms in equation (3.5).it is convenient to define two variables F and D to represent the convective mass flux per unit area and diffusion conductance at cell faces

$$F = \rho u \quad \text{and} \quad D = \frac{\Gamma}{\partial x} \qquad (3.15)$$

The cell face values of the variables *F* and D written as

$$F_w = (\rho u)_w \quad , F_e = (\rho u)_e \tag{3.16}$$

$$\mathrm{D}_w = \frac{\Gamma_w}{\partial x_{WP}} \quad , \mathrm{D}_e = \frac{\Gamma_e}{\partial x_{PE}} \tag{3.17}$$

Assuming that $A_w=A_e=A$, *and* employ the central differencing approach to represent the contribution of the diffusion terms. The integrated convection – diffusion equations (3.5) written as

$$F_e\phi_e - F_w\phi_w = \mathrm{D}_e(\phi_E - \phi_P) - \mathrm{D}_w(\phi_P - \phi_W) + S_u + S_P\phi_P \tag{3.18}$$

To solve equation (3.18) we calculate the transported property ϕ at the *e* and *w* faces. In this thesis used QUICK Scheme by FLUENT programs to calculate ϕ at the *e* and *w* faces.

3.2.2.2 QUICK Scheme

The QUICK Scheme uses a three point upstream weighted quadratic interpolation for cell face values. The face value of ϕ is obtained from a quadratic function passing through two bracketing nodes (on each side of the face) and a node on the upstream side, shown in Figure 3.5 (Versteeg and Malalasekera, 1995).

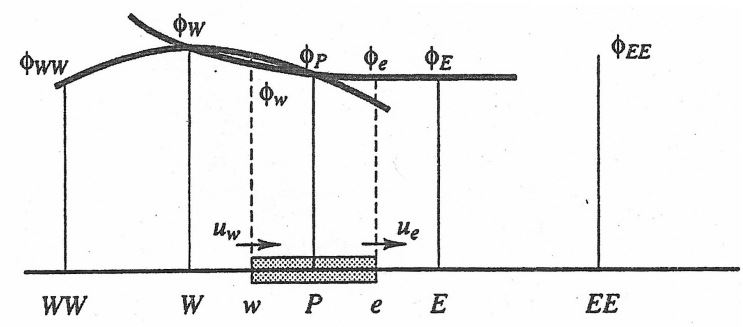

Figure 3.5 quadratic profiles used in the QUICK scheme

When $u_w>0$ and $u_e>0$ a quadratic fit through *WW,W* and *P* is used to evaluate ϕ_w and a further quadratic fit through *W,P* and *E* to calculate ϕ_e. for $u_w<0$ and $u_e<0$ values of ϕ at *W ,P* and *E* are used for ϕ_w and values at *P,E* and *EE for* ϕ_e.for a

uniform grid the value of ϕ at the cell face between two bracketing nodes *i* and *i-1* ,and upstream node *i-2* is given by the following formula :

$$\phi_{face} = \frac{6}{8}\phi_{i-1} + \frac{3}{8}\phi_i - \frac{1}{8}\phi_{i-2} \qquad (3.19)$$

When $u_w>0$, the bracketing nodes for the west face *"w"* are *W* and *P*, the upstream node is *WW (*Figure 3.5).

$$\phi_w = \frac{6}{8}\phi_W + \frac{3}{8}\phi_P - \frac{1}{8}\phi_{WW} \qquad (3.20)$$

When $u_e>0$, the bracketing nodes for the east face *"e"* are *P* and *E*, the upstream node is *W*, so

$$\phi_e = \frac{6}{8}\phi_P + \frac{3}{8}\phi_E - \frac{1}{8}\phi_W \qquad (3.21)$$

Equations (3.20) and (3.21) use for the convective terms and central differencing for the diffusion terms , the discretised form of the one- dimensional convection diffusion transport equation with absence of sources (3.18) written as

$$\left[F_e\left(\frac{6}{8}\phi_P + \frac{3}{8}\phi_E - \frac{1}{8}\phi_W\right) - F_w\left(\frac{6}{8}\phi_W + \frac{3}{8}\phi_P - \frac{1}{8}\phi_{WW}\right)\right] = D_e(\phi_E - \phi_P) - D_w(\phi_P - \phi_W) \qquad (3.22)$$

When arranged equation (3.22) to give

$$\left[D_w - \frac{3}{8}F_w + D_e + \frac{6}{8}F_e\right]\phi_P = \left[D_w + \frac{6}{8}F_w + \frac{1}{8}F_e\right]\phi_W + \left[D_e - \frac{3}{8}F_e\right]\phi_E - \frac{1}{8}F_w\phi_{WW} \qquad (3.23)$$

The coefficients of ϕ_W and ϕ_E , in Equation (3.23) can be defined as a_W , and a_E and the coefficient of ϕ_P as a_P , hence the general form of the discretized equation can be written as

$$a_P\phi_P = a_W\phi_W + a_E\phi_E + a_{WW}\phi_{WW} \qquad (3.24)$$

With

a_W	a_E	a_{WW}	a_P
$D_w + \frac{6}{8}F_w + \frac{1}{8}F_e$	$D_e - \frac{3}{8}F_e$	$-\frac{1}{8}F_w$	$a_W + a_E + a_{WW} + (F_e - F_w)$

For F_w<0 and F_e<0 the flux across the west and east boundaries is given by the expressions

$$\phi_{w=} \frac{6}{8}\phi_P + \frac{3}{8}\phi_W - \frac{1}{8}\phi_E \qquad (3.25a)$$

$$\phi_{e=} \frac{6}{8}\phi_E + \frac{3}{8}\phi_P - \frac{1}{8}\phi_{EE} \qquad (3.25b)$$

Substitution of these two formulas for the convective terms in the discretised convection diffusion equation (3.18) together with central differencing for the diffusion terms leads, and re-arrangement as above, to the following coefficients.

a_W	a_E	a_{EE}	a_P
$D_w + \frac{3}{8}F_w$	$D_e - \frac{6}{8}F_e - \frac{1}{8}F_w$	$\frac{1}{8}F_e$	$a_W + a_E + a_{EE} + (F_e - F_w)$

The QUICK scheme for one- dimensional convection -diffusion can be summarized as follows

$$a_P\phi_P = a_W\phi_W + a_E\phi_E + a_{WW}\phi_{WW} + a_{EE}\phi_{EE} \qquad (3.26)$$

With central coefficient

$$a_P = a_W + a_E + a_{WW} + a_{EE} + (F_e - F_w) \qquad (3.27)$$

And neighbor coefficients

a_W	a_E	a_{WW}	a_{EE}
$D_w + \frac{6}{8}\alpha_w F_w + \frac{1}{8}\alpha_e F_e + \frac{3}{8}(1-\alpha_w)F_w$	$D_e - \frac{3}{8}\alpha_e F_e - \frac{6}{8}(1-\alpha_e) F_e - \frac{1}{8}(1-\alpha_w)F_w$	$-\frac{1}{8}\alpha_w F_w$	$\frac{1}{8}(1-\alpha_e)F_e$

Where

$\alpha_w = 1$ for $F_w > 0$ and $\alpha_e = 1$ for $F_e > 0$
$\alpha_w = 0$ for $F_w < 0$ and $\alpha_e = 0$ for $F_e < 0$

The QUICK differencing scheme has greater formal accuracy than the central differencing or hybrid schemes and it retains the upwind weighted characteristics. Figure (3.6) shows a comparison between upwind and QUICK for the two dimensional test, the QUICK scheme matches the exact solution much more accurately than the upwind scheme on a 50×50 grid (Versteeg and Malalasekera, 1995).

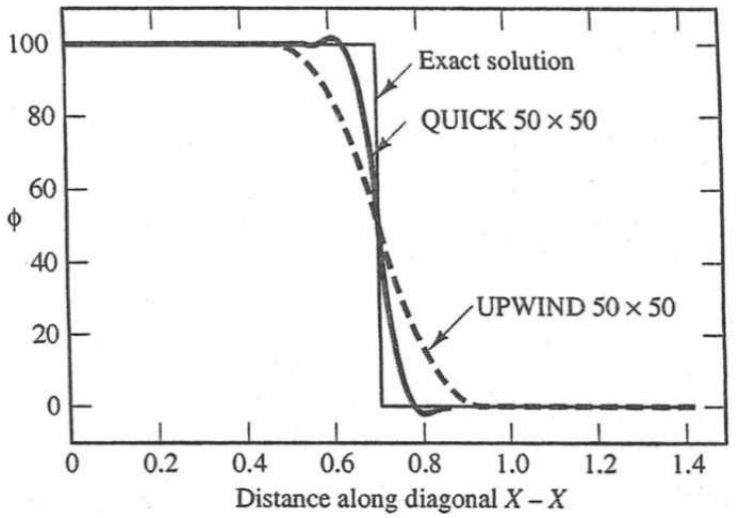

Figure 3.6 comparisons of QUICK and Upwind solutions for the 2D test

Thus, set of algebraic equations can be obtained by means of discretizing the governing equations related to the boundary conditions to obtain the ϕ distribution of the solution domain, as in Figure 3.2. The boundary side coefficient is set to zero and the flux crossing the boundary is introduced such a source term which is appended to any existing S_u and S_P terms. This process results a system of linear algebraic equations which needs to be solved. The complexity and size of the set of equations depends on the dimensionality of the problem, the number of grid nodes and the discretization practice (Versteeg and Malalasekera, 1995).

To solve the algebraic equations, there exist several computer algorithms which are divided into two main groups of solution techniques;

- *Direct methods* (requiring no iteration)
- *Indirect methods* (or iterative methods).

For linear problems, which require the solution of algebraic equations only once, that arise N equations with N unknowns, direct methods may be appropriate. Besides, for two- or three- dimensional problems, solving the algebraic equations becomes more complicated and requires rather large amounts of computer memory and time. Common used examples of direct methods are *Cramer's rule matrix inversion* and *Gaussian elimination*. (Patankar 1980; Versteeg and Malalasekera, 1995)

On the other hand, iterative methods are based on the repeated application of a relatively simple algorithm leading to eventual convergence after a –sometimes large– number of repetitions. Well–known examples are the *Jacobi* and *Gauss–Seidel* iterative methods. In simple computer programs, this method can be useful; however, they can be slow to converge when the system of equations is large. Thomas (1949) developed a technique for rapidly solving tri-diagonal systems that is called Thomas algorithm or *Tri-Diagonal Matrix Algorithm* (TDMA). In addition to this, there are several methods that have been developed recently, such as, *Strongly Implicit procedure* (SIP) by Stone (1968), *Conjugate Gradient Method* (CGM) by Hestenes and Steifel (1952), and *Strongly Implicit Solver* (SIS) by Lee (1989).

CHAPTER FOUR
CFD SIMULATION AND VALIDATION WITH EXPERIMENTAL DATA

Experimental investigation is a time-consuming and expensive process, while numerical modeling is relatively fast and inexpensive. However, numerical modeling usually requires experimental validation in order to be considered a viable alternative to measurements. Therefore, comparison between experimental result (Herchang Ay, JiinYuh Jang, and Jer-Nan Yeh, 2002) and numerical result for the temperature distribution and averaged convective heat transfer coefficients over a plate-fin surface are performed. In experimental study used an infrared thermovision to monitor temperature distribution over a plate-fin surface inside the plate finned-tube heat exchangers .In addition, the local convection heat transfer coefficients over the fin are determined by means of a control volume based finite difference formulation after the temperature value identified over the tested surface. Computational Fluid Dynamics (CFD) software, Fluent is used in numerical study for model the same experiment. Numerical and experimental data are compared to understand the discrepancies between them.

4.1 Experimental Equipment and Procedure

4.1.1 Experimental Apparatus

The experimental setup, as schematically illustrated in Figure 4.1, used to investigate the local heat transfer performance of a plate consisted of a three-row plate-fin and tube heat exchanger situated in a subsonic blowdown open-circuit wind tunnel. The wind tunnel consisted of an axial flow, diffusers, a settling chamber, construction sections, test section, and provides an approach velocity that is flat to within one percent, with a turbulent intensity less than one percent. The airflow is driving by the 5.6 kW (7.5 h.p.) axial flow fan with an inverter to adjust the output power. Eight type-K thermocouples are mounted at the corners of the center test core; four each on the inlet and outlet section of the tested model. The data signals are individually recorded and then averaged.

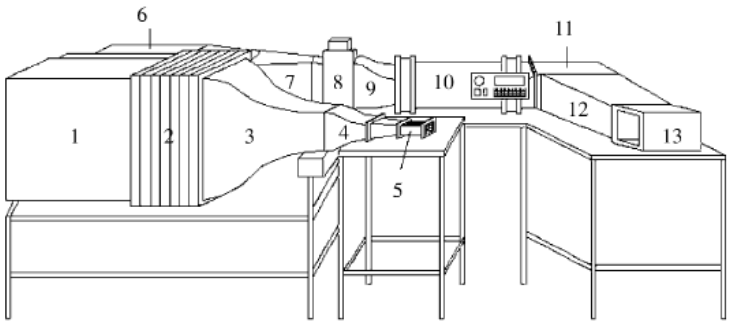

1: corner
2: settling chamber
3: contraction section (contraction area ratio:10.17:1)
4. contraction section
5: test section
6: corner
7: diffuser
8: heater, removable rack
9: C/R transition section
10: fan, power section
11: corner
12: diffuser
13: corner

Figure 4.1 Schematic diagram of the experimental setup.

4.1.2 Test Model

The test section, shown schematically in Figure 4.2(a), is constructed of stainless steel for large scale testing of a bank of tubes shared continuous plate-fins. Figure 4.2(b) and (c) are the description of coordinate systems and nomenclature for the tested fins. Their detailed geometrical parameters are tabulated in Table 4.1. Each tube is locally heated by means of joulean dissipation in a wire inserted in the central region of a cylinder installed in the tube. In order to measure the temperature distribution on the surface of plate-fin inside test core by an infrared camera, a transparent sheet, Figure 4.2(a), replaces the top plate-fin of the test core. A portion of the thermal electromagnetic radiation emitted by the test fin will absorb and reflect on the transparent sheet.

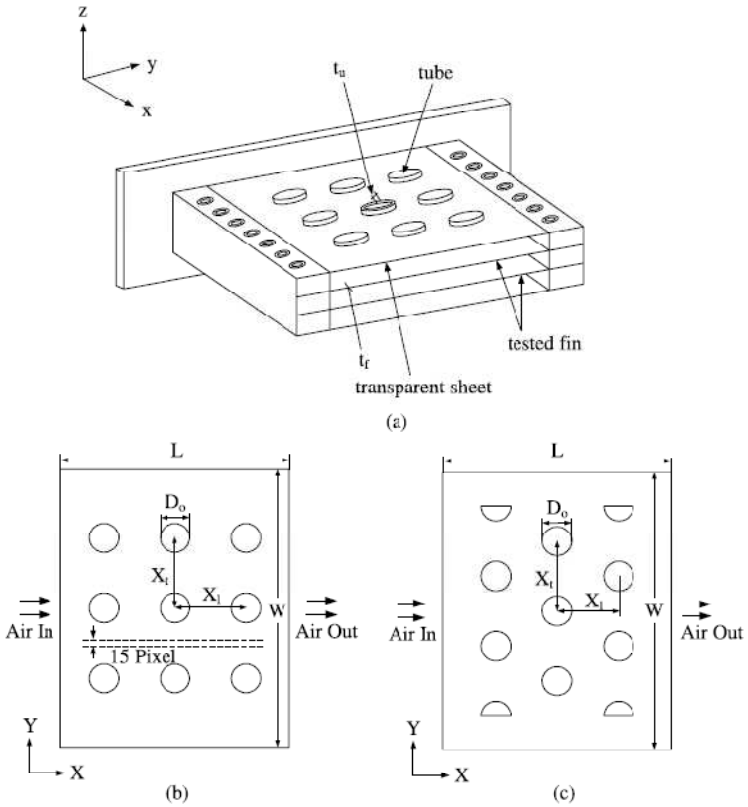

Figure 4.2 the experimental test models: (a) schematic of the wind tunnel test section, and sketch illustrating nomenclature for (b) in-line tube arrangements, and (c) staggered tube arrangements.

Table 4.1 Geometrical data

Test section	**Tube arrangement**	
	(In-line)	**(staggered)**
Width of the test section (W)	240 mm	240 mm
Length of the test section (L)	196 mm	196 mm
Fin spacing (H)	20 mm	20 mm
Outside diameter of the tube (D_o)	25.4 mm	25.4 mm
Row number	3	3
Tube number (N)	9	9
Transverse pitch (X_t)	60.7 mm	60.7 mm
Longitudinal pitch (X_l)	60.7 mm	52.6 mm
Thickness of the fin (t_f)or(δ)	0.5 mm	0.5 mm
Thickness of the tube (t_u)	2 mm	2 mm
Reynolds numbers ($\mathrm{Re} = UH/\nu$)	543 - 1096	543 - 1096

The experimental apparatus for infrared temperature measurements used in AGEMA Themovision 550 (THV550). The sensing system of THV550 is a focal plane array (FPA) detector made of a matrix with 320 (H) × 240 (V) PtSi elements. The electromagnetic energy radiated in the infrared spectral band by an object will convert into an electronic signal from all the sensors and acquire simultaneously in the whole field of view.

4.1.3 Experimental Procedure

For testing, the fan was started. The frontal air velocity, U, was measured by a hot wire with ± 2.0% accuracy. Nine power supplies were turned on and adjusted to bring the outside wall temperature of nine tubes to 60 ^{o}C, respectively. When steady state values had been established, the temperature map of the plate-fin surface was recorded. The imaging size of the map was a plane matrix array with 220 pixels × 220 pixels for in-lined and 194 pixels × 246 pixels for staggered arrangements. Following the temperature value identified at each pixel by the infrared thermovision system, the local convective heat transfer coefficients over the fin were determined by means of a control volume based finite difference formulation. For steady conduction we consider the energy-balance equation for a small control volume illustrated in Figure 4.3, stated as

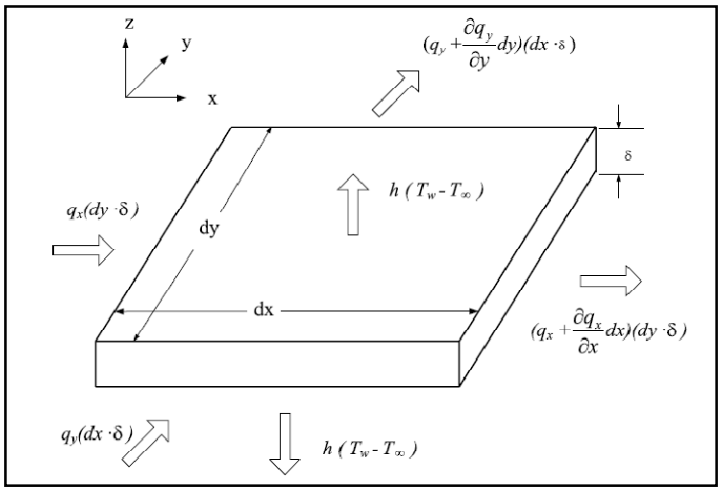

Figure 4.3 Differential control volume for three-dimensional conduction with heat dissipation by convection in rectangular coordinates.

$$2h(T_w - T_\infty)dxdy = -\frac{\delta q_x}{\delta x}dxdy\delta - \frac{\delta q_y}{\delta x}dxdy\delta \qquad (4.1)$$

Where δ is the thickness of the fin and T_∞ is the bulk mean temperature of the stream. A uniform temperature on the plate along the z-direction is assumed in Equation (4.1) due to the Biot number based on δ estimated about 10^{-3}. In terms of Fourier's law,

$$q_x = -k\frac{\delta T}{\delta x}, \qquad q_y = -k\frac{\delta T}{\delta y} \qquad (4.2)$$

The substitution of Equation (4.2) into Equation (4.1) yields

$$h = \frac{k\delta}{2(T_w - T_\infty)}\left(\frac{\delta^2 T}{\delta x^2} + \frac{\delta^2 T}{\delta y^2}\right) \qquad (4.3)$$

The control volume approach was used to discretize the derivatives in Equation (4.3) given by

$$h = \frac{k\delta}{2(T_w - T_\infty)}\left(\frac{T_{x+1,y} - 2T_{x,y} + T_{x-1,y}}{\Delta x^2} + \frac{T_{x,y+1} - 2T_{x,y} + T_{x,y-1}}{\Delta y^2}\right) \qquad (4.4)$$

If we assume a square mesh $\Delta x = \Delta y = \ell$ Equation (4.4) simplifies to

$$h = \frac{k\delta}{2(T_w - T_\infty)}\left(\frac{T_{x+1,y} + T_{x-1,y} + T_{x,y+1} + T_{x,y-1} - 4T_{x,y}}{\ell^2}\right) \qquad (4.5)$$

Here, ℓ is the length of the imaging element (pixel) estimated as 0.77 mm in the thermograms. Using Equation (4.5), a conservatively, and estimated uncertainty of ±7.0% for the buck mean temperature of fluid, T_∞, and the uncertainty estimation method of (Kline and McClintock,1953), the maximum uncertainty of the calculated

the local convective heat transfer coefficient is ±7.5%. The averaged heat transfer coefficient, $\overline{h}$, then can be obtained by

$$\overline{h} = \frac{1}{A}\int_A h dA \qquad (4.6)$$

Where dA is the control surface element of the fin and defined as $dx * dy$ in Figure 4.3. The uncertainty in the averaged heat transfer coefficient is ±7.6% estimated by the similar method (S.J. Kline and F.A. McClintock, 1953). Note that the highest uncertainties are associated with lower Reynolds number.

4.2 Numerical Analysis

In order to compare with experimental study performed by (Herchang Ay, JiinYuh Jang, and Jer-Nan Yeh, 2002), the temperature distribution and convective heat transfer coefficients over a plate-fin surface inside the plate finned-tube heat exchangers is determined by computational fluid dynamics (CFD) software, FLUENT. The model geometry is described in detail in Figure 4.2 and in Table 4.1. The creating and meshing of the model and boundary conditions given to this meshed model is performed by GAMBIT program. Mesh refinement is investigated and explained clearly in Chapter 5. Vertexes, edges, faces, and volumes are created and meshed, respectively (Figure 4.4) and (Figure 4.5)

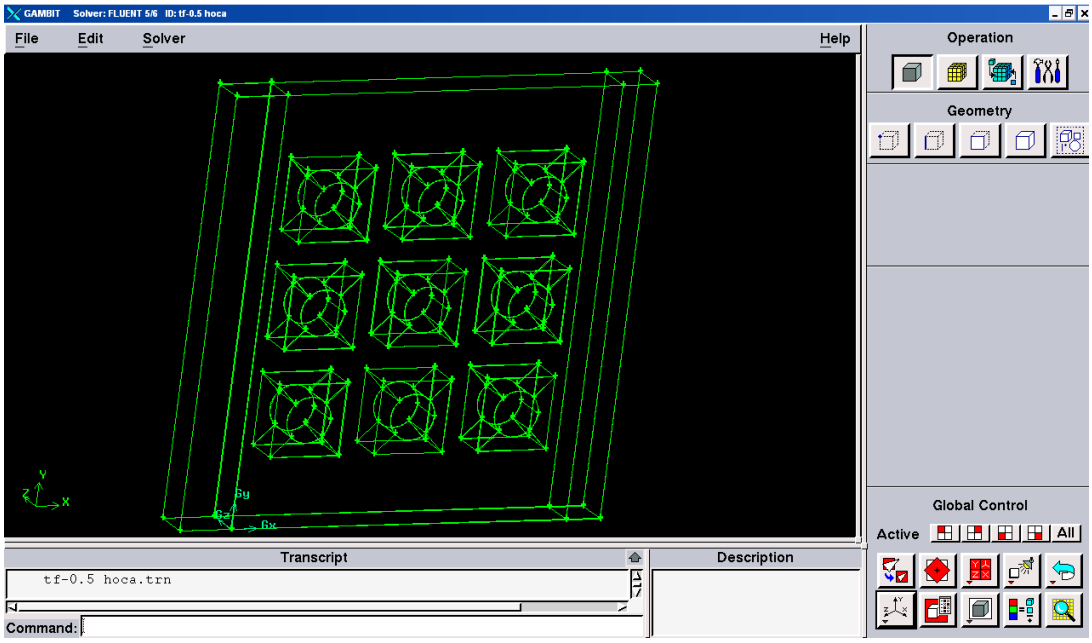

Figure 4.4 Model geometry

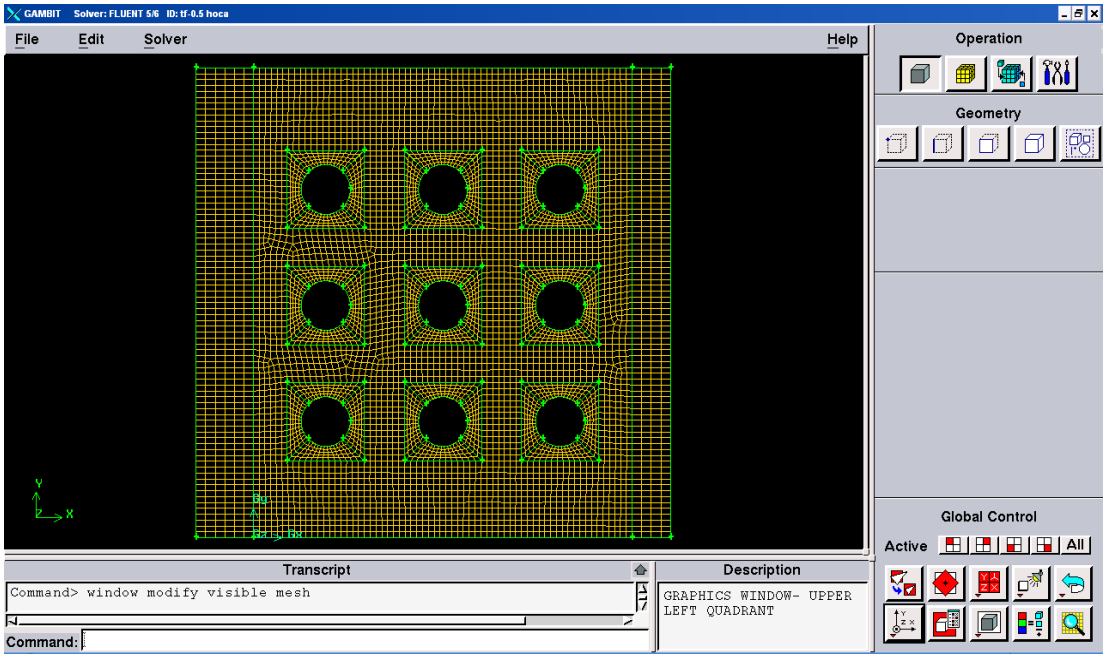

Figure 4.5 Volume mesh

Mass inlet boundary condition is defined for left surface, since air enters from that cross section. The air exits from the right side of the model. So, the outflow boundary condition is given to this surface. Wall boundary conditions are given to the top and bottom surfaces of the model as isothermal ($\left.\frac{\partial T}{\partial y}\right|_{y=0} = 0, \left.\frac{\partial T}{\partial y}\right|_{y=W} = 0$).

Also, wall boundary conditions are given to the side, front and back surfaces of the model, since convection heat transfer occurs from these surfaces. Tube inner surfaces are defined as wall (constant temperature 60 ^{o}C). Solid and fluid volumes must be defined in order to obtain proper heat transfer results, shown in Figure 4.6.

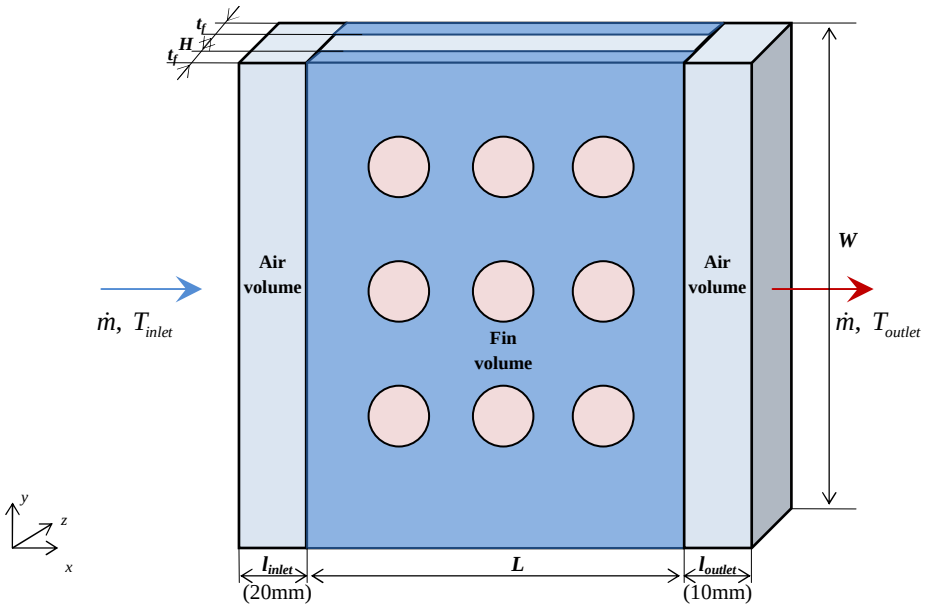

Top	Bottom
$x = 0 \rightarrow L + l_{inlet} + l_{outlet}$, $y = W$, $z = 0 \rightarrow H + 2t_f$: $\frac{\partial T}{\partial y} = 0$	$x = 0 \rightarrow L + l_{inlet} + l_{outlet}$, $y = 0$, $z = 0 \rightarrow H + 2t_f$: $\frac{\partial T}{\partial y} = 0$

Front	Back
$x = 0 \rightarrow L + l_{inlet} + l_{outlet}$, $y = 0 \rightarrow W$, $z = 0$: $\frac{\partial T}{\partial z} = h(T - T_\infty)$	$x = 0 \rightarrow L + l_{inlet} + l_{outlet}$, $y = 0 \rightarrow W$, $z = H + 2t_f$: $\frac{\partial T}{\partial z} = h(T - T_\infty)$

Figure 4.6 Boundary condition surfaces

3D version of the Fluent is selected in order to analyze heat transfer. The flow is assumed to be steady, incompressible and laminar flow because of the low Reynolds number of the flow. Steel is selected for fin, and tube. Air is selected as fluid. Inlet air temperature is 298 K.

Mass flow rate is 5.68×10^{-3} m/sec for U=1 m/s and H=20 mm, for other frontal velocity U, mass flow rate changes while the other conditions remain the same. After solution total heat transfer rate is calculated from flux reports and calculated temperature from surface integrals reports.

Some of the results are calculated manually using the FLUENT results and theoretical equations:

Logarithmic Mean Temperature Difference (LMTD) method is used in this study. Air-side heat transfer coefficient is calculated from Equation (4.7) (Incropera, 2002),

$$\bar{h} = \left(\frac{Q}{\Delta T_{lm} * A_{total}} \right) \qquad (4.7)$$

$\bar{h}$: The averaged convective heat transfer coefficient (W/m^2k)

Q : Heat transfer capacity (W), taken from the Fluent results

ΔT_{lm} : log-mean temperature difference

A_{total} : Total air-side surface heat transfer area (m^2)

Log-mean temperature difference is calculated from Equation (4.8) (Incropera, 2002),

$$\Delta T_m = \left[\frac{(T_s - T_i) - (T_s - T_o)}{Ln\left(\frac{T_s - T_i}{T_s - T_o} \right)} \right] \qquad (4.8)$$

T_S : air-side surface temperature

T_i : Air inlet temperature (25 ^oC)

T_o : Air outlet temperature, taken from the Fluent results

Air-side surface temperature is calculated from Equation (4.9) (Incropera, 2002),

$$T_s = \frac{T_f * A_f + T_u * A_u}{A_{total}} \quad (4.9)$$

T_f : Air side fin surface temperature taken, from the Fluent results

T_u : tube surface temperature (60 ^oC)

A_f : the surface area of the fin (mm^2)

A_u : the surface area of the tube (mm^2)

The surface area of the fin and tube are calculated from Equation (4.10), (4.11), (4.12) and (4.13) (Incropera, 2002),

$$A_{f\,(in-line)} = 2(W * L - N(\frac{\pi * D_o^2}{4})) \quad (4.10)$$

$$A_{f\,(staggered)} = 2(W * L - (N-2)(\frac{\pi * D_o^2}{4}) - 4(\frac{\pi * D_o^2}{8})) \quad (4.11)$$

$$A_{u(in-line)} = N * \pi * D_o * H \quad (4.12)$$

$$A_{u(staggered)} = (N-2) * \pi * D_o * H + 4 * ((\frac{\pi * D_o}{2}) + D_o * H) \quad (4.13)$$

W : Width of the test section (240 mm)

L : Length of the test section (196 mm)

N : Number of tube (9)

D_o : Outside diameter of the tube (mm)

H : Fin spacing (mm)

Total air-side heat transfer area is are calculated from Equation (4.14) (Incropera, 2002),

$$A_{total} = A_f + A_u \quad (4.14)$$

4.3 Results and Discussion

The temperature distribution on the plate-fin surface for fin spacing H=10 mm and frontal velocity U =1.0 m/s inside the plate finned-tube heat exchangers is present experimentally and numerically, in Figures 4.7 and 4.8, respectively. A 20-step color palette for thermograms (≈1.1 ^{o}C per step) map is used in Figure 4.7.

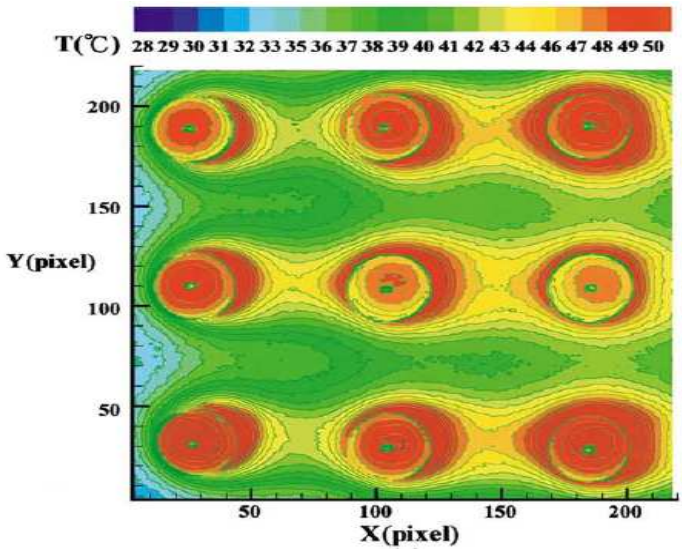

Figure 4.7 experimentally temperature distribution on the plate-fin surface for H=10 mm, and U =1.0 m/s.

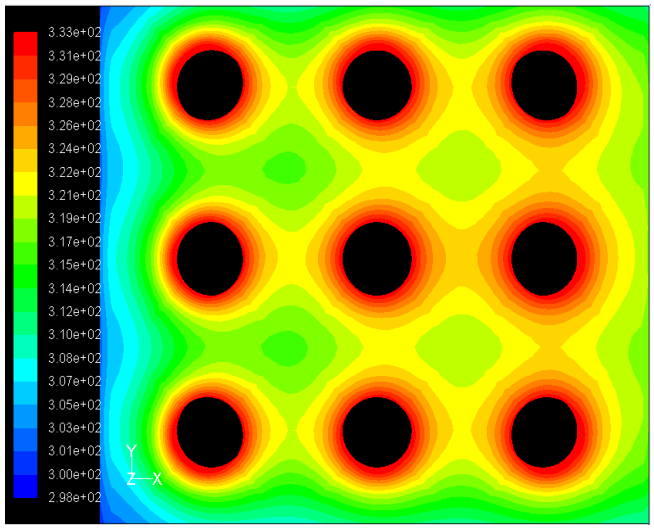

Figure 4.8 numerically temperature distribution on the plate-fin surface for H=10 mm, and U =1.0 m/s.

At the leading edge of the plate-fin, the results indicate lower temperature, as shown in Figures 4.7 and 4.8, because the velocity boundary layer is initially developed in the z-direction. The temperature gradient on the fin surface is sharper near the front and sides of the first two row tubes due to the repeated growth and destruction of the boundary layer by tubes. However, at the rear of the tube, the temperature gradient is gentler because the airflow is swept downstream into the wake. A different characteristic occurs after the third row due to an additional exit effect.

To investigate the accuracy of the numerical models in the plate finned-tube heat exchangers, A comparison between experimental and numerical result of the averaged convective heat transfer coefficients ($\bar{h}$) on a fin at various Reynolds numbers ranging from 543 to 1096, under U = 1 m/s and H =20 mm are presented.

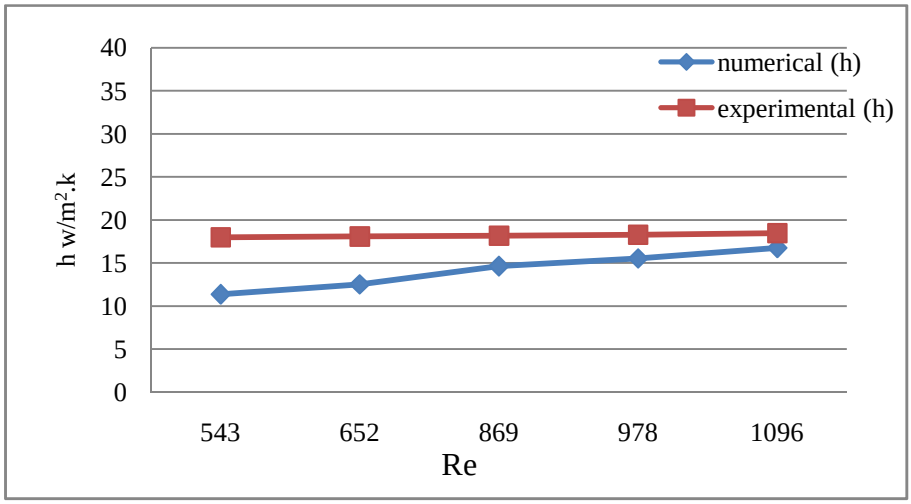

Figure 4.9 A comparison of the averaged convective heat transfer coefficients ($\bar{h}$) on a fin at various Reynolds numbers ranging under U = 1 m/s and H =20 mm for in-line array

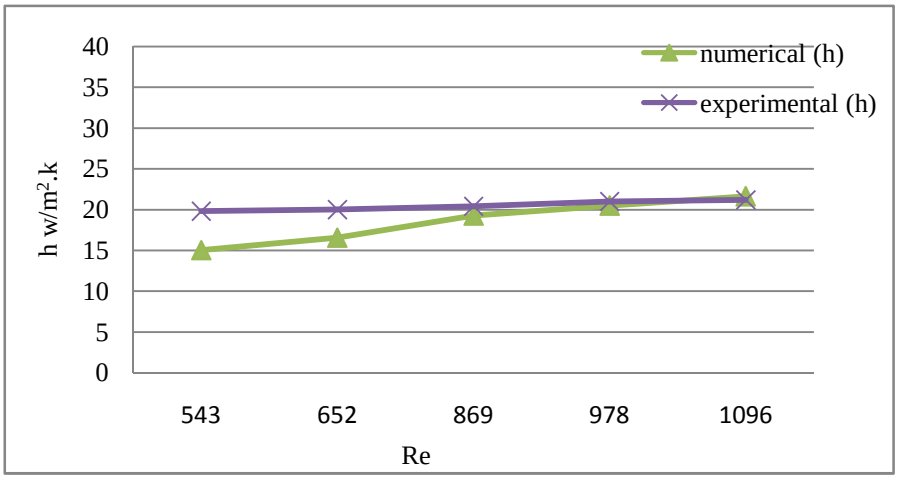

Figure 4.10 A comparison of the averaged convective heat transfer coefficients ($\bar{h}$) on a fin at various Reynolds numbers ranging under U = 1 m/s and H =20 mm for staggered array

The results of the comparison are shown in Figures 4.9 and 4.10, show that the comparison between them gives error about 14% for in-line array and 2% for staggered array because of few information about properties of metal and detail of geometrical parameter are used in experimental test. Therefore, the numerical model, a reasonably good agreement is obtained in comparison with the experimental models for the temperature distribution and the averaged convective heat transfer coefficients on the plate-fin surface inside the plate finned-tube heat exchangers.

CHAPTER FIVE

NUMERICAL STUDY

In this study, a plate fin type heat exchanger with one row tube configuration is analyzed for different geometrical parameters by using a numerical computation technique. Numerical optimization of a finned tube gas to liquid heat exchanger will be realized. In order to find the optimum geometrical dimensions, several fin geometries investigated. The main purpose is to enhance heat transfer rate from the flue gas, which is the combustion products, to water which flows through the tube of the heat exchanger. The other significant point is to minimum flue gas pressure drop while flue gas passing through the gap between fins. The effects of the distance between two fins, tube center location, fin height, tube thickness, and tube ellipticity on heat transfer and pressure drop across the heat exchanger are investigated for 10 different models, numerically. Figure 5.1 shows a typical plate fin and tube heat exchanger of a heater used in the analyses.

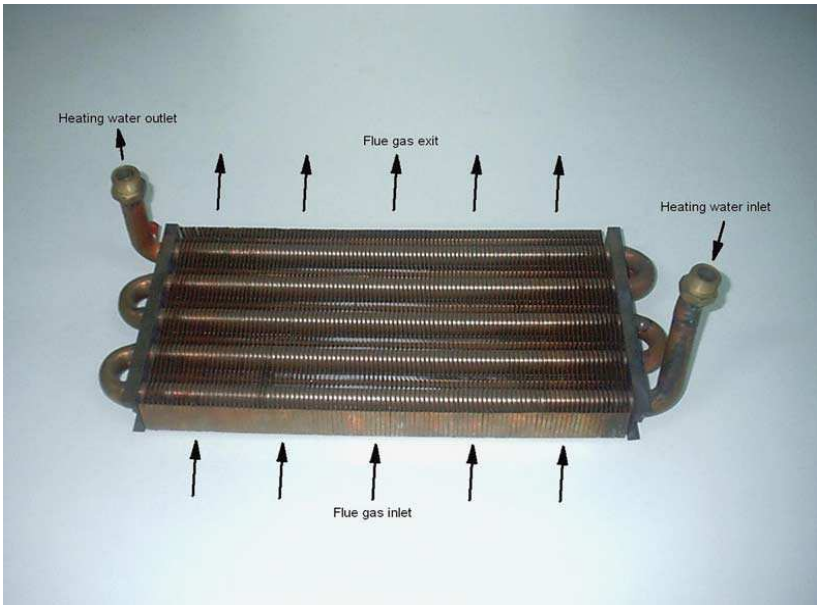

Figure.5.1 View of an analyzed plate fin and tube heat exchanger.

Computational Fluid Dynamics (CFD) software (FLUENT), will be used to evaluate different fins. FLUENT is a computer program written in the C computer language for modeling fluid flow and heat transfer in complex geometries.

5.3 Model Description

5.1.1 Geometry

The studied model consists of two fins with half fin thickness, fin tube, tube cover, and flue gas between the fins. Due to the symmetry, only one-tenth segment of the fin is modeled Symmetrical conditions and geometrical view of the model is shown in Figure 5.2, Figure 5.3 shows the dimensions taken into consideration as geometrical parameters. The model is created and meshed by using GAMBIT software, which is the modeling program used with “Fluent” software.

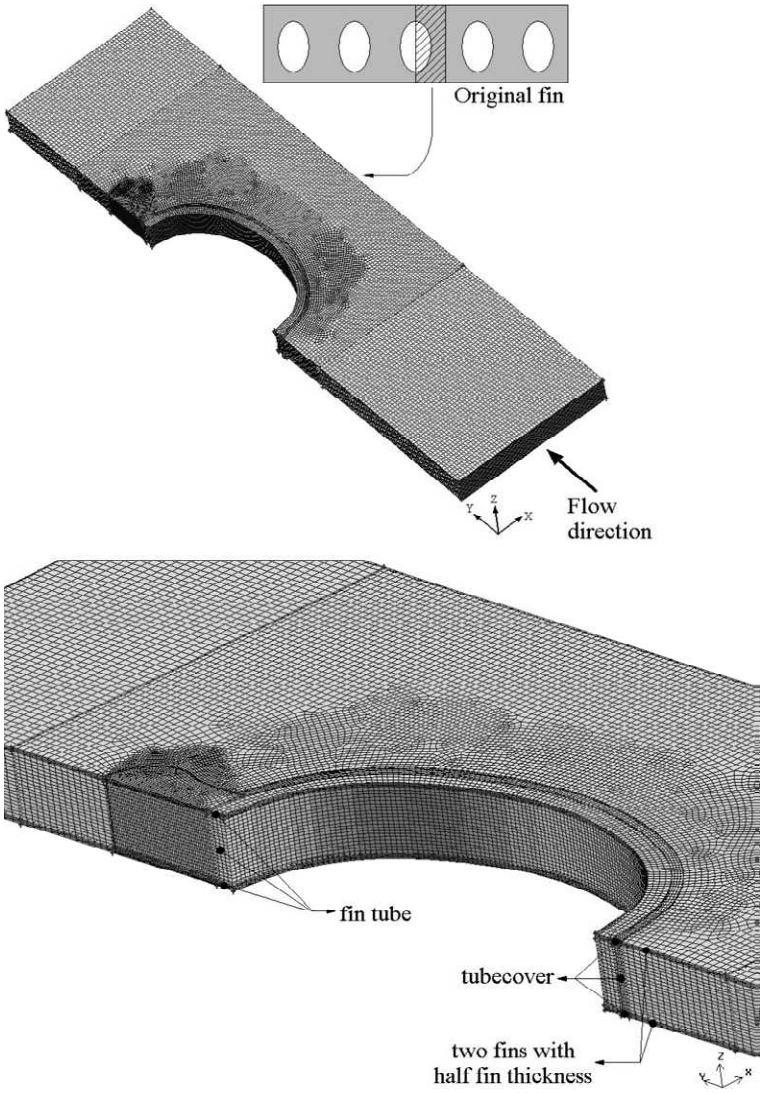

Figure 5.2 Original fin and the segment used in the modeling.

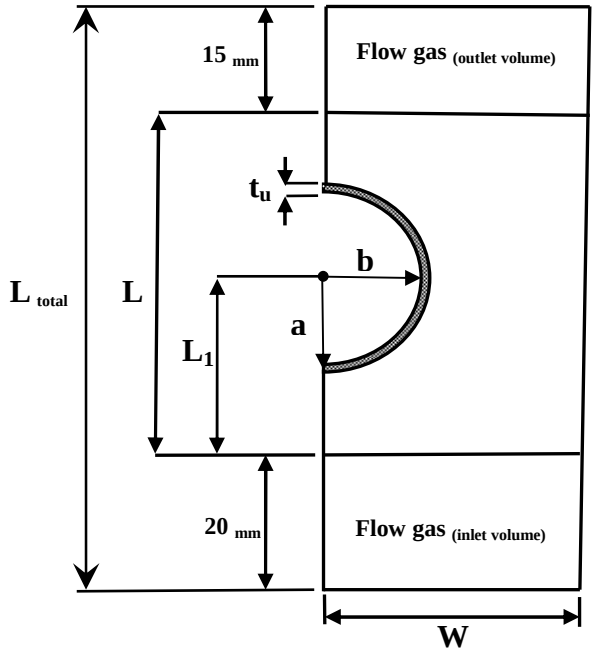

Figure 5.3 Schematic view of fin dimensions.

Dimensions of the models, which are taken from commercially available products, are given in Table 5.1. Distance between the fins is 2.6 mm, except for the Model (b) which has a 2.7 mm gap. The width of the fin is 17.5 mm. Creating geometry is the first step of the modeling. Vertexes, edges, faces, and volumes are created, respectively (Figure 5.4).

Table 5.1 Dimensions of the models

Model type	**L (mm)**	**L1 (mm)**	**t_u (mm)**	**t_f (mm)**	**D_o**		**Ellipticity b/a**
					a(mm)	**b(mm)**	
A	35	15.5	0.8	0.4	9.2	6.7574	0.7345
B	35	15.5	0.8	0.3	9.2	6.7574	0.7345
C	35	18.5	0.8	0.4	9.2	6.7574	0.7345
d	35	12.5	0.8	0.4	9.2	6.7574	0.7345
E	38	18.5	0.8	0.4	9.2	6.7574	0.7345
F	38	15.5	0.8	0.4	9.2	6.7574	0.7345
G	35	15.5	0.6	0.4	9.2	6.7574	0.7345
H	35	15.5	1.2	0.4	9.2	6.7574	0.7345
I	35	18.5	0.8	0.4	9.2	3.7388	0.4064
j	35	15.1	0.8	0.4	9.2	9.2	1

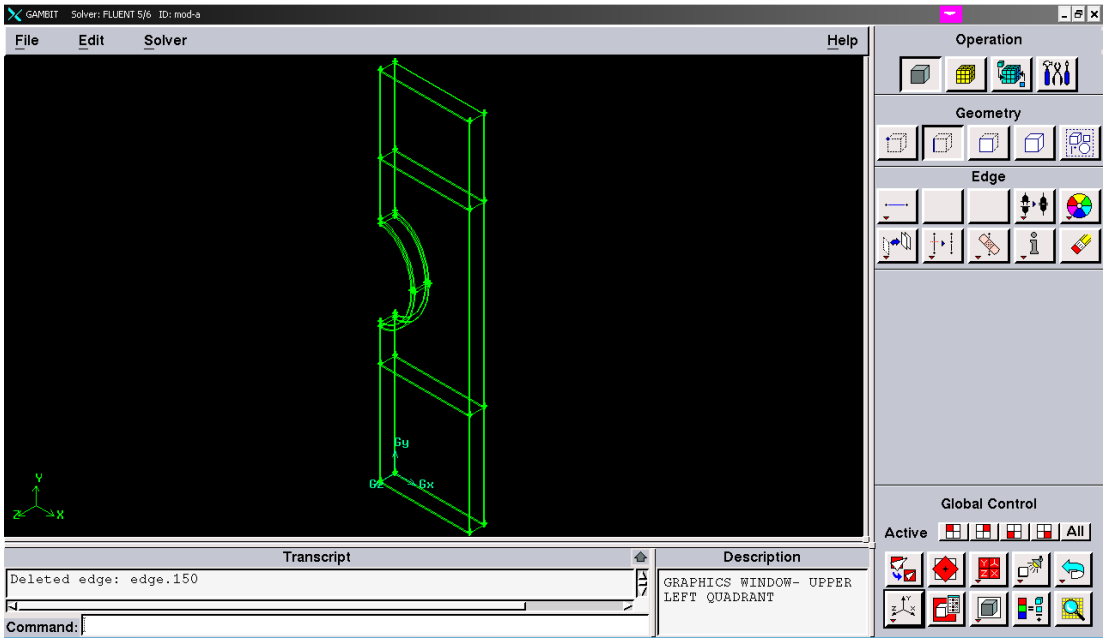

Figure 5.4 Model geometry

The volume representing the flue gas which is passing through the gap between two fins is extended in y directions at both inlet and exit sides, since this configuration enables more accurate boundary condition application.

5.1.2 Mesh

Meshing the geometry is the second step of the modeling. Edges, faces, and volumes are meshed, respectively. Tube thickness is meshed for interval size of 0.2. Tube side face and Fin side face are meshed for interval size of 0.2. Computational faces are meshed for interval size of 1 (Figure 5.5). Four hexahedral finite volume elements along the thickness of the half fin and twenty of the same elements along the distance between two fins are used (Figure 5.6).

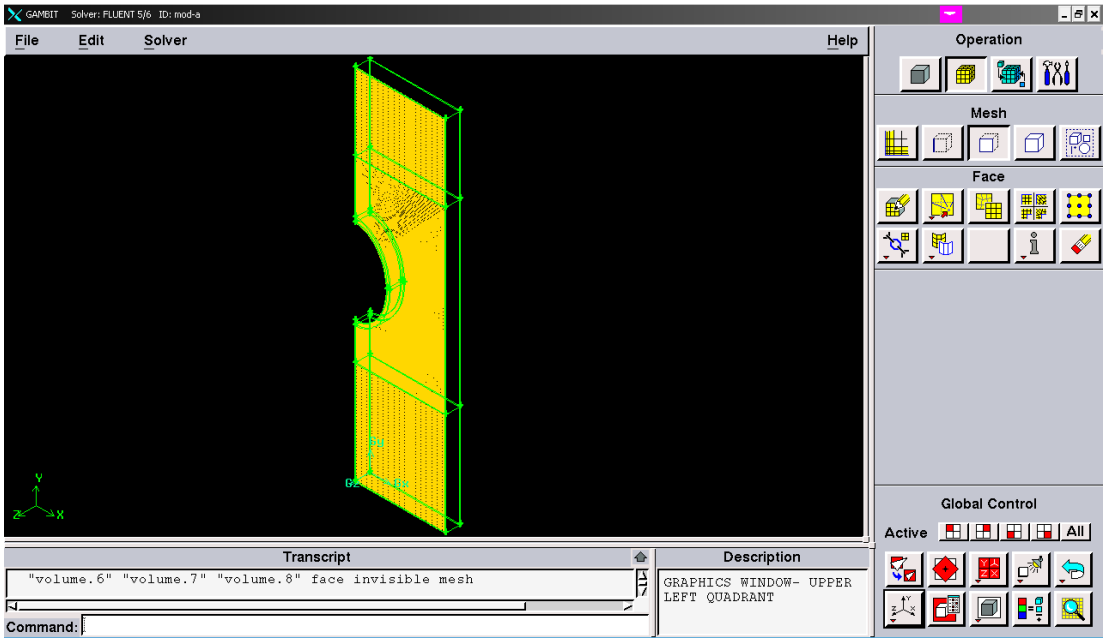

Figure 5.5 Face mesh

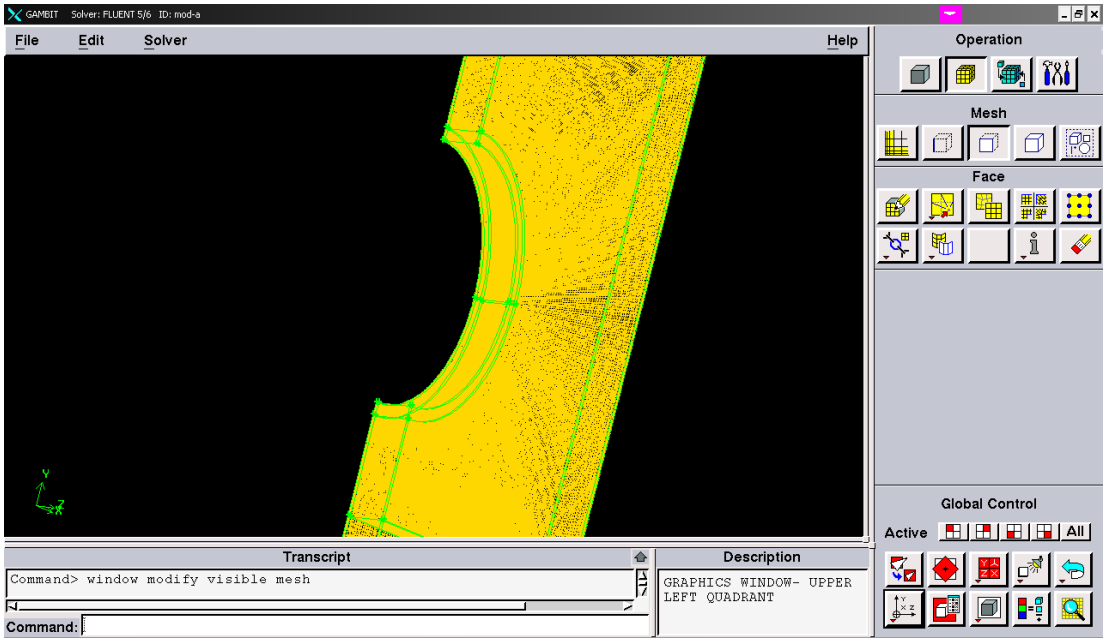

Figure 5.6 volume mesh

Then, the created model in GAMBIT software is exported to the FLUENT software in which boundary conditions and material properties are defined.

5.1.2.1 Mesh Refinement

Mesh refinement has significant effect on accuracy of results in numerical studies. Therefore, the effect of mesh size on heat transfer for model (A) taken as an example to explain this effect. Number of mesh ranging from 48,150 to 1,051,680 cell, shown in Figure (5.7).

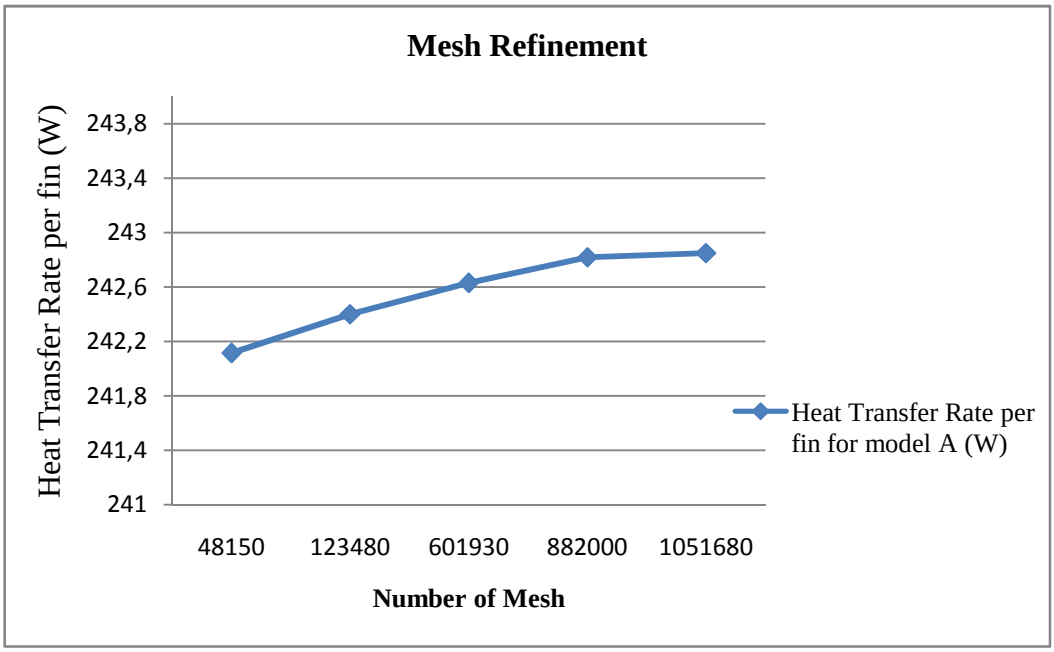

Figure 5.7 Mesh Refinement for model (A)

Figure 5.7, shows the effect of number of mesh on heat transfer rate for model (A). From the result, it can be seen that the heat transfer rate has no significant change after 882000 mesh number, therefore, about 882000 meshes taken in all models.

5.2 Governing Equations

The following assumptions have been taken; steady-state, Newtonian fluid, incompressible flow, no internal heat generation, laminar flow and negligible radiation. In the conservative form, the balance equations for continuity, momentum, energy become (Versteeg and Malalasekera, 1995).

Continuity equation $$\frac{\partial u}{\partial x}+\frac{\partial v}{\partial y}+\frac{\partial w}{\partial z}=0$$

x-momentum equation

$$\rho\left[\, div(u\vec{v})\right]=div\left(\mu\ grand(u)\right)-\frac{\partial p}{\partial x}$$

y-momentum equation

$$\rho\left[\, div(v\vec{v})\right]=div\left(\mu\ grand(v)\right)-\frac{\partial p}{\partial y}$$

z-momentum equation

$$\rho\left[\, div(w\vec{v})\right]=div\left(\mu\ grand(w)\right)-\frac{\partial p}{\partial z}$$

Energy equation

$$\rho c_p\left(u\frac{\partial T}{\partial x}+v\frac{\partial T}{\partial y}+w\frac{\partial T}{\partial z}\right)=\frac{\partial}{\partial x}\left(k\frac{\partial T}{\partial x}\right)+\frac{\partial}{\partial y}\left(k\frac{\partial T}{\partial y}\right)+\frac{\partial}{\partial z}\left(k\frac{\partial T}{\partial z}\right)$$

In this study, the governing equations have been integrated by using Fluent program which makes use of the Finite Volume Method. The continuity, momentum, and energy equations have been discretized by using the Quick Scheme. The SIMPLE model was employed in the pressure-velocity coupling, in which the pressure profile is calculated via the continuity conservation equation. The convergence criterion for all balance equations was set at 10^{-4} RMS, the exception being the energy equation for which the convergence criterion was set at 10^{-8} RMS.

5.3 Boundary Conditions

Boundary conditions are given to the meshed model. Mass flow inlet boundary condition is defined for bottom surface, which is illustrated as red surface in Figure 5.8, since flue gas enters from that cross section. The flue gas is exhausted from the top side of the heat exchanger. So, the outflow boundary condition is given to this surface, shown in Figure 5.8. Symmetrical boundary conditions have been applied to the side, front and back surfaces of the model, shown as yellow surfaces in Figure 5.8, due to the symmetry. Tube inner surface is defined as wall, since convection

heat transfer occurs from this surface, shown as white surface in Figure 5.8. Solid and fluid volumes must be defined in order to obtain proper heat transfer results.

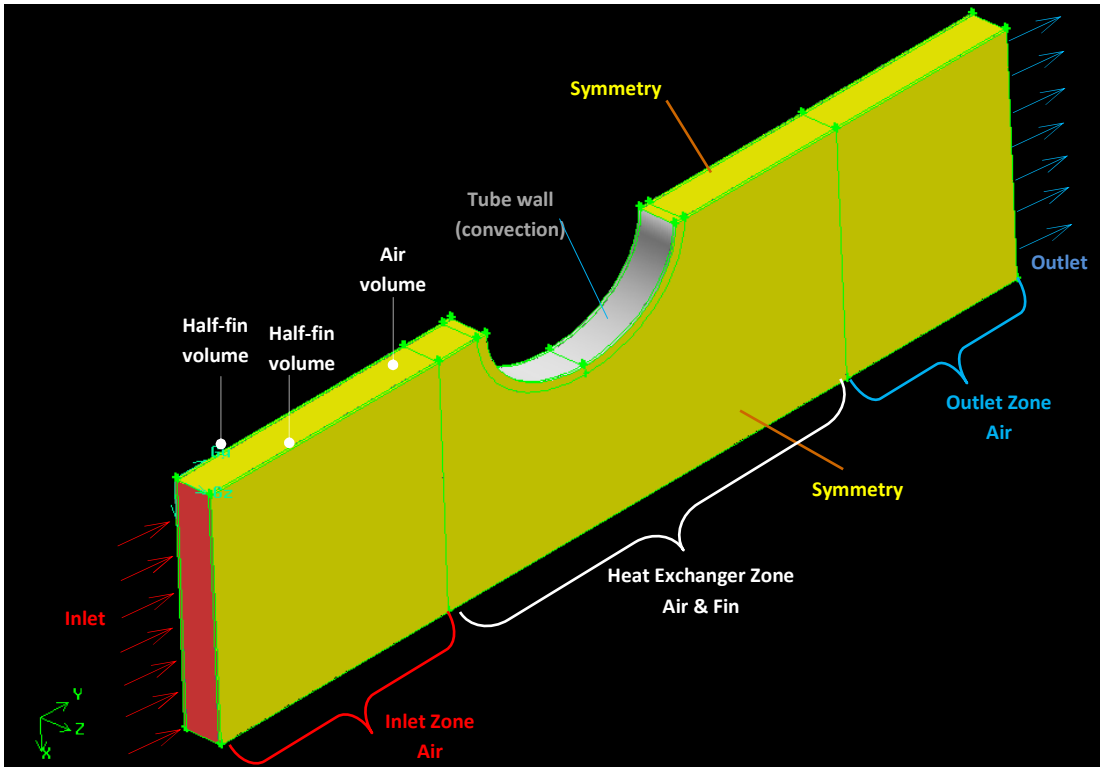

Figure 5.8 Boundary condition surfaces

5.4 Thermal Analysis

3D version of the Fluent is selected in order to analyze heat transfer and pressure drop. The flow is assumed to be laminar because of the low Reynolds number of the flow. The Reynolds number is calculated from Equation (5.1), (Kakaç, 1998).

$$\mathrm{Re} = \frac{GD_h}{\mu} \tag{5.1}$$

where

$$G = \rho U_{\max} = \frac{\dot{m}}{A_{\min}} \tag{5.2}$$

$$\mathrm{D}_h = 4\frac{LA_{\min}}{A} \tag{5.3}$$

G_{max} : Mass velocity in minimum area (kg/m²s)

D_h :Hydraulic diameter (m)

ρ : Air density (kg/m^3)

μ : Air dynamic viscosity(kg/m.s)

U_{max} : Air velocity in minimum flow area (m/s)

A_{min} : Minimum flow cross sectional area (m²)

The material of fin and tube is assumed to be copper. The physical properties of copper are taken as constant. Whereas the flue gas properties are taken as a function of temperature. The values used for the simulations are given below, this values taken from (Erek, 2005).

- Flue gas

$$k = 6.409*10^{-5}*T + 5.774*10^{-3}$$

$$\mu = -6.534*10^{-12}*T^2 + 4.267*10^{-8}5.054*10^{-6}$$

$$c_p = -3.97*10^{-5}*T^2 + 2.932*10^{-1}*T + +977.7$$

- Copper

$$k = 387.6\left(W / m.K\right)$$

$$\rho = 8978\left(kg / m^3\right)$$

$$c_p = 381\left(j / kg.K\right)$$

Boundary conditions; The mass flow rate used in all of the models is $1.904x10^{-5}$ kg/s. Temperature value of the flue gas at the inlet is 1500 K. These values are taken from the application results. The convection coefficients between the water flowing inside the tubes and the inner wall are calculated by using the Gnielinski correlation shown in equation (5.4) for fully developed turbulent forced convection through a duct (S. Kakac and Y. Yener, 1995).

$$Nu = \frac{\left(f/2\right)(\mathrm{Re}-1000)\,\mathrm{Pr}}{1+12.7\left(f/2\right)^{1/2}\left(\mathrm{Pr}^{2/3}-1\right)} \tag{5.4}$$

where, $f = (1.58\ln \mathrm{Re} - 3.28)^{-2}$

Free stream temperature is defined as boundary condition for the inner wall of fin tube. The middle section of fin is taken into consideration and free stream temperature is assumed as 343 K.

After solution is converged, temperature and pressure contours, velocity vectors can be displayed for visual consideration of the results. Total heat transfer rate is calculated from flux reports. Pressure drop is calculated from surface integrals.

5.5 Results and Discussion

Fluent software is run for each model after determining boundary conditions and material properties. The heat transferred from the flue gas passing through the gap between fins to the water flowing through the fin tube, the static and total pressure drop values of flue gas across the heat exchanger are also, obtained from the solution of the models and tabulated in Table 5.2 and show in Figures 5.9 and 5.10. Since the transferred heat is corresponding to one-tenth segment of the fin, actual heat transfer from one fin, also, is indicated as heat transfer per fin.

Table 5.2 Comparison of the models

Model type	Q (per segment) (W)	Q (per fin) (W)	Normalized Q (%)	Static pressure drop (Pa)	Normalized static pressure drop (%)	Total pressure drop (Pa)	Normalized total pressure drop (%)
A	24.2824	242.824	100	2.2545	100	1.937	100
B	24.06319	240.6319	99.09725	2.045	90.70747	1.734	89.51988
C	24.454	244. 54	100.93	2.2857	101.3839	1.93	99.63862
D	24.21351	242.1351	99.7163	2.26388	100.4161	1.97166	101.7894
E	24.5558	245.558	101.1259	2.3504	104.2537	2.0394	105.2965
F	24.54039	245.4139	101.0625	2.3445	103.992	2.05	105.9338
G	24.30155	243.0155	100.0789	2.2662	100.519	1.9586	101.1151
H	24.20979	242.0979	99.70098	2.31085	102.4994	2.0014	103.3247
I	24.37493	243.7493	100.3811	1.8578	82.40408	1.56688	80.8921
j	23.85057	238.5057	98.22163	2.96	131.293	2.556	131.9566

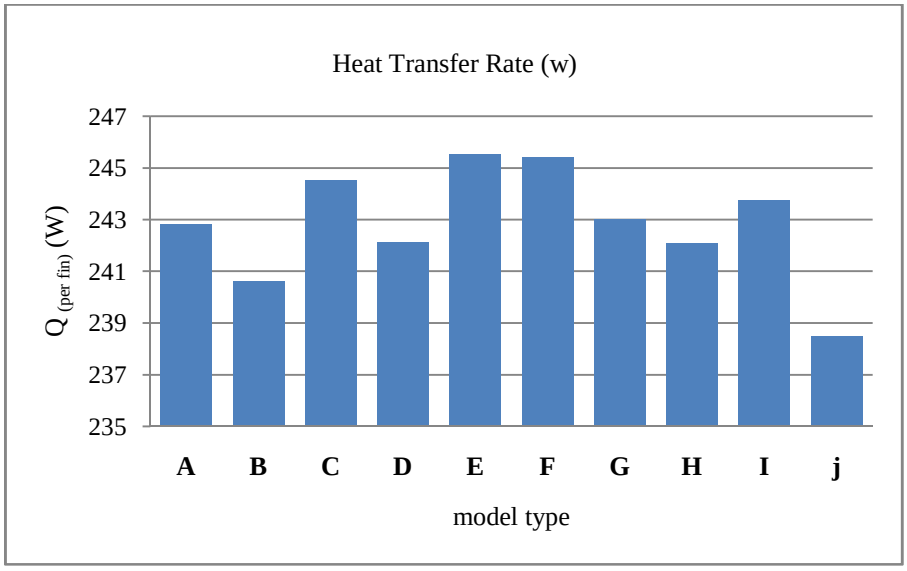

Figure 5.9 Heat transfer rate per fin for all models

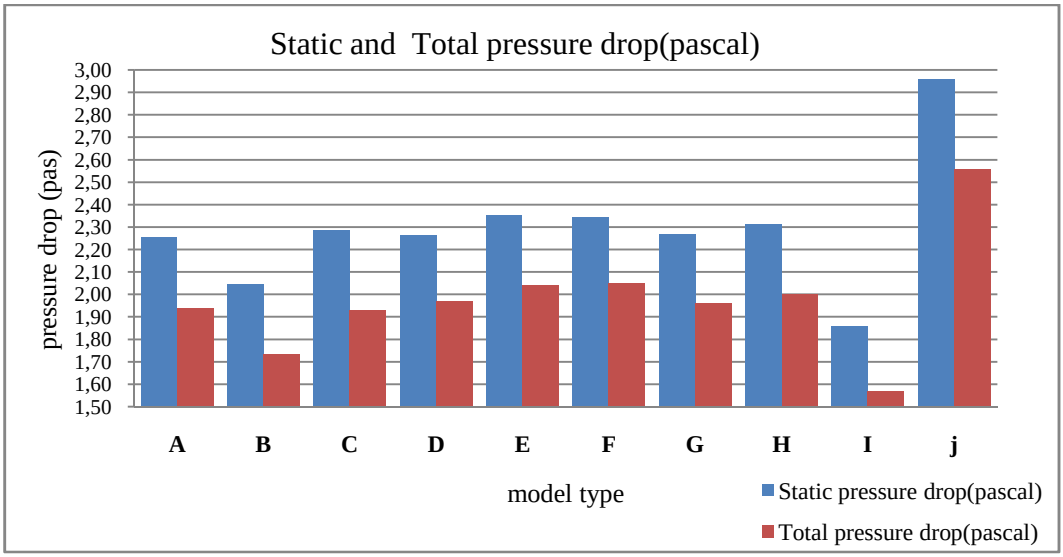

Figure 5.10 Static and Total pressure drop for all models

Normalized heat transfer, static and total pressure drop values, given in Table 5.2 and show in Figures 5.11 and 5.12, are calculated by taking the values of the Model (A) as 100%. These normalized values make the comparison of the models easier.

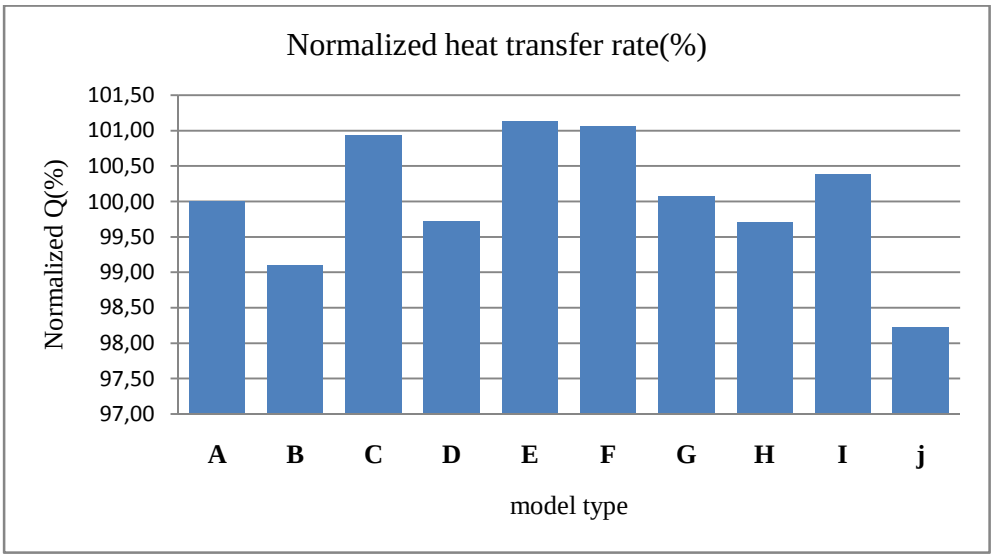

Figure 5.11 Normalized heat transfer rate for all models

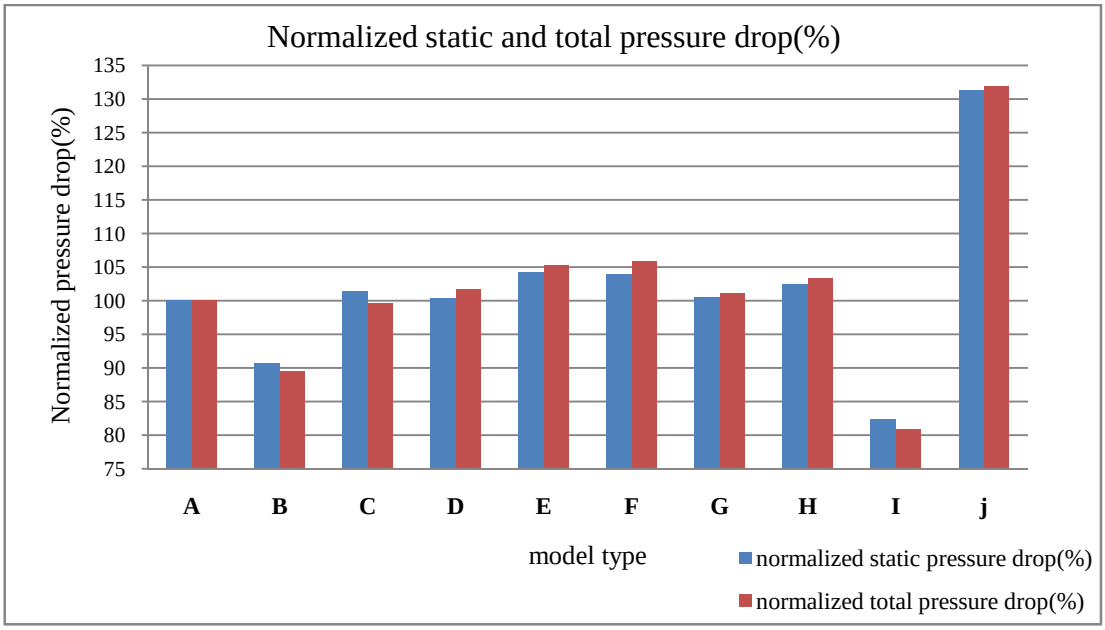

Figure 5.12 Normalized static and total pressure drop for all models

In Table 5.2 and Figures 5.9 and 5.11, the effect of the distance between fins on the heat transfer rate can be clearly seen in model (B); the heat transfer rate is higher for a small distance between fins than for a larger fin distance.

The distance between fins has significant effect on the pressure drop, as in model (B) has the smallest static and total pressure drops. Since flue gas velocity is decreased, the lower pressure drop value is obtained, shown in Table 5.2 and Figures 5.10 and 5.12.

The effects of the distance between fins on temperature contours, velocity vectors, and pressure contours are shown in Figure 5.13 to 5.18, respectively.

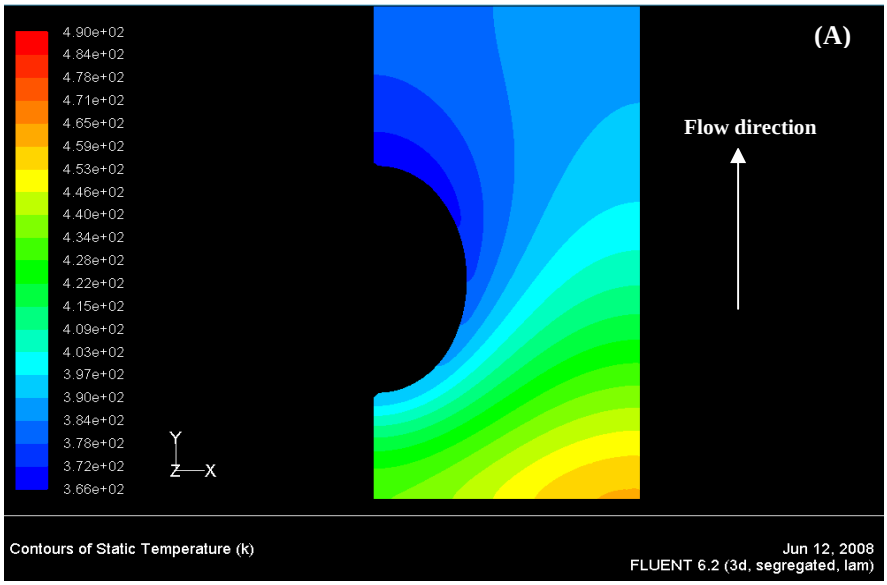

Figure 5.13 Temperature distributions on the surface of the fin for model (A)

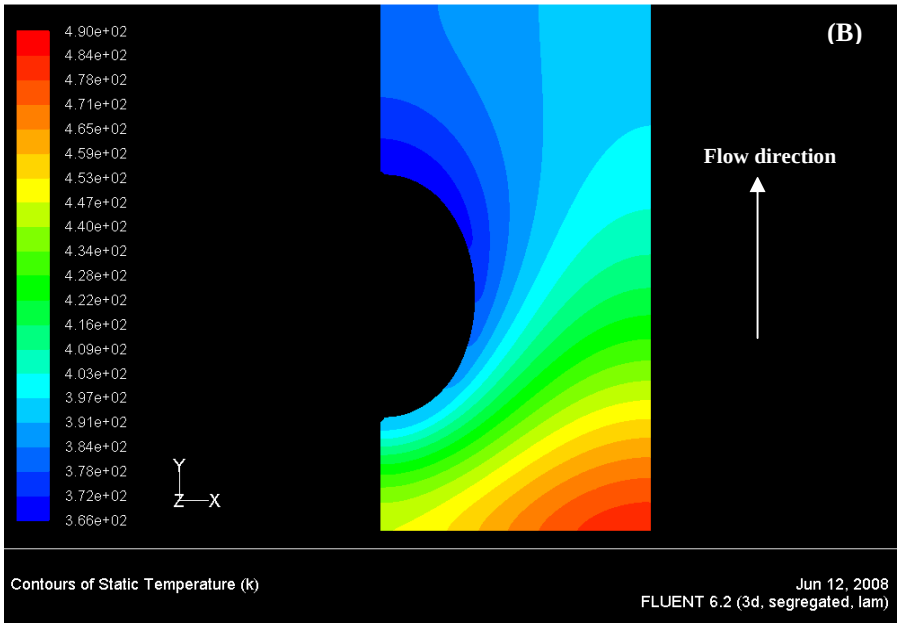

Figure 5.14 Temperature distributions on the surface of the fin for model (B)

In Figures 5.13 and 5.14, it can be seen the temperature distribution on the surface of fin in model (B) better than the model (A), but heat transfer rate less than the model (A) due to smallest fin thickness in the model (B). Also, the temperature distribution on the surface of fin is highest at the leading edge due to the thin boundary layer and at the front of the tube when a horseshoe vortex system is present there.

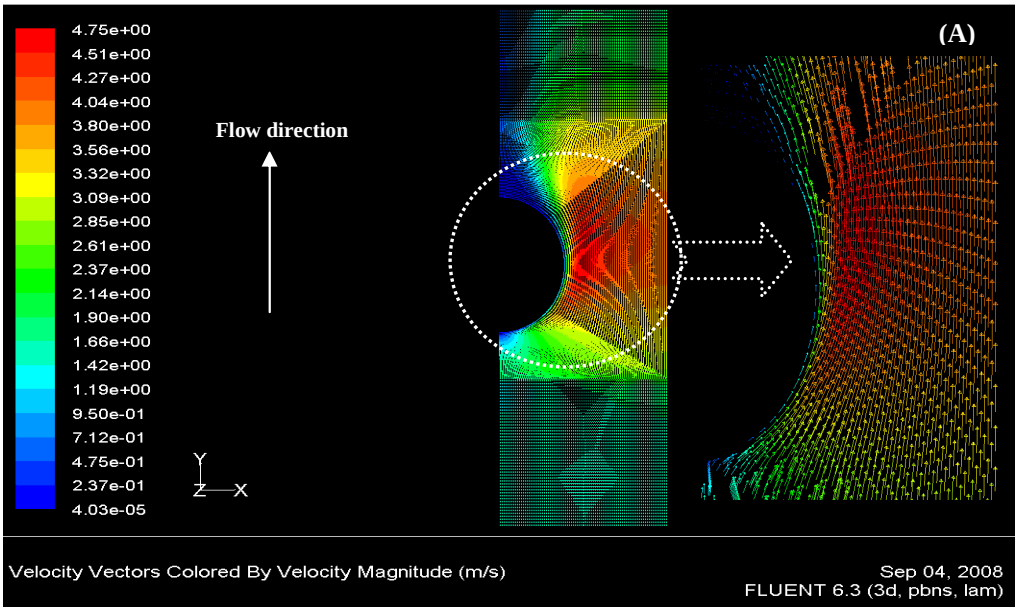

Figure 5.15 Flow velocity distributions at middle plane inside the gap domain for model (A)

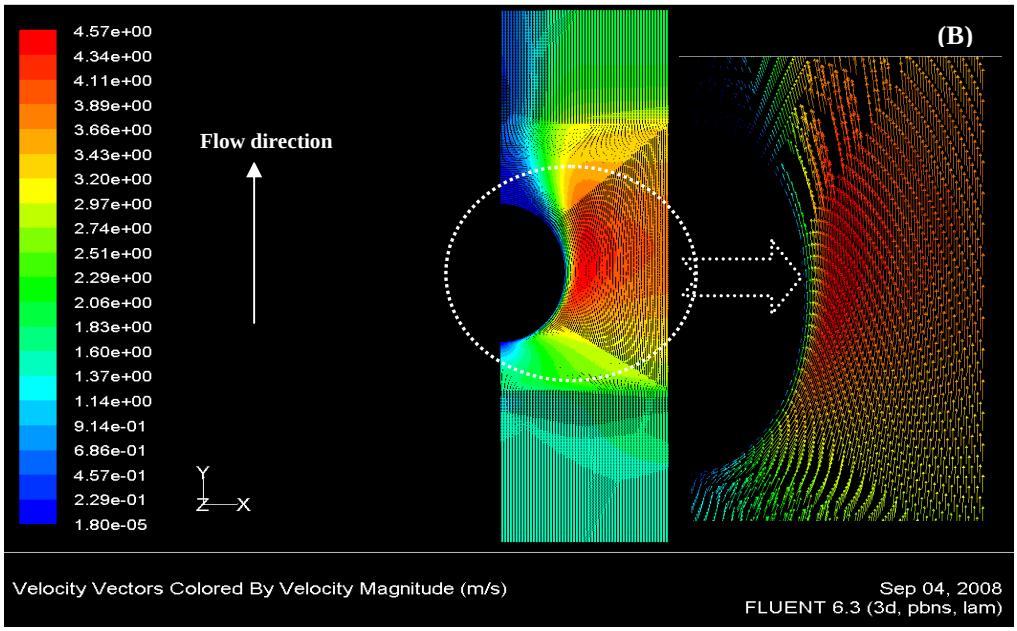

Figure 5.16 Flow velocity distributions at middle plane inside the gap domain for model (B)

Figures 5.15 and 5.16, shows the flue gas velocity between fins in the model (A), greater than the model (B) because of small distance between fins in the model (A). Therefore, the pressure drops in the model (A) greater than the model (B); this can be clearly seen in Figures 5.17 and 5.18.

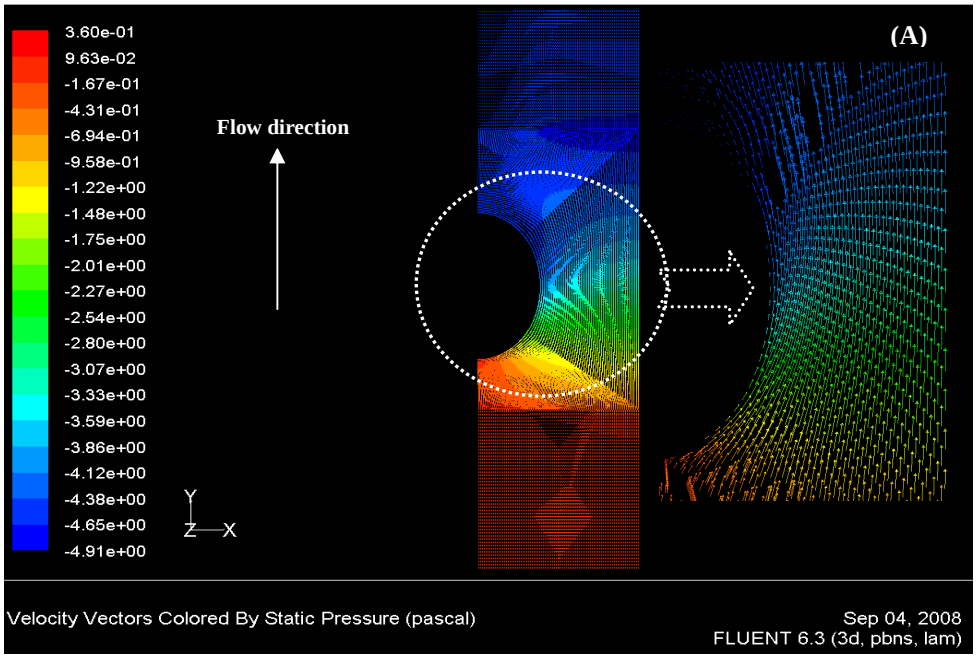

Figure 5.17 pressure contours at middle plane inside the gap domain for model (A)

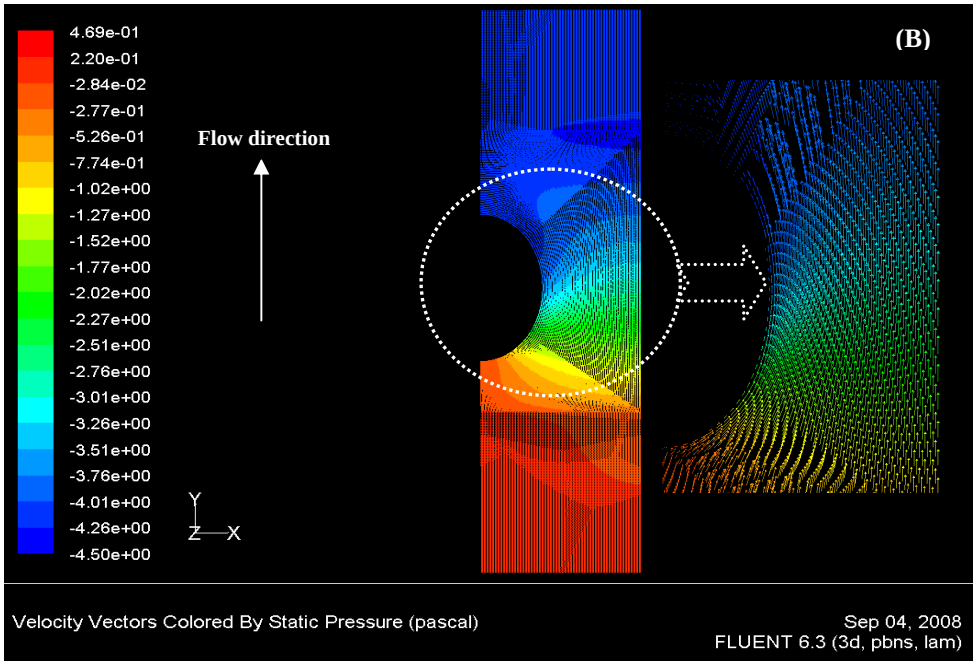

Figure 5.18 pressure contours at middle plane inside the gap domain for model (B)

In Table 5.2 and Figures 5.9 and 5.11, shows the effect of tube center location on heat transfer rate between flue gas and water, as in Model (C). Placement of the tube in downstream region, increases heat transfer rate between flue gas and water because of horseshoe vortex effect. If the fin tube is placed in the upstream region, heat transfer augmentation caused by horseshoe vortex could not be noticed at

sufficient level. But, if it is placed in the downstream region which has lower Nusselt number, horseshoe vortex can be noticed strongly. In addition to this, recirculating vortices formed behind the tube attenuate negative effect on heat transfer when the fin tube is placed at the downstream region. This effect can be seen for the results of Models (E) and (F), as well.

As shown in Table 5.2 and Figures 5.10 and 5.12, the tube center location has no significant effect on the pressure drop.

The effects of the tube center location on temperature contours, velocity vectors, and pressure contours are shown in Figure 5.19 to 5.30, respectively.

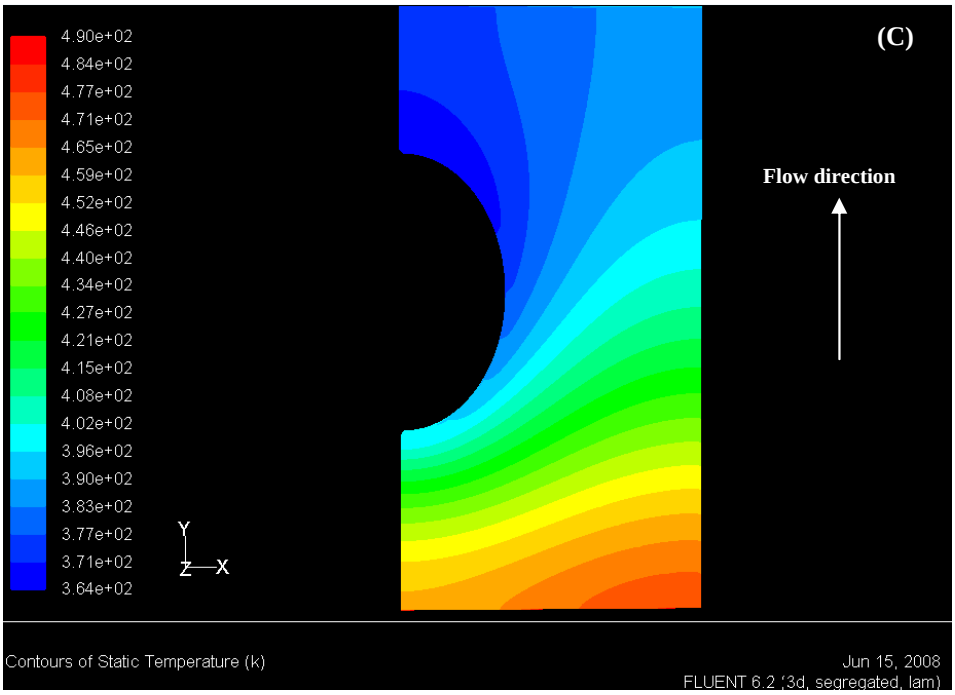

Figure 5.19 Temperature distributions on the surface of the fin for model (C)

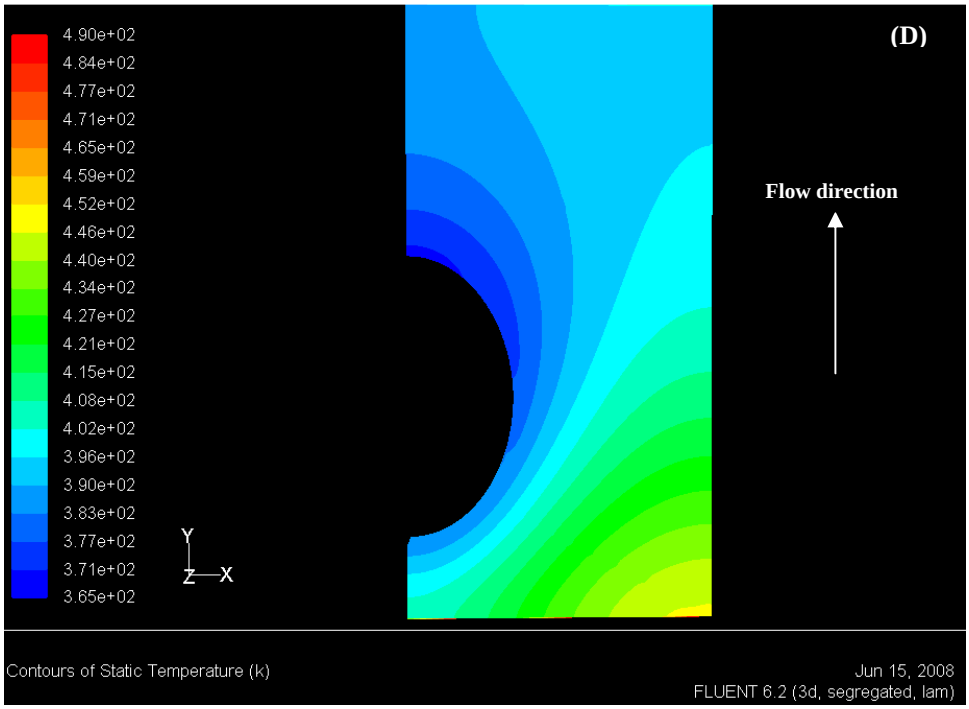

Figure 5.20 Temperature distributions on the surface of the fin for model (D)

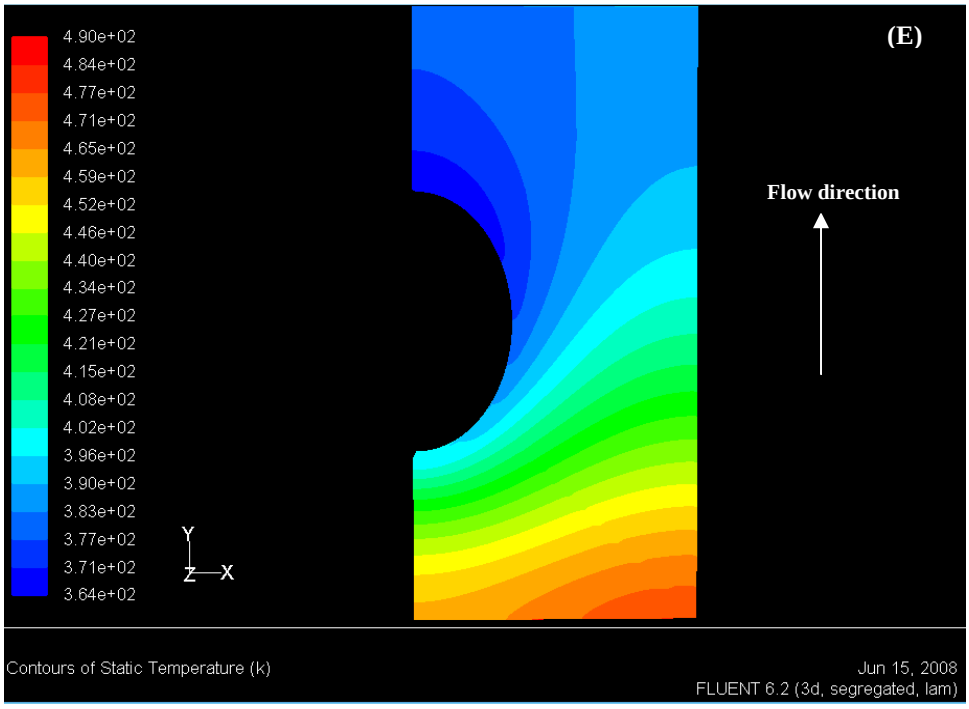

Figure 5.21 Temperature distributions on the surface of the fin for model (E)

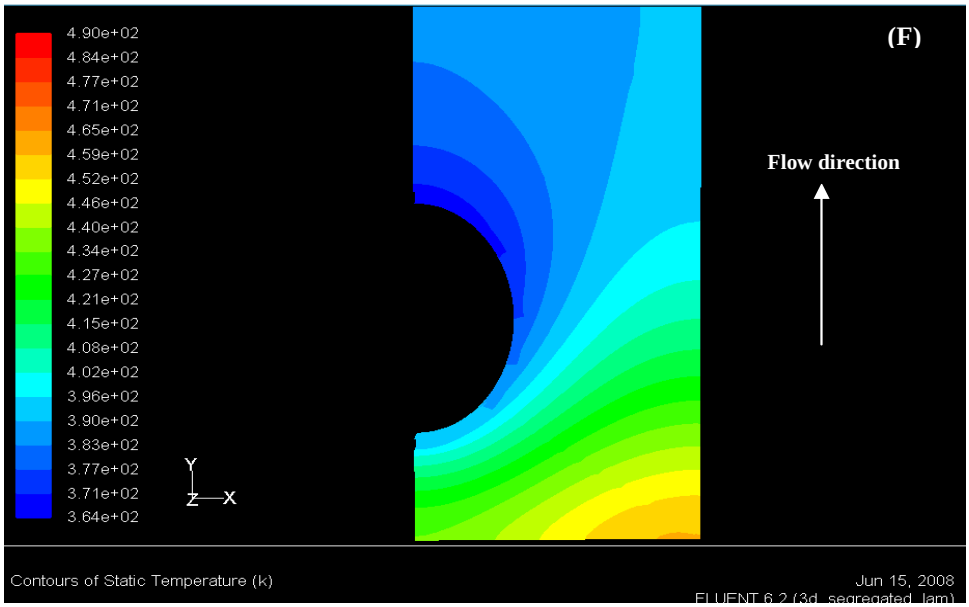

Figure 5.22 Temperature distributions on the surface of the fin for model (F)

In Figures 5.19 to 5.22, it can be seen that the temperature distribution on the surface of fin in the model (C) is better than the model (D) and the model (E) is better than the model (F) due to the placement of the tube in downstream region. Also, the temperature distribution on the surface of fin in the model (E) is better than the model (C) and the model (F) has better conditions than the model (D) due to the fin height in models (E), (F) more than the models (C), (D).

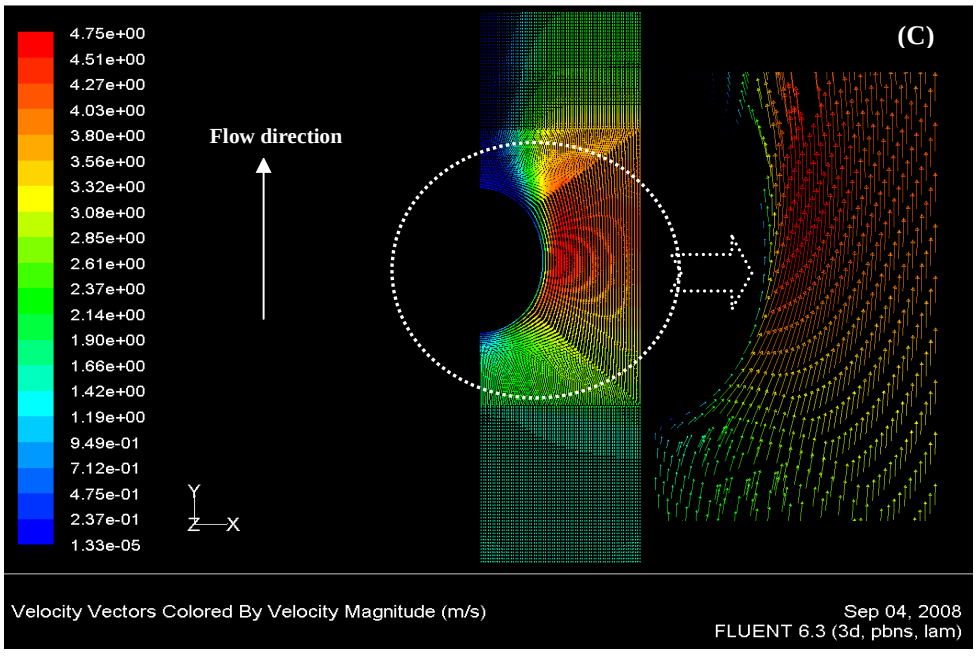

Figure 5.23 Flow velocity distributions at middle plane inside the gap domain for model (C)

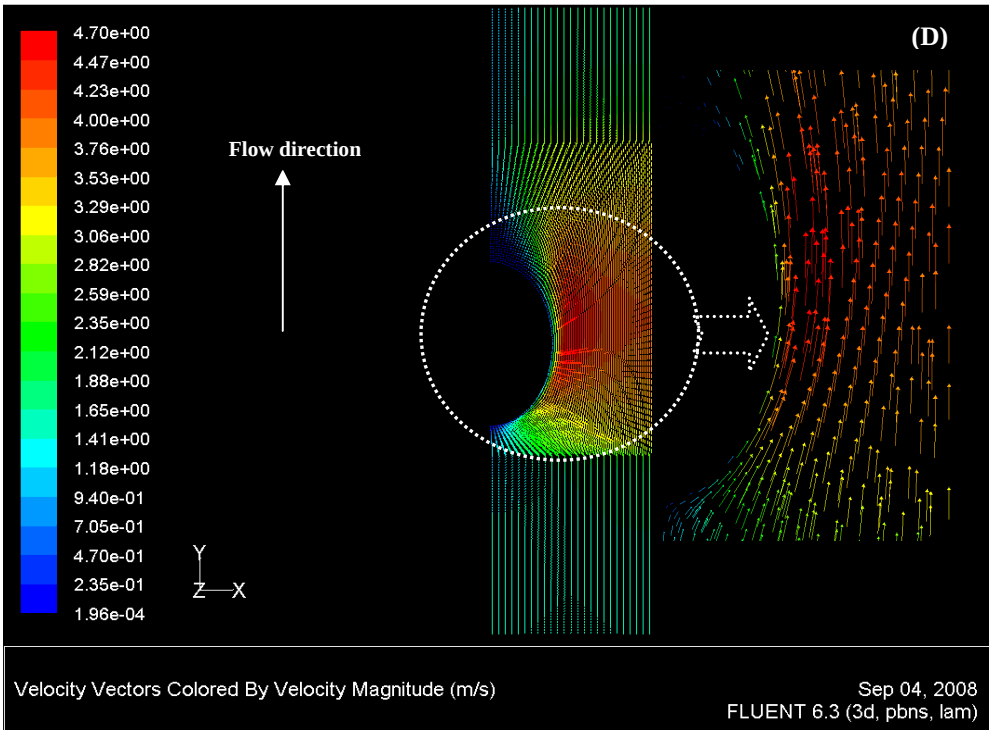

Figure 5.24 Flow velocity distributions at middle plane inside the gap domain for model (D)

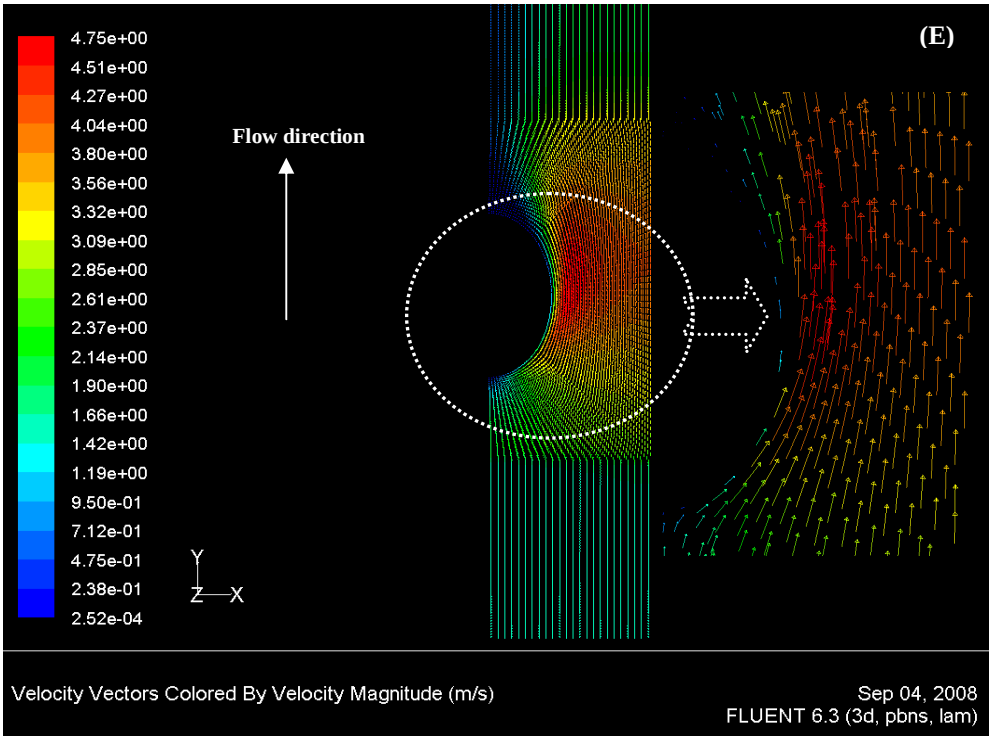

Figure 5.25 Flow velocity distributions at middle plane inside the gap domain for model (E)

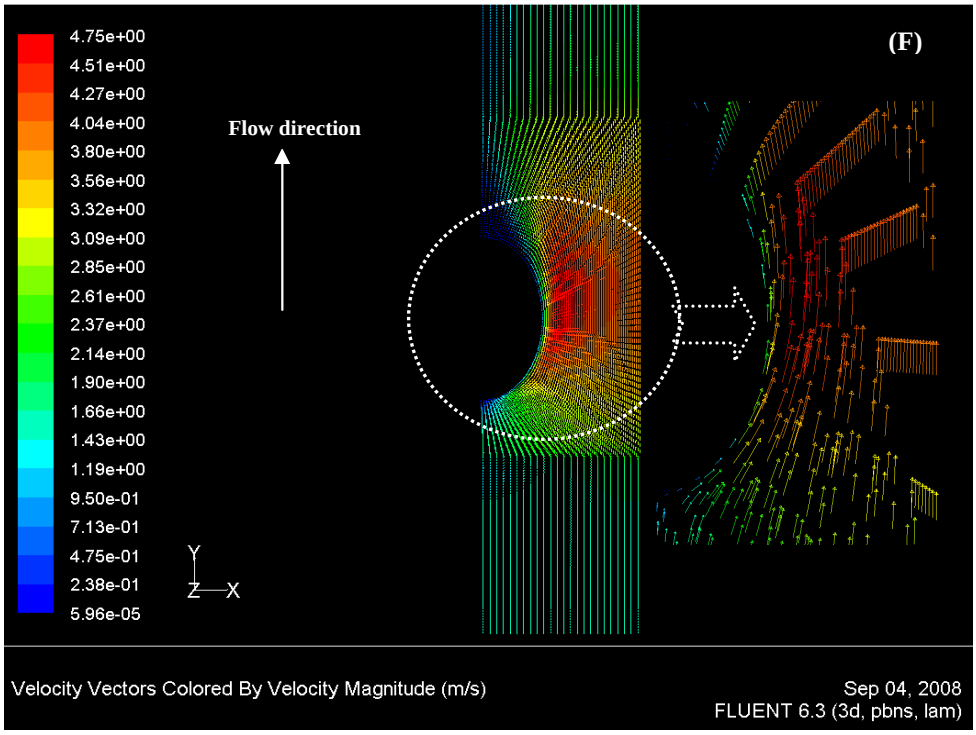

Figure 5.26 Flow velocity distributions at middle plane inside the gap domain for model (F)

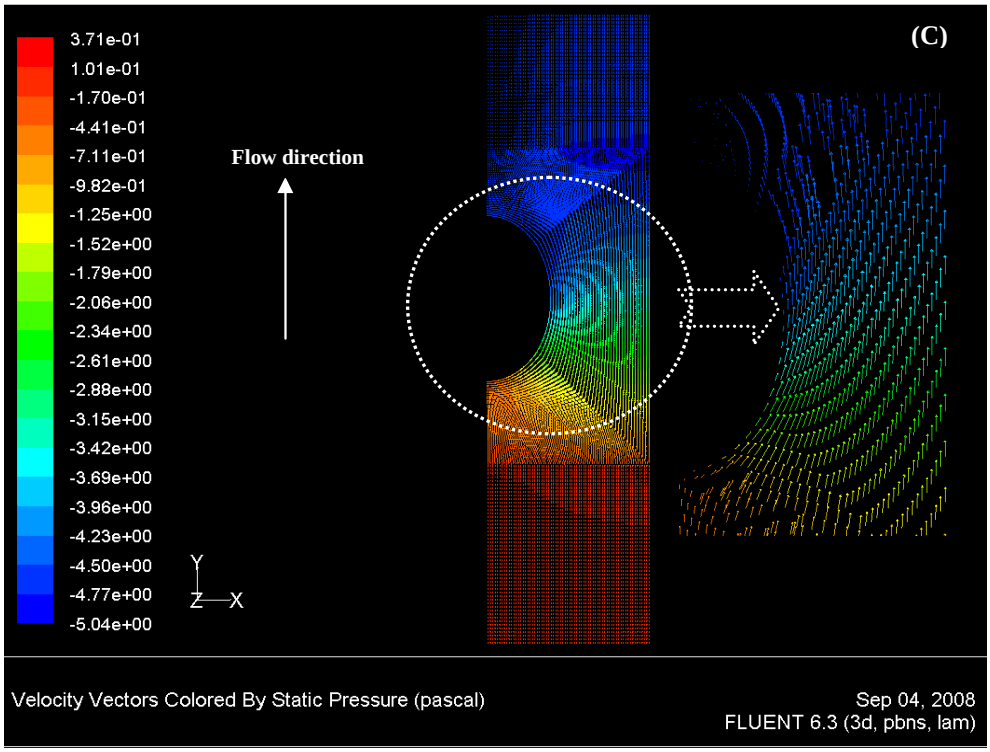

Figure 5.27 pressure contours at middle plane inside the gap domain for model (C)

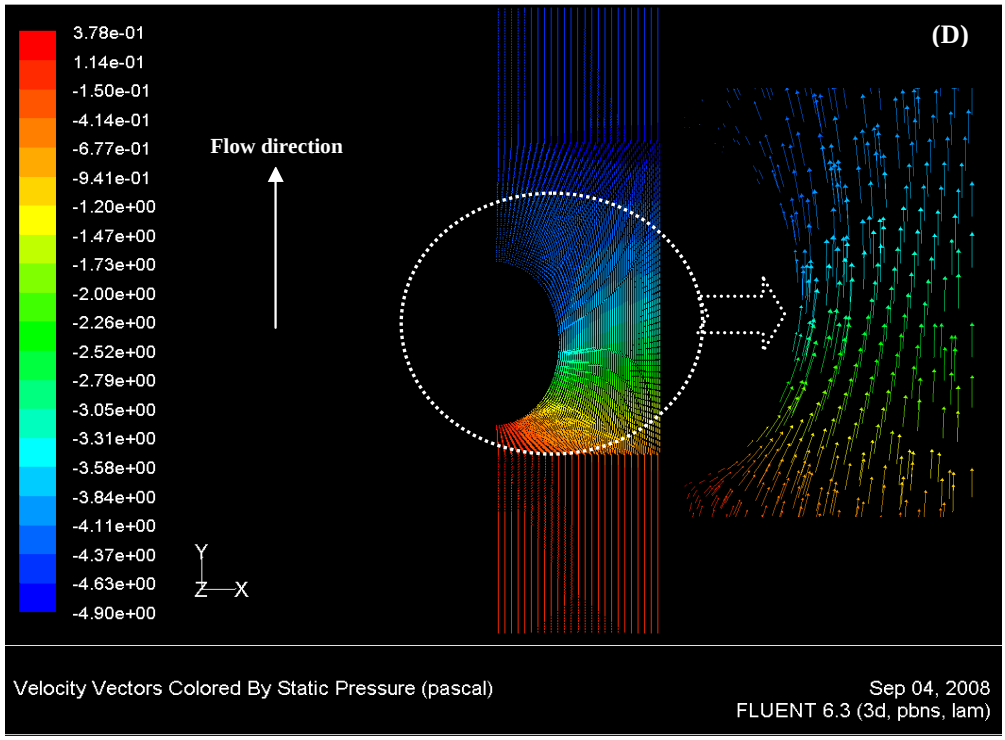

Figure 5.28 pressure contours at middle plane inside the gap domain for model (D)

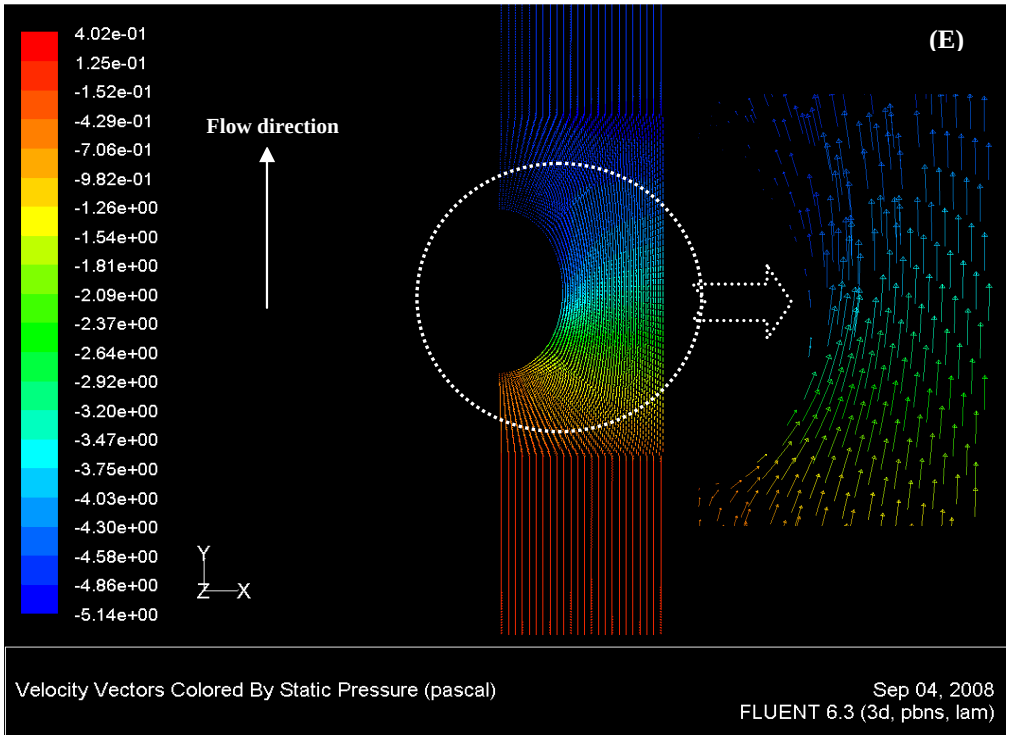

Figure 5.29 pressure contours at middle plane inside the gap domain for model (E)

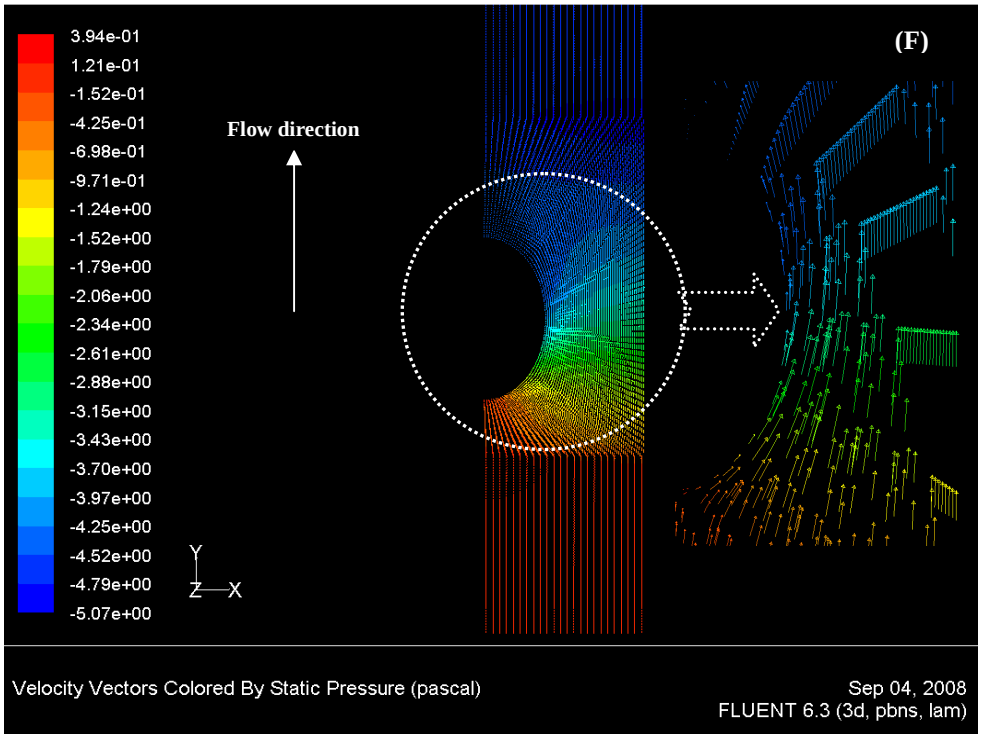

Figure 5.30 pressure contours at middle plane inside the gap domain for model (F)

In Figures 5.23 to 5.26, shows that the change in the flue gas velocitiy for models (C), (D) and models (E), (F) has no great significance. Hence, the pressure drop in these models have nearly same. But in models (E), (F) the pressure drop is greater than the models (C), (D) because of the increasing of fin heights, as shown in Figures 5.27 to 5.30, respectively.

Figures 5.9, 5.11 and Table 5.2, shows that, greater heat transfer rates are obtained as the fin height increases, due to the increased heat transfer area, as in model (E) and model (F).

As shown in Figures 5.10, 5.12 and Table 5.2, the pressure drop increases with the rise of fin height, as in model (E) and model (F).

The effects of the fin height on temperature contours, pressure contours, and velocity vectors are shown in Figures 5.13, 5.19, 5.21, 5.22, 5.15, 5.23, 5.25, 5.26, 5.17, 5.27, 5.29 and 5.30, respectively.

The effects of the tube thickness on the heat transfer and the pressure drop are shown in Table 5.2 and Figures 5.9 to 5.12, respectively. Heat transfer increases with decreasing tube thickness, whereas pressure drop is decreased with decreasing tube thickness because heat resistance between water and flue gas is lower for this case, as in model (G).

The effects of the tube thickness on temperature contours, pressure contours, and velocity vectors are shown in Figures 5.31 to 5.37, respectively.

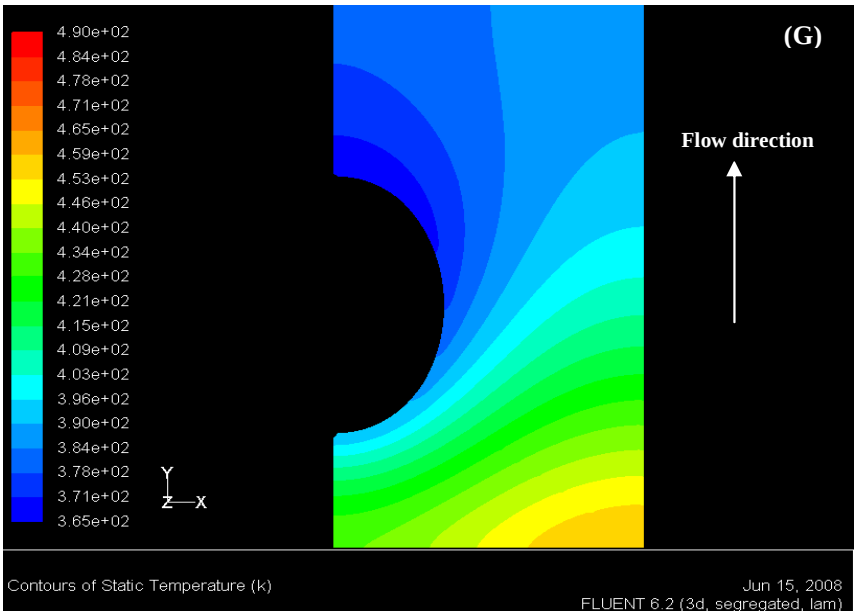

Figure 5.31 Temperature distributions on the surface of the fin for model (G)

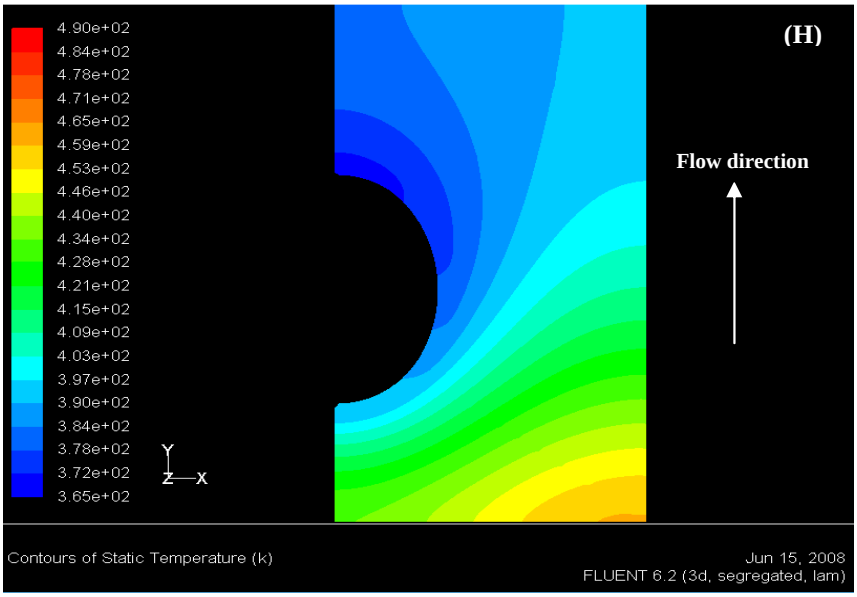

Figure 5.32 Temperature distributions on the surface of the fin for model (H)

In Figures 5.31 and 5.32, it can be seen that the temperature distribution on the surface of fin in model (G) better than the model (H) because of heat resistance between water and flue gas is lower for model (G) than the model (H) that's result from decrease tube thickness in model (G).

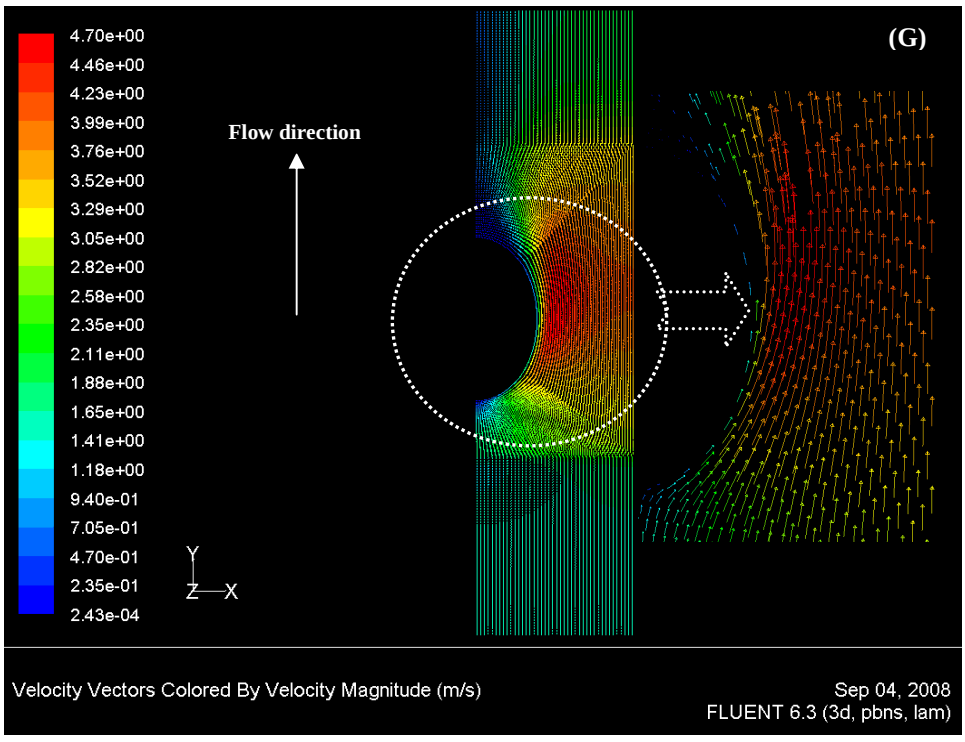

Figure 5.33 Flow velocity distributions at middle plane inside the gap domain for model (G)

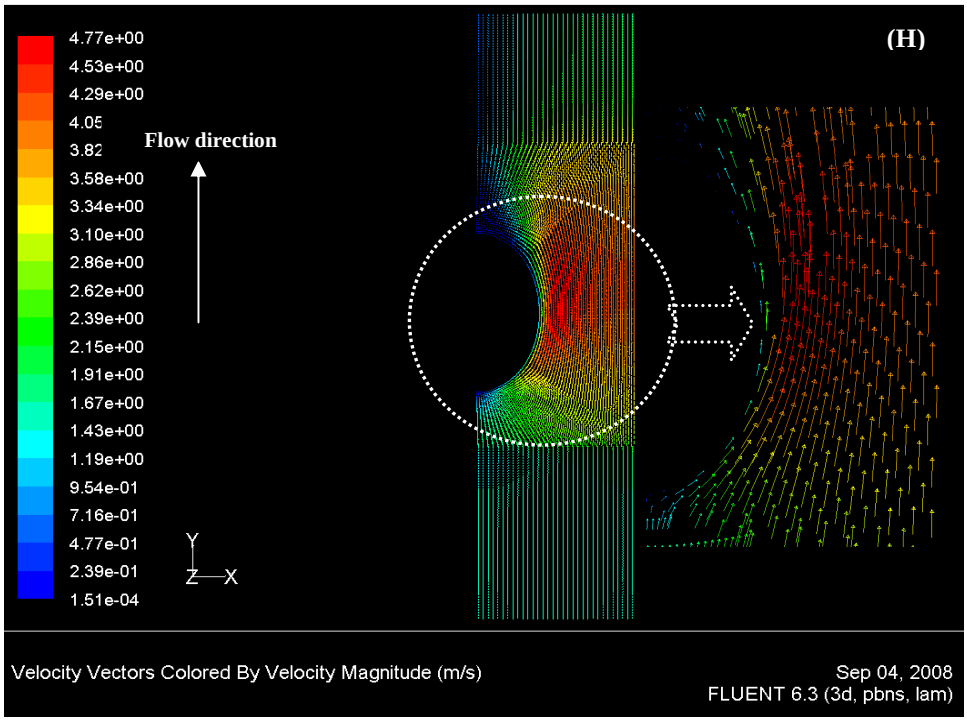

Figure 5.34 Flow velocity distributions at middle plane inside the gap domain for model (H)

Figures 5.33 and 5.34 shows that the flue gas velocity change in models (H) higher than model (G), Therefore, the pressure drop in model (H) higher than the model (G); this can be clearly seen in Figures 5.35 and 5.36.

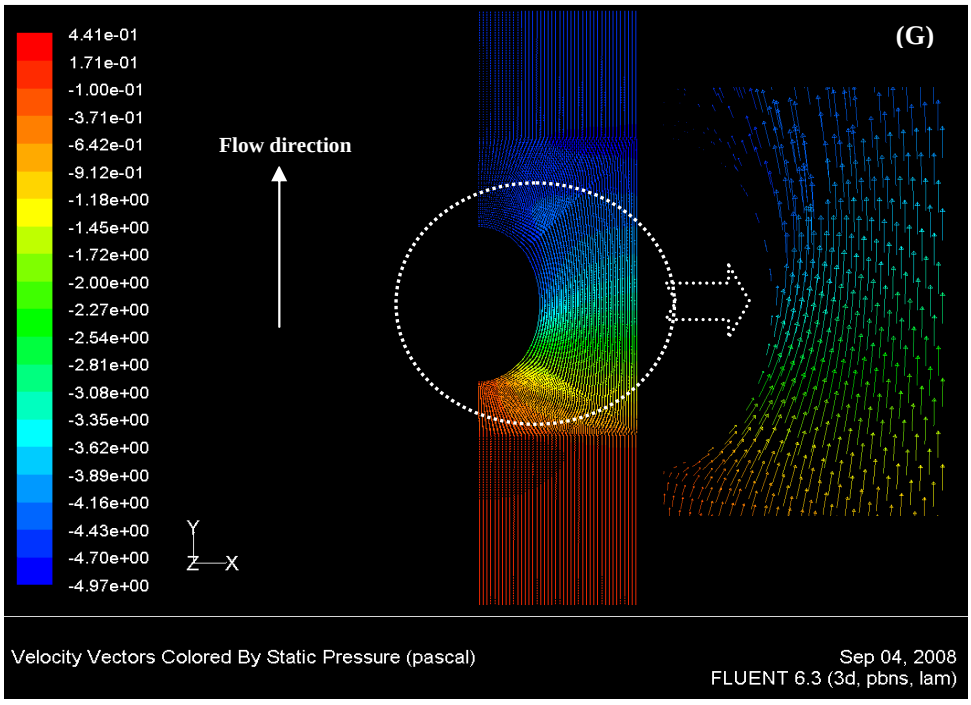

Figure 5.35 pressure contours at middle plane inside the gap domain for model (G)

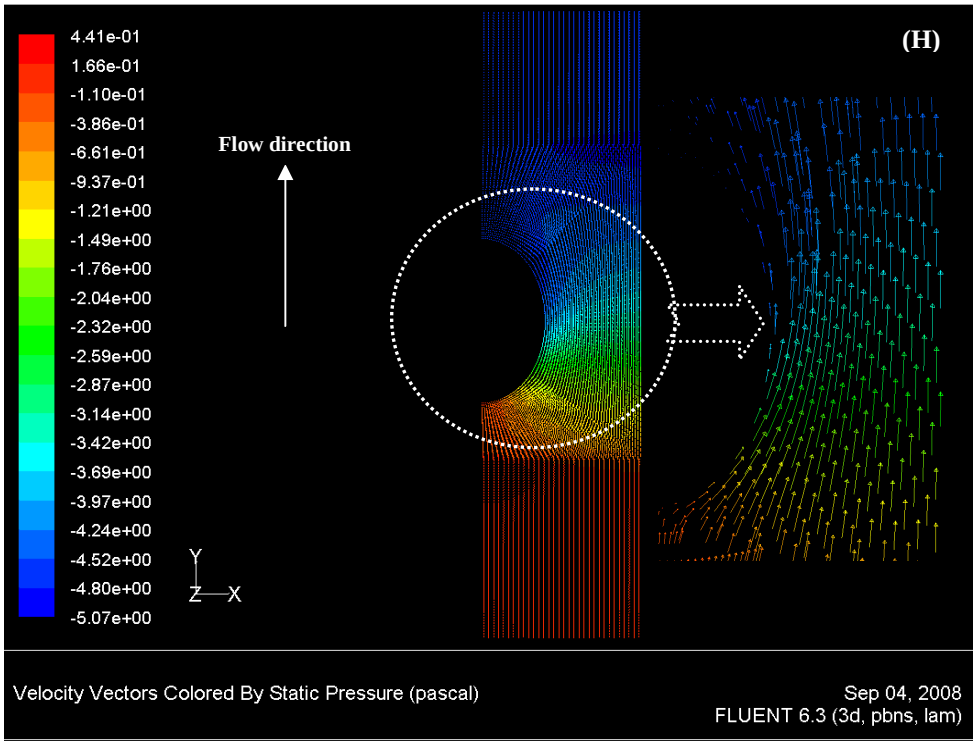

Figure 5.36 pressure contours at middle plane inside the gap domain for model (H)

The effects of the tube ellipticity on the heat transfer and pressure drop across the heat exchanger are shown in Table 5.2 and Figures 5.9 to 5.12, respectively. Heat transfer increases with ellipticity increases in a tube, also, the ellipticity affects the pressure drop positively because when ellipticity increases, the cross section of flue gas flow, also, increases, as in model (I). Elliptical tube results small drag effect than the circular tube, as in model (J); due to the elliptic tube geometry has a better aerodynamic shape than the circular shape.

The effects of the tube ellipticity on temperature contours, pressure contours, and velocity vectors are shown in Figures 5.19, 5.37, 5.38, 5.23, 5.39, 5.40, 5.27, 5.41 and 5.42, respectively

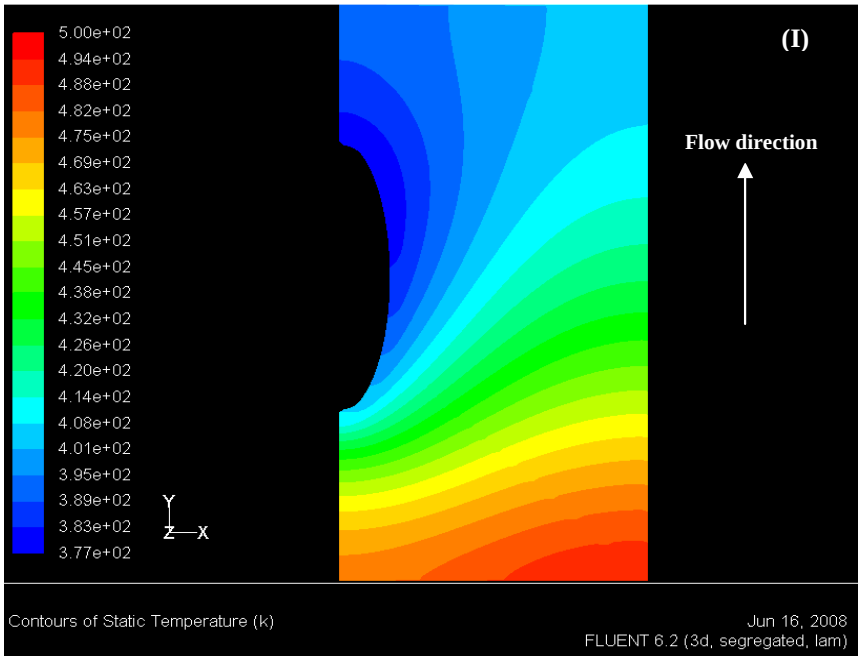

Figure 5.37 Temperature distributions on the surface of the fin for model (I)

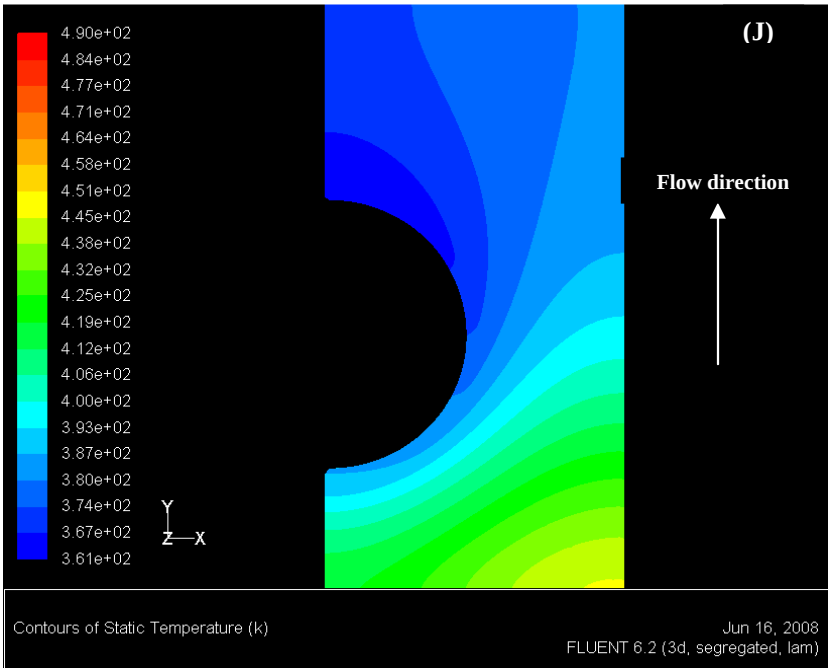

Figure 5.38 Temperature distributions on the surface of the fin for model (J)

Figures 5.37 and 5.38 shows that, the temperature distribution on the surface of fin in model (I) is better than the model (J). Because the shape in model (I) has better aerodynamic.

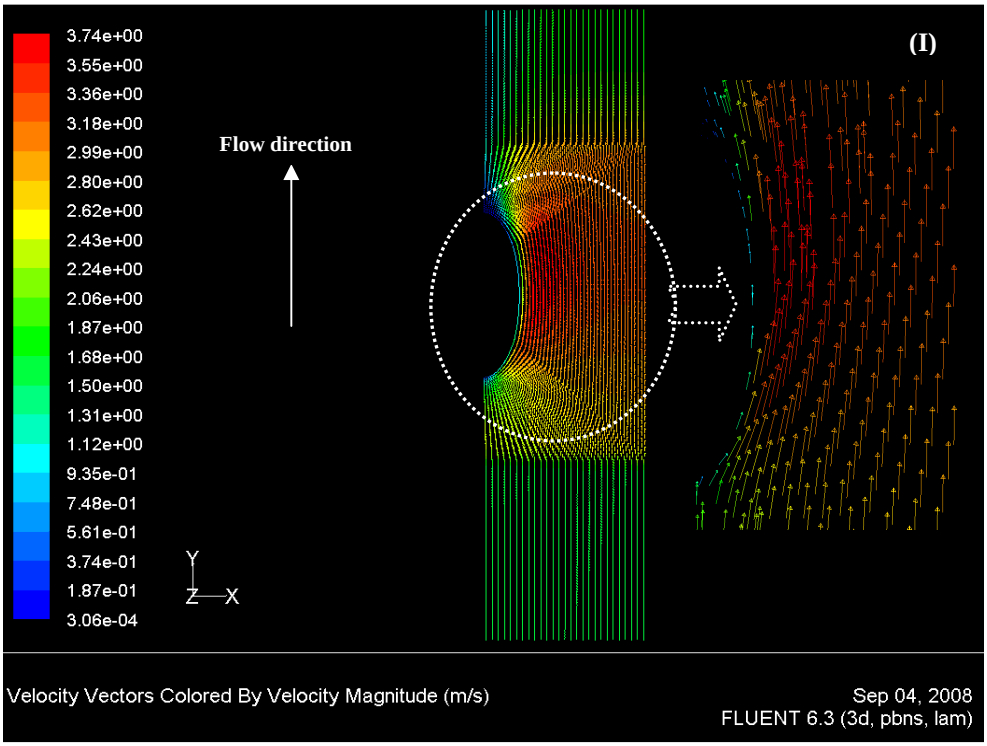

Figure 5.39 Flow velocity distributions at middle plane inside the gap domain for model (I)

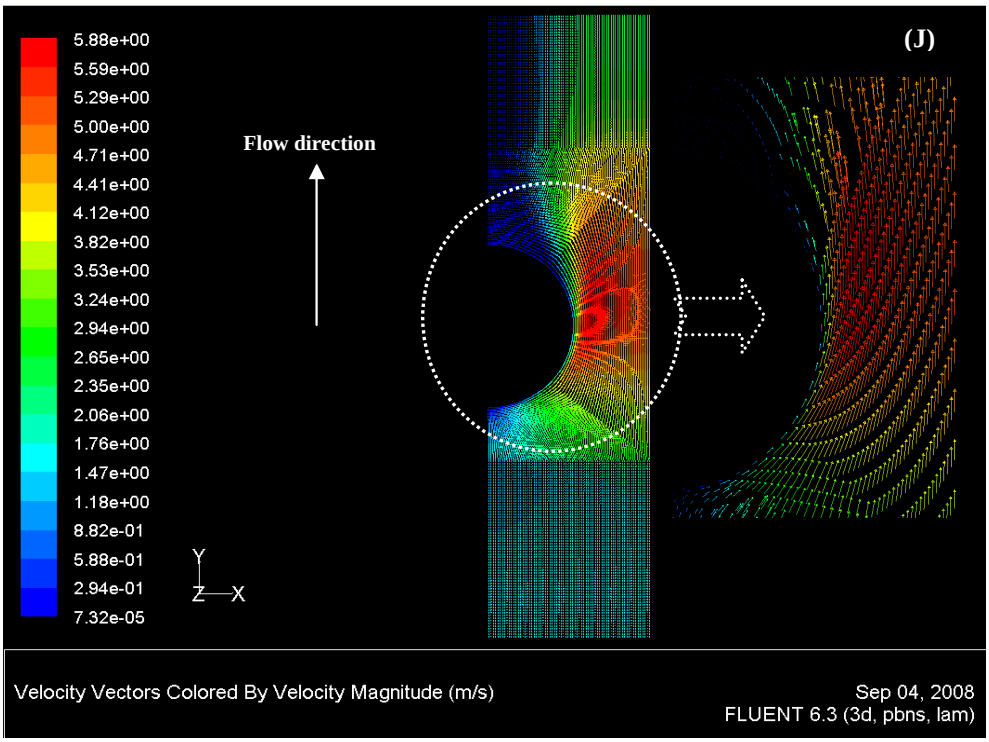

Figure 5.40 Flow velocity distributions at middle plane inside the gap domain for model (J)

In Figures 5.39 and 5.40, the flue gas velocity change in models (I) is smaller than the model (J) due to the cross section of flue gas flow increases when the ellipticity

increases. Therefore, the pressure drop in the model (J) is higher than the model (I); this difference can be clearly seen in Figures 5.41 and 5.42

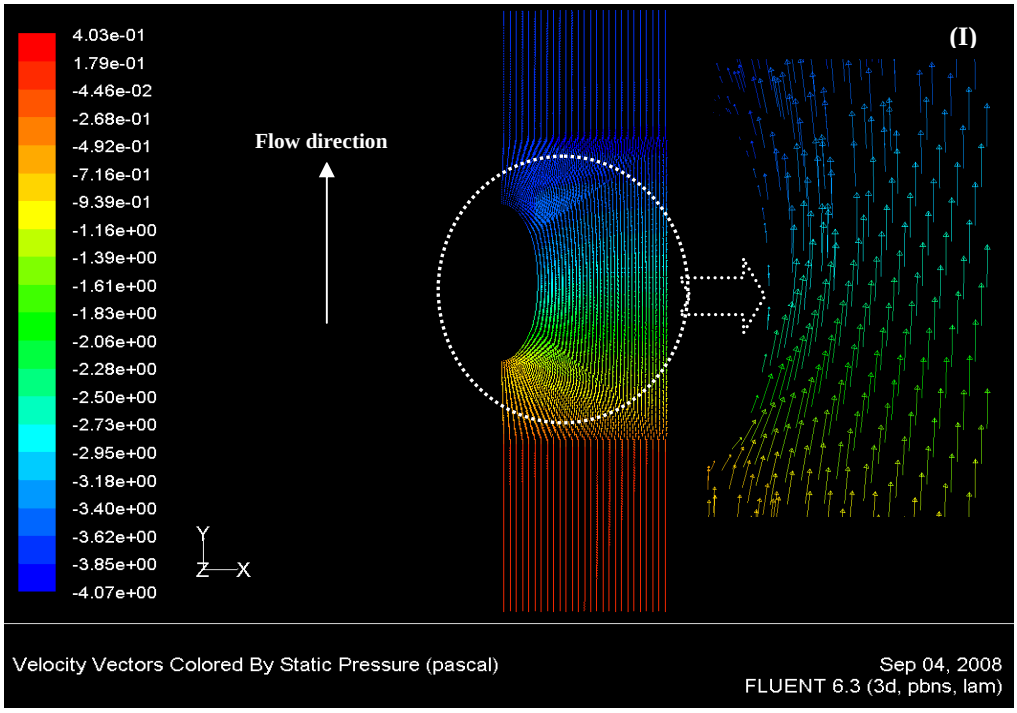

Figure 5.41 pressure contours at middle plane inside the gap domain for model (I)

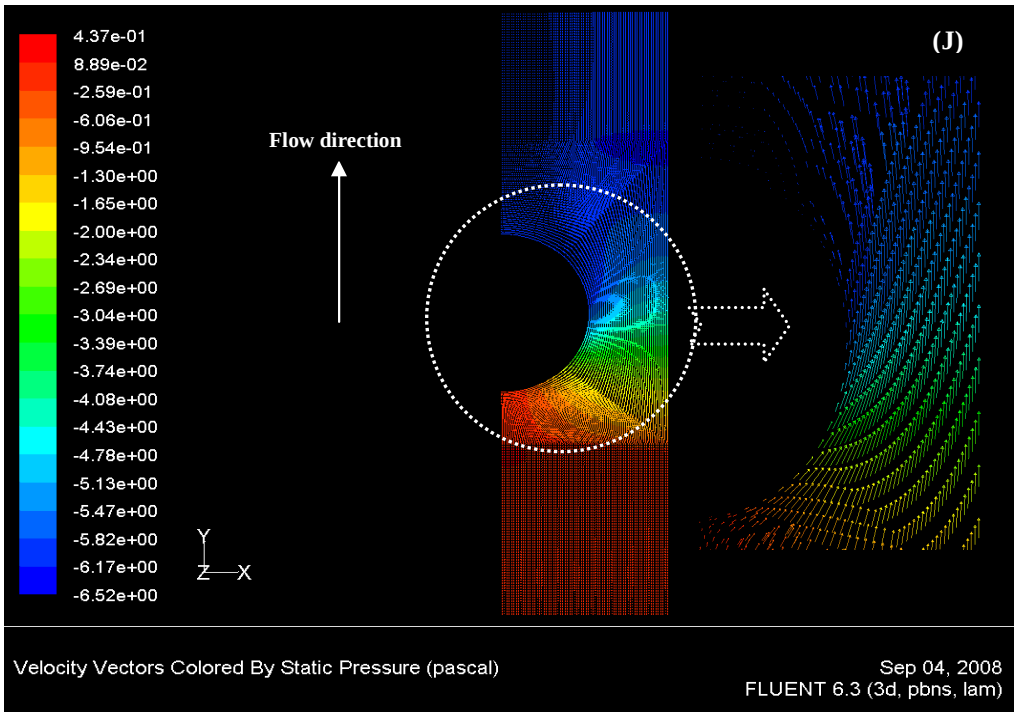

Figure 5.42 pressure contours at middle plane inside the gap domain for model (J)

CHAPTER SIX

CONCLUSION

In this study, a literature survey about the heat transfer and pressure drop characteristics of heat exchangers are performed. Heat exchanger types are mentioned, briefly. A comparison between experimental and numerical result for the temperature distribution and averaged convective heat transfer coefficients over a plate-fin surface are performed. Computational Fluid Dynamics (CFD) software, Fluent is using to simulation of three-row plate-fin and tube heat exchanger and validation with experimental data. At the leading edge of the plate-fin, the results indicate lower temperature because the velocity boundary layer is initially developed in the z-direction. At the rear of the tube, the temperature gradient is gentler because the airflow is swept downstream into the wake. A different characteristic occurs after the third row due to an additional exit effect.

A comparison between experimental and numerical result for the averaged convective heat transfer coefficients ($\overline{h}$), show that the error about 14% for in-line array and 2% for staggered array because of few information about properties of metal and detail of geometrical parameter are used in experimental test. The numerical results are a reasonably in good agreement with experimental results.

In numerical study, one row plate fin and tube heat exchanger is analyzed for different geometrical parameters by using Computational Fluid Dynamics (CFD) software (FLUENT). The effects of the distance between two fins, tube center location, fin height, tube thickness, and tube ellipticity on heat transfer between flue gas and water and pressure drop of flue gas across the heat exchanger are investigated for 10 different models.

- The distance between fins has an important effect on heat transfer and pressure drop. Figures 5.9 and 5.11 show the heat transfer rate is higher for a small distance between fins than for a larger fin distance, as in model (B). For the models with ellipticity value of 0.7345, Model (B) has the smallest static and total pressure drops. Since flue gas velocity is decreased, the lower pressure drop value is obtained.

- Placement of the tube in downstream region, as in Model (c), increases the heat transfer between flue gas and water. The reason of this augmentation can be revealed as horseshoe vortex effect. If the fin tube is placed in the upstream region, heat transfer augmentation caused by horseshoe vortex could not be noticed at sufficient level. But, if it is placed in the downstream region which has lower Nusselt number, horseshoe vortex can be noticed strongly. In addition to this, recirculating vortices formed behind the tube attenuate negative effect on heat transfer when the fin tube is placed at the downstream region. This effect can be seen for the results of Models (e) and (f), as well. Figures 5.10 and 5.12 show the tube center location has no significant effect on the pressure drop.

- Greater heat transfer and pressure drop values are obtained as the fin height is increased, due to the increased heat transfer surface area, as in Model (E) and model (F).

- As the tube thickness is decreased, heat transfer is increased whereas pressure drop is decreased. Because heat resistance between water and flue gas is lower for this case, as in Model (G).

- As ellipticity increases in a tube, the heat transferred across a heat exchanger increases. The ellipticity, also, affects pressure drop positively. This result can be revealed that as ellipticity increases the cross section of flue gas flow, also, increases, as in Model (I). Elliptical tube results in a lesser drag than the circular tube, as in Model (J); due to its better aerodynamic shape. This shape causes better heat transfer characteristics, as well.

NOMENCLATURE

A	: Area (m^2)
A_{total}	: Total air-side surface heat transfer area (m^2)
a	: Bigger radius of elliptical tube (mm)
b	: Smaller radius of elliptical tube (mm)
c_p	: specific heat at constant pressure (J kg^{-1} K^{-1})
D_o	: outside diameter of the tube (mm)
f	: Fanning friction factor
H	: fin spacing (mm)
h	: the local convective heat transfer coefficient (W/m^2 ^oC)
$\overline{h}$	: the averaged convective heat transfer coefficient (W/m^2 ^oC)
k	: thermal conductivity (W m^{-1} K^{-1})
L	: Fin height (mm)
L_1	: Fin tube center location (mm)
l	: length of the imaging element (mm)
N	: Number of tube
Nu	: Average Nusselt number
N_{faces}	: number of faces enclosing cell
Pr	: Prandtl number
Q	: Heat transfer rate (W)
Re	: Reynolds number
$\overline{S}$	: source term
T	: temperature (^oC)
T_∞	: bulk mean temperature of the stream (^oC)

T_w : local wall temperature of the fin surface (^oC)

t_u : Fin tube thickness (mm)

t_f : Fin thickness (mm)

U : frontal velocity (m/s)

W : width of the fin(mm)

x : x-direction coordinate

X : imaging pixel in x coordinate

X_t : transverse pitch (mm)

X_l : longitudinal pitch (mm)

y : y-direction coordinate

Y : imaging pixel in y coordinate

z : z-direction coordinate

Greek symbols

δ : thickness of fin (mm)

ε : emissivity

ν : kinematic viscosity (m2/s)

ϕ : diffusion property

Γ : diffusion coefficient

$\dot{m}$: mass flow rate (kg s^{-1})

μ : dynamic viscosity (N s m^{-2})

ρ : density (kg m^{-3})

$\vec{v}$: velocity vector $\left(=u\vec{i}+v\vec{j} \text{ in 2D}\right)$

S_ϕ : source of ϕ per unit volume

Subscripts

e : east interface of the control volume

f	: fin condition
$face$	: face condition
i	: inlet condition
lm	:log mean condition
o	: outlet condition
s	:surface condition
u	: tube condition
w	: wall (surface) or west interface of the control volume
∞	:free stream condition

REFERENCES

Abu Madi, M., Johns, R.A., Heikal, M.R. (1998). Performance characteristics correlation for round tube and plate finned heat exchangers. *Int. J. Refrig. 21* (7) 507–517.

Bordalo, S. N. and Saboya, F. E. M. 1995. Experimental determination of pressure drop coefficients in circular and elliptical tubes and plate fin heat exchangers. *Proc. 13th COBEM, Brazilian Conference on Mechanical Engineering*, Belo Horizonte, Brazil (in Portuguese).

Brauer, H. August 1964. Compact heat exchangers. *Chem. Process Eng.*, 451-460.

D.G. Shepherd, Performance of one-row tube coils with thin-plate fins, low velocity forced convection, Heating, Piping Air Cond. 28 (1956) 137–144.

E.C. Rosman, P. Carajilescov, F.E.M. Saboya, Performance of one and two-row tube and plate fin heat exchangers, *J. Heat Transfer 106* (1984) 627–632.

Erek, A. (1999). Phase change around finned horizontal cylinder: a conjugate problem. PhD thesis. İzmir: Graduate School of Natural and Applied Sciences of Dokuz Eylul University.

Erek, A., Özerdem, B., Bilir, L., & Ilken, Z. Effect of geometrical parameters on heat transfer and pressure drop characteristics of plate fin and tube heat exchangers. *Applied Thermal Engineering* 25 (2005) 2421–2431

F. Schulemberg, Finned elliptical tubes and their applications in air-cooled heat exchangers, *J. Eng. Ind. 88* (1966)179–190.

F.E.M. Saboya, E.M. Sparrow, Local and average transfer coefficients for one-row plate fin and tube heat exchanger configurations, *J. Heat Transfer 96* (1974) 265–272.

F.E.M. Saboya, E.M. Sparrow, Transfer characteristics of two-row plate fin and tube heat exchanger configurations, *Int. J. Heat Mass Transfer 19* (1976) 41–49.

F.E.M. Saboya, E.M. Sparrow, Experiments on a three-row fin and tube heat exchanger, *J. Heat Transfer 98* (1976) 520–522.

Fluent, User Manuals & Tutorials

Friterm Brochures & Catalogues

Gambit, User Manuals & Tutorials

Herchang Ay, JiinYuh Jang, Jer-Nan Yeh. Local heat transfer measurements of plate finned-tube heat exchangers by infrared thermography. *International Journal of Heat and Mass Transfer 45* (2002) 4069–4078.

Incropera, F. (2002). *Fundamentals of Heat and Mass Transfer*. (5th ed.), John Wiley & Sons, Inc.

Jang, J.Y., Wu, M.C., Chang, W.J. (1996). Numerical and experimental studies of three-dimensional plate-fin and tube heat exchanger. *Int. J. Heat Mass Transfer, 39,* 3057–3066.

Jang, J.Y., Lai, J.T., Liu, L.C. (1998). The thermal-hydraulic characteristics of staggered circular finned-tube heat exchangers under dry and dehumidifying conditions. *Int. J. Heat Mass Transfer, 41,* 3321 – 3337.

Kakaç, S. (1998). *Heat Exchangers: Selection, Rating, and Thermal Design*. CRC Press.

Kuan, D. Y., Aris, R. and Davis, H. T. 1984. Estimation of fin efficiencies of regular tubes arrayed in circumferential fins. *Int. J.Heat Mass Transfer,* 22, 148-151.

L.A.O. Rocha, F.E.M. Saboya, J.V.C. Vargas, A comparative study of elliptical and circular sections in one and two row tubes and plate fin heat exchangers, *Int. J. Heat Fluid Flow 18* (1997) 247–252.

Patankar, S.V. (1980). *Numerical Heat Transfer and Fluid Flow*. NY: McGraw-Hill.

R.L. Webb, Air-side heat transfer in finned tube heat exchangers, *Heat Transfer Eng. 1 (3)* (1980) 33–49.

R. Romero-Me´ndez, M. Sen, K.T. Yang, R. McClain, Effect of fin spacing on convection in a plate fin and tube heat exchanger, *Int. J. Heat Mass Transfer 43* (2000) 39–51

Shah, R. K. 1985. Compact Heat Exchangers. In *Handbook of Heat Transfer Applications*, 2nd ed., W. M. Rohsenow,. P. Hartnett, and E. N. Ganic (eds.). McGraw-Hill, New York, 4-174-4-311.

S.J. Kline, F.A. McClintock, Describing uncertainties single-sample experiments, *Mech. Eng. 75* (1953) 3–8.

S. Kakac¸, Y. Yener, *Convective Heat Transfer*, second ed., CRC Press Begell House, Boca Raton, Florida, 1995,pp. 279–309.

S.N. Bordalo, F.E.M. Saboya. pressure drop coefficients for elliptic and circular sections in one ,two and three–row arrangements of plate fin and tube heat exchangers, *J. Braz. Soc. Mech. Sci.XXL(4)* (1999) 600-610.

Versteeg, H.K., & Malalasekera W. (1995). *An Introduction to Computational Fluid Dynamics: the finite volume method*, London: Prentice Hall.

Wang CC, Fu WL, Chang CT. (1997). Heat transfer and friction characteristics of typical wavy fin and tube heat exchangers. *Exp Thermal Fluid Sci, 14(2)*, 174–86.

Wang CC, Tsi YM, Lu DC. (1998). A comprehensive study of convex-louver and wavy fin and tube heat exchangers. *AIAA J Thermophys Heat Transfer, 12(3),* 423–30.

Wang CC, Lin YT, Lee CJ, Chang YJ. (1999). Investigation of wavy fin and tube heat exchangers: a contribution to databank. *Exper. Heat Transfer, 12*, 73–89.

Wang, C.C., Chi, K.Y. (2000). Heat transfer and friction characteristics of plain finand- tube heat exchangers, part I: new experimental data. *Int. J. Heat Mass Transfer 43*, 2681–2691.

Wang, C.C., Chi, K.Y., Chang, C.J. (2000). Heat transfer and friction characteristics of plain fin-and-tube heat exchangers, part II: Correlation. *Int. J. Heat Mass Transfer 43*, 2693–2700.

Wang, C.C., Lee, W.S., Sheu, W.J. (2001). A comparative study of compact enhanced fin-and-tube heat exchangers. *Int. J. Heat Mass Transfer, 44*, 3565 – 3573.

Ximenes, M. P. 1981. Heat and mass transfer in elliptical tubes and plate fin heat exchangers. Ph.D. *thesis, Mechanical Engineering division, Air Force Institute of Technology*, Sao Jose dos Campos, Brazil (in Portuguese).

Zabronsky, H. 1955. Temperature distribution and efficiency of a heat exchanger using square fins on round tubes. *J. Appl. Mech.*, 22, 119-122.